NOTE TO USERS

Design Optimization of an Adaptive Laminated Composite Beam with Piezoelectric Actuators

MEHRAD AHARI

A Thesis

in

The Department

of

Mechanical and Industrial Engineering

Presented in Partial Fulfillment of the Requirements
for the Degree of Master of Applied Science (Mechanical Engineering) at
Concordia University
Montreal, Quebec, Canada.

July 2005

Your file Votre référence
ISBN: 0-494-10260-8
Our file Notre référence
ISBN: 0-494-10260-8

Abstract

Design Optimization of an Adaptive Laminated Composite Beam with Piezoelectric Actuators

MEHRAD AHARI

Adaptive laminated composite structures are being increasingly used in the aerospace and automotive industries due to their capability of shape control, precise positioning, and vibration suppression. In the present work, the behavior of a laminated composite beam under static and dynamic loading is being modeled using an efficient finite element model, being developed based on the CLPT and FSDT. Responses of the beam to an impact loading, where the effect of each mode of actuation is taken into account, have been plotted and the two theories have been compared.

Later, the model has been modified to incorporate the effect of surface-bonded piezoelectric actuators. The effect of size and location of the piezoelectric patches, while they actively stiffen the beam, on the first three natural frequencies and also on the maximum deflection of the beam under various boundary conditions has been studied. The effect of active stiffening on the frequency and amplitude of the dynamic response of the beam to an impact loading has also been investigated.

Optimization technique based on the SQP method has been applied to control the shape of a beam by minimizing the mean-square error between the actual and the desired shape. The overall mass of the beam is also minimized by changing the thicknesses of composite layers and/or actuators while various constraints are applied. Finally, optimization techniques are used to find the appropriate voltages to control the shape of a piezo-laminated beam, performing as laser beam or reflection mirror controller.

Table of Contents

List of Figures

List of Tables

List of Symbols

σ_{ij}	Stress components
ε_{ij}	Strain components
C_{ij}	Material coefficients
S_{ij}	Compliance coefficients
θ	Angle between fiber orientation and the reference axis
Q_{ij}	Plane stress-reduced stiffness
E_1	Young's moduli in fiber direction
E_2	Young's moduli in transverse direction
G_{12}	Shear moduli in the 1-2 plane
G_{13}	Shear moduli in the 1-3 plane
G_{23}	Shear moduli in the 2-3 plane
ν_{ij}	Poison ratio
t	Time
u	Displacement in x-direction
w	Deformation in the thickness direction
ϕ_x	Rotation about y-axis
N_x^i	Initial axial force along x-axis
$q(x)$	Distributed transverse load on the beam
b	Width of the beam
N_0	Axial force
q_0	Uniform transverse load
M_x	Bending moment about the y-axis
B_{11}	Coefficients of coupling stiffness matrices
D_{11}	Coefficients of bending stiffness matrices
I_0	Mass inertia of the beam
I_2	Rotary inertia of the beam
ρ	Density
H,h	Height of the beam
v_i	Weight function
(u_0, w_0)	The displacements along the coordinate of a material point on the xy-plane
$[K]^e$	Element's stiffness matrix
$[G]^e$	Element's geometric stiffness matrix
$[M]^e$	Element's mass matrix
$\{F\}^e$	Force vector

l	Length of the beam
γ	Transverse shear strain
n	Total number of plies in the laminate
t_k	Thickness of individual ply in the laminate
μ	Shear correction factor
φ_i	Shape functions
S_i	Shape functions
ω	Natural frequency
[C]	Damping matrix
α, β	Coefficients in Newmark method
$\{\dot{w}\}, \{\ddot{w}\}$	Velocity and acceleration vectors, respectively
$\{D\}$	Electric displacement vector
$\{E\}$	Electric field vector
$[e]$	Dielectric constant matrix
$[p]$	Piezoelectric constant matrix
d_{31}, d_{32}, d_{15}	Piezoelectric constant
M_x^P	Piezoelectric moment
N_x^P	Axial piezoelectric force
N_a	Number of piezoelectric layers in the laminate.
$V^{(k)}$	Applied voltage
F^P	Bending force due to the actuators
Q_x^P	Transverse shear force

1 Introduction

1.1 Motivations and objectives

The traditional passive structures can not modify their response mechanism and are unable to perform successfully under varying load conditions. Such performance limitations have motivated considerable interests in developing a new class of structures called adaptive structures which can modify their shapes in a controlled manner.

The study of adaptive composite structures is extremely important because of their demonstrated potential to outperform conventional structures in different applications, such as precise positioning and vibration control. Their high strength-to-weight ratio and adaptation capability have made them very attractive in applications like aerospace structures and transportations. Although extensive research has been conducted to formulate the behavior of these new emerging structures, design optimization, shape and position control of adaptive laminated composites structures have not received appropriate attention. In this study, the capability of piezoelectric actuators to change the static and dynamic shape of laminated composite structures is investigated. Furthermore, the structure has been optimized under different constraints in order to achieve the desired shape or minimum weight. Finally, optimization technique is used as an effective tool to find the appropriate voltages required for a piezoelectric laminated beam, to act as a precise position controller.

1.2 Laminated composite materials

Development of composite materials is one of the boldest technological advances of the modern engineering. Composites refer to materials created by the synthetic assembly of two or more components, in order to tailor specific characteristics and properties mostly considerable high strength-to-weight ratio, compared to metals and other industrial materials. These specific characteristics have made composites the suitable material to be used in a variety of domain from aerospace and automobiles to medical and sport equipments. But the most astonishing characteristic of composite materials is the opportunity they create for designers to tailor the mechanical properties based on their specific needs.

Selected materials to create a composite material are a reinforcing component and a compatible matrix binder. Composite materials are usually subdivided into the following classes according to the structural constituents [2]: (i) laminar: composed of layers or laminar constituents; (ii) particulate: the dispersed phase consists of small particles; (iii) fibrous: the dispersed phase consists of fibers; (iv) flake: the dispersed phase consists of flat flakes.

Fiber reinforced composites are the most common materials used in aerospace, construction and automotive industries. In fibrous composite materials, the fibers provide virtually all strength and stiffness while the matrix is to bind the reinforcements together and keep them in proper orientation, to transfer the load to and between them and

distribute it evenly, to protect the fibers from hazardous environments and handling, to provide resistance to crack propagation and damage, to provide all the inter-laminar shear strength of the composite, and to offer protection from high temperature and corrosion. The key point behind the fibrous composite is that the individual fibers are stiffer and stronger than the same material in bulk form whereas matrix materials have their usual bulk-form properties . By changing the orientation of the fibers, one can optimize the composite material for strength, stiffness, fatigue, heat and moisture resistance. Fiber reinforced composite materials for structural applications are often made in the form of a thin layer, which is called lamina.

The structural elements, such as bars, beams and plates are made by stacking together many plies of fiber reinforced layers in different angles to achieve the desired properties. The different layers of lamina are permanently bonded together under heat and pressure using a hot press or autoclave [2,3].

1.3 Piezoelectric actuator and sensors

The concept of using sensors and actuators to design a self-controlling and self-monitoring smart laminated structure has drawn considerable interest among the research community. The advantage of incorporating these types of materials into the structures can combine the superior mechanical properties of laminated composites and sensing and actuating capabilities of smart elements. Therefore sensing and actuating mechanism becomes part of the structure so that monitoring and adaptive capabilities are added to the great advantages of conventional composite materials. The smart system is potentially

capable to be applied in designing large scaled space structures, aircraft structures, satellites, and even in commercial automotive industry.

There are a number of materials that have the capability to be used as sensors and or actuators or both. Piezoelectric materials, magneto-strictive materials, electro-strictive materials, shape memory alloys, and electro and magneto-rheological fluids are examples of such materials. Among these, piezoelectric materials due to their coupled mechanical and electrical properties have capability to serve as both sensors and actuators. They also act linearly within a certain limits of applied voltages which make them a good choice for designers. The basic characteristics of piezoelectric materials are direct and reverse piezoelectric effect. In the direct piezoelectric effect, applying mechanical loads on piezoelectric induces an electrical response where as in the reverse piezoelectric effect, an electrical input to the piezoelectric results in mechanical strain. The development of intelligent composite materials with piezoelectric component offers great potential for use in various fields such as advanced automobile and aerospace structural applications. In order to make these adaptive structures applicable for structural design, it is necessary to formulate the appropriate analysis and optimization techniques [5].

1.4 Adaptive laminated structures

The development of smart laminated composite structures with adaptive capabilities may further improve the performance and reliability of the laminated structure. These novel smart structures will combine the superior mechanical properties of conventional composite materials, and incorporate the additional inherent capability of piezoelectric

layers to sense and adapt their static and dynamic response. These advanced laminated structures potentially have the capability to cope with unforeseen loading conditions. They can speed up the damping process of the structures and can also alter the natural frequencies and the amplitude as well as other characteristic of the structure under dynamic excitation. An adaptive laminated composite structure as shown in Figure 1.4-1 involves robust structure, distributed actuators and sensors, and a control mechanism that analyze the feedback response from the sensors in order to command the actuators to apply localized actuations in an attempt to alter the system response and control the response of the structures.

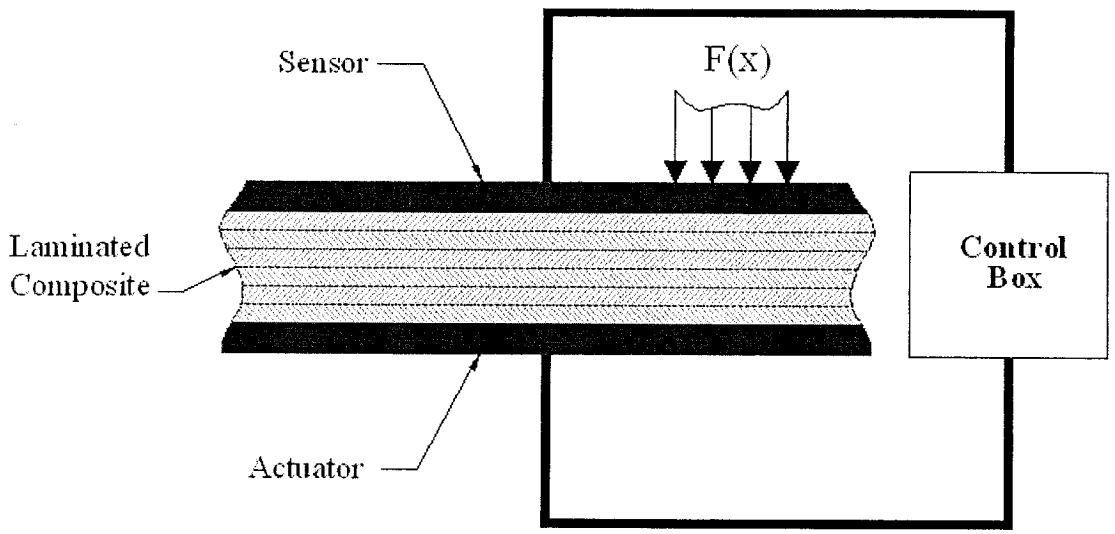

Figure 1.4-1: Schematic image of a smart laminated beam with piezoelectric sensor and actuator

Adaptive laminated structures can be designed to actively react to disturbance forces in order to maintain structural integrity while maintaining or even improving the level of performance [5].

1.5 Literature survey

In the past twenty years, numerous studies have been taken place on the modeling and analysis of adaptive laminated structures and multitude of papers has been published so far in this field. The following survey has been confined to the most recent publications mainly in the past fifteen years. The publications have been selected from English language and most relevant to the preset targets of this research.

Various theories have been developed for the analysis of laminated composite, mainly by improvement of the plate theories [1,2]. The classical lamination plate theory (CLPT) and the first-order shear deformation theory (FSDT) are two examples [3]. Simplicity and exactness of the foregoing theories, specially in predicting the behavior of thin laminates (regardless of interlaminar interactions and delamination phenomenon), is one the most important reasons of their popularity despite of the existence of more complex theories such as higher order and layer-wise (which need excessive amount of calculations where as in several applications do not result in considerable difference in predicting the behavior of laminate). The Subject of impact and dynamic response of a laminated composite structure was explained in details by Abrate [4].

Numerous investigators have recently demonstrated the feasibility of the adaptive laminated structures on various applications. A thorough investigation on piezoelectricity was performed by Piefort [5]. Lee *et al* [6] discussed the transient response of laminated plate with embedded piezoelectric layers using equivalent-single layer theories. They also investigated the effects of lamination orientations, and piezoelectric position on the

vibration suppression. Reddy [7] developed a finite element formulation for laminated composite plate with sensors and actuators using the most common single-layer theories namely, classical laminated plate, first-order and third-order shear deformation theories. Ghosh and Batra [8] used piezoelectric layers to control the geometric shape of a symmetric laminated plate based on the first-order shear deformation theory. Shape control of non-symmetric piezolaminated beam was presented by Eisenberger and Abramovich [9-10]. Ray *et al* [11] derived the close form solutions for the deflection of a simply supported rectangular plate with distributed piezoelectric layers attached on top and bottom surfaces of the plate under sinusoidal loading. Study on precise deflection and static shape control of the intelligent structures can be found in [12-14]. Finite element formulation for laminated composite plates with distributed sensors and actuators has been presented in a few publications [15-22] alongside with Benjeddou [23] who performed an investigation about advances in piezoelectric finite element modeling. Edery-Azulay and Abromovich [24] investigated the actuation and sensing mechanism of a shear piezoelectric layer embedded in composite laminated beams. They derived a close form solution based on the first-order shear deformation theory for the static deflection of a laminated beam with embedded piezoelectric layers as continuous or distributed patches. Suleman and Venkayya [25] applied classical laminated plate theory and variational principles to present a finite element formulation for laminated plate with piezoelectric layers. Ray *et al* [26] extended the application of finite element method in smart structures by considering higher-order shear deformation theory to develop the static deflection of laminated composite rectangular plate with PVDF layers. Donthireddy *et al* [27] used piezo-laminated beam for shape control of the beam under static loading.

Benjeddou *et al* [28] obtained the exact solutions for the free vibration of laminated composite plate with bonded piezoelectric layers on top and bottom using first-order shear deformation theory. Thirupathi *et al* [29] used a quad-lateral piezo-laminated shell element with eight nodes to model static deflection of turbine blades. Waisman and Abramovich [30-31] used piezoelectric actuators to alter the stiffness and natural frequencies of a composite laminated beam and investigated the effect of length and location of actuator patches on the natural frequencies in a procedure called active stiffening control. Laminated composite beams with piezoelectric sensors and actuators have been discussed by Clinton *et al* [32]. Also Some valuable and benchmark experimental studies on deflection of a cantilever bimorph beam has been conducted by Koconis *et al* [33].

Design of adaptive composite laminates demands a large number of parameters such as materials and geometric properties as well as loading conditions to be involved. Thus conventional design methodology leads to very long and expensive procedures which sometimes make the design infeasible. During the past few years the adaptive structures community has focused on the development of formal design methodologies and optimized methods for these novel structures. The objective function in most of the existing works in this area may be classified as: (i) maximization/ minimization of the deflection, (ii) minimization of the mass, (iii) minimization of the voltage and a very few research are also available which considered the optimization of the natural frequency of the adaptive structure as objective function. Actuator size and location are the most common design variables in all of the published works. This is due to very small

actuating force produced by the piezoelectric patches, thus this small amount of force should be arranged in an optimal way in order to be used for controlling the response of the laminated structures. It is noted that the produced actuating force is related to the thickness, size, and location of the piezoelectric patches bonded on the laminated beam.

Soares *et al* [34] applied sensitivity analysis and optimization techniques to maximize the effect of piezoelectric actuator and minimize the weight of the structure. Correia *et al* [35] presented a model to optimize the lamination schemes of the adaptive composite structures with surface bonded piezoelectric actuators. The design variables in this study were considered as layer thickness, actuator size and location of piezoelectric layers. Birman [36] presented the optimal design of a sandwich plate with embedded piezoelectric materials to minimize the transverse static deflection. In this research, the optimization variables are the ratios of the cross-sectional areas of the piezoelectric patches in each direction to their respective spacing. Bruant *et al* [37] developed a model to determine the optimal location of piezoelectric actuator by minimizing the mechanical energy of the system and sensor location by maximizing the energy of the state output. Carlos *et al* [38] presented a finite element model based on the higher-order shear displacement field to the optimal design of laminated composite plate structures. The objective of optimization in this work was the determination of the optimum location of the piezoelectric actuators in order to maximize their efficiency for static deformation. Yan and Yam [39] considered the bending moment induced by piezoelectric patch actuators as objective function to investigate the optimal thickness and embedded depth of piezoelectric in order to maximize piezoelectric actuating force in active vibration

control. Barboni *et al* [40] modeled the bending moment produced by single actuators by means of the pin-force model and optimized size and position of the actuators using an analytical method. Batra and Geng [41] studied the transient elastic deformations of a plate with piezoceramic element bonded to the top and bottom surfaces and analyzed the effect of the shape and size of the piezoceramic actuators on the increasing the buckling load of the plate. Correia *et al* [42] found the optimal location of the integrated piezoelectric actuators and also fiber orientation angles to maximize the buckling load of the adaptive plate structures. Baz and Poh [43] solved the problem of location optimization of a pre-selected actuator size. They used beam finite elements to model a cantilever beam and included the mass and the stiffness of the actuator in the model. Aldraihem [44] optimized the size and location of single or two pairs of actuators based on the beam modal cost and controllability index. Suleman and Goncalves [45] used physical programming to perform multi-objective optimization of an adaptive composite beam with piezoelectric actuators bonded to its surface to find optimal size and placement of the actuators pairs, in order to maximize the performance of their actuation power, to minimize the mass of the piezoelectric material and to maintain required actuation voltage below maximum operating values. Optimization techniques using the software MATLAB was explained by Venkataraman [46] alongside with useful information about different techniques available for this purpose. For other advances in optimization of smart structures one may consult the survey done by Frecker [47] who reviewed the most recent publications in this subject.

As it can be realized, the field of adaptive laminated composite structures is new and

although extensive research study has been conducted to formulate the mechanics of the system, not much research has been focused on the sensitivity and design optimization aspects of these emerging structures. Also the effect of shear deformation on the response of the adaptive laminated composite has not received appropriate attention. The main aim of this study is two folds: 1- To develop an efficient finite element model of the adaptive laminated beam with and without consideration of shear deformation to predict the response of the beam under various static and dynamic (impact) loading and boundary conditions and to investigate the effect of shear deformation and sensitivity of the response under the variation of different parameters. 2- To formulate the relevant design optimization road map and develop efficient optimization algorithm to find the optimal adaptive laminated beam used for different applications.

1.6 Thesis Organization

In the present chapter, a brief introduction explaining the general goals and important description along with literature survey are presented.

In the second chapter, a finite element model for predicting the behavior of a laminated composite beam based on the classical lamination theory (CLPT) as well as the first order shear deformation theory (FSDT) is developed. After validating the finite element model by comparing the results with available exact solutions, the model is used to investigate the static and dynamic response of the beam to various applied load conditions. Effect of each mode of vibration on the general response of the beam to an impact loading is

analyzed using both theories. Later, the theories are compared in predicting the deflections as well as natural frequencies and the limits in which the CLPT can be used with an acceptable accuracy are obtained.

Third chapter deals with the development of the finite element model to incorporate the effect of surface bonded piezoelectric actuators. After making sure of validity of the model, it is employed to investigate the effect of active stiffening (the procedure in which, the actuators are used to stretch the beam, instead of bending it) on elements of dynamic response of the beam such as amplitude and damping characteristic. Subsequently, the effect of the location and length of actuators on the alteration of the first three natural frequencies of the beam has been thoroughly investigated.

Optimization of piezo-laminated beams using powerful Sequential Programming techniques implemented in MATLAB environment is the main core of chapter four. First, the shape of a beam structure is controlled by minimizing the mean-square error between the actual and the desired shape of the beam as the objective function where the appropriate applied voltages to each pair of piezoelectric actuators are found as variables. Then, overall weight of the structure is minimized by changing the thicknesses of the composite layers and actuators as variables where different constraints are applied. In this set of examples, optimization takes place under static and dynamic loading and actuators are used to create bending or active stiffening depending on the nature of the problem. At the end, two interesting possible application of a piezo-laminated beam in precise position controlling which are controlling the point that a laser beam points on a target

wall and the angle of a reflection mirror, are discussed. The optimization techniques are used to find the appropriate voltages to achieve these purposes. Final discussions and conclusions will be presented in the last chapter.

2 Laminated composite beam

2.1 Introduction

Composite materials are materials formed by combining two or more materials such that the results posses improved engineering properties than conventional ones. Strength, stiffness, weight reduction, corrosion resistance, thermal properties, fatigue life, noise and vibration suppression are among these properties.

Most of the man-made composite materials are made from a reinforced material called fiber and base material called matrix which can both be made of either metallic or non-metallic materials. Fibrous composites are made from fibers of a material in matrix material of another where as in particulate composites; the role of fibers is played by macrosize particles. Laminated composites which are made of layers of different materials, including particulate and fibrous composites, are another popular form of composites.

The strength and stiffness of a fibrous composite material is usually being dictated by those of fibers which are stiffer and stronger than the same material in bulk form. The matrix material, not only protects fiber from environmental damages, but most importantly acts as a load-transfer medium between fibers while keeping them together.

A fundamental building block of a composite material is a ply or lamina. It is made of many fibers embedded in a matrix material. By stacking a set of lamina in different

angles and directions and bond them with usually the same material used as matrix, a laminate is created. Using highly directional properties of the plies, mechanical properties of the laminated composite materials can be tailored. Hence one can design and produce laminates which are perfectly customized for the specific use in the structures. This is one of the most important advantages of the laminated composite materials to the common materials such as steel [3].

2.1.1 Constitutive equations of a lamina

Based on the generalized Hook's law, assuming that the lamina is continuum and behaves as a linear elastic material (the first assumption neglects any fiber breakage and fiber-matrix de-bonding which require micromechanics approach and the second assumption states that the generalized Hook's law is valid), the stress-strain and strain-stress relations when the coordinate planes are chosen parallel to the three orthogonal planes of material symmetry (principal coordinate system), can be written as [3]:

$$\begin{Bmatrix} \sigma_{11} \\ \sigma_{22} \\ \sigma_{33} \\ \sigma_{23} \\ \sigma_{13} \\ \sigma_{12} \end{Bmatrix} = \begin{bmatrix} C_{11} & C_{12} & C_{13} & 0 & 0 & 0 \\ C_{12} & C_{22} & C_{23} & 0 & 0 & 0 \\ C_{13} & C_{23} & C_{33} & 0 & 0 & 0 \\ 0 & 0 & 0 & C_{44} & 0 & 0 \\ 0 & 0 & 0 & 0 & C_{55} & 0 \\ 0 & 0 & 0 & 0 & 0 & C_{66} \end{bmatrix} \begin{Bmatrix} \varepsilon_{11} \\ \varepsilon_{22} \\ \varepsilon_{33} \\ \varepsilon_{23} \\ \varepsilon_{13} \\ \varepsilon_{12} \end{Bmatrix} \qquad \textbf{2.1-1}$$

$$\begin{Bmatrix} \varepsilon_{11} \\ \varepsilon_{22} \\ \varepsilon_{33} \\ \varepsilon_{23} \\ \varepsilon_{13} \\ \varepsilon_{12} \end{Bmatrix} = \begin{bmatrix} S_{11} & S_{12} & S_{13} & 0 & 0 & 0 \\ S_{12} & S_{22} & S_{23} & 0 & 0 & 0 \\ S_{13} & S_{23} & S_{33} & 0 & 0 & 0 \\ 0 & 0 & 0 & S_{44} & 0 & 0 \\ 0 & 0 & 0 & 0 & S_{55} & 0 \\ 0 & 0 & 0 & 0 & 0 & S_{66} \end{bmatrix} \begin{Bmatrix} \sigma_{11} \\ \sigma_{22} \\ \sigma_{33} \\ \sigma_{23} \\ \sigma_{13} \\ \sigma_{12} \end{Bmatrix} \qquad \textbf{2.1-2}$$

where σ_{ij} are the stress components, ε_{ij} are the strain components, C_{ij} are the material coefficients and S_{ij} denotes the compliance coefficients, $[S]=[C]^{-1}$.

The foregoing equations are written based on the principal material coordinate system. The coordinate system which is practically used does not usually coincide with the principal material coordinate system. Further, a laminate consists of several layers, each posses a different orientation. So in practice, these equations must be transformed to global coordinate system used to solve problems. For flat laminates, fiber-reinforced laminas are stacked in a way that their z-axis always coincides with the z-axis of the global coordinate system and x-axis (and eventually y-axis) makes an angle θ (Figure 2.1-1). By using the following equations, stresses and strains can be transformed from principal material coordinate system to global coordinate system as [3]:

$$\begin{Bmatrix} \sigma_{xx} \\ \sigma_{yy} \\ \sigma_{zz} \\ \sigma_{yz} \\ \sigma_{xz} \\ \sigma_{xy} \end{Bmatrix} = \begin{bmatrix} \cos^2\theta & \sin^2\theta & 0 & 0 & 0 & -\sin 2\theta \\ \sin^2\theta & \cos^2\theta & 0 & 0 & 0 & \sin 2\theta \\ 0 & 0 & 1 & 0 & 0 & 0 \\ 0 & 0 & 0 & \cos\theta & \sin\theta & 0 \\ 0 & 0 & 0 & -\sin\theta & \cos\theta & 0 \\ \sin\theta\cos\theta & -\sin\theta\cos\theta & 0 & 0 & 0 & \cos^2\theta-\sin^2\theta \end{bmatrix} \begin{Bmatrix} \sigma_{11} \\ \sigma_{22} \\ \sigma_{33} \\ \sigma_{23} \\ \sigma_{13} \\ \sigma_{12} \end{Bmatrix} \qquad \textbf{2.1-3}$$

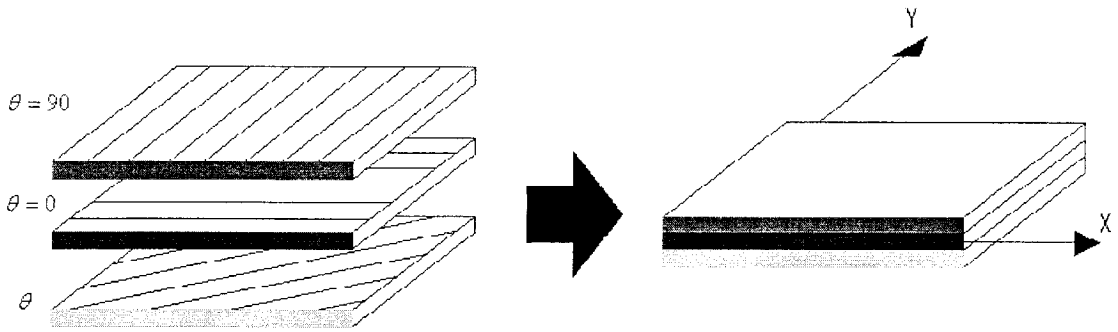

Figure 2.1-1: A laminate made up of laminae with different fiber orientations

2.1.2 Plane stress constitutive relations

Since most laminates are typically thin, the assumption of plane state of stress, in which the normal stress is negligible, gives an acceptable accuracy. For a lamina in x-y plane, σ_{zz}, is assumed to be negligible compared to σ_{xx}, σ_{yy} and σ_{xy}.

For the plane stress, and for the case in which transverse shear stresses, σ_{yz} and σ_{xz}, are also assumed to be negligible (such as assumptions made in classical lamination theory), the constitutive equation for an orthotropic lamina, may be expressed as [3]:

$$\begin{Bmatrix}\sigma_1\\ \sigma_2\\ \sigma_6\end{Bmatrix}=\begin{bmatrix}Q_{11} & Q_{12} & 0\\ Q_{12} & Q_{22} & 0\\ 0 & 0 & Q_{66}\end{bmatrix}\begin{Bmatrix}\varepsilon_1\\ \varepsilon_2\\ \varepsilon_6\end{Bmatrix} \qquad \textbf{2.1-4}$$

However, considering the effect of transverse shear stresses (such as the first-order shear deformation theory) leads to an additional equation to state the transverse shear effects:

$$\begin{Bmatrix}\sigma_4\\ \sigma_5\end{Bmatrix}=\begin{bmatrix}Q_{44} & 0\\ 0 & Q_{55}\end{bmatrix}\begin{Bmatrix}\varepsilon_4\\ \varepsilon_5\end{Bmatrix} \qquad \textbf{2.1-5}$$

where $Q_{ij}^{(k)}$ are the plane stress-reduced stiffness, calculated as follows:

$$Q_{11}=\frac{E_1}{1-\nu_{12}\nu_{21}};Q_{12}=\frac{\nu_{12}E_2}{1-\nu_{12}\nu_{21}};Q_{22}=\frac{E_2}{1-\nu_{12}\nu_{21}} \qquad \textbf{2.1-6}$$
$$Q_{66}=G_{12};Q_{44}=G_{23};Q_{55}=G_{13}$$

where E_1 and E_2 are the young's moduli in fiber and transverse direction, G_{12}, G_{23} and G_{13} are the shear moduli in the 1-2, 2-3 and 1-3 planes, respectively and ν_{ij} is poison ratio, defined as ratio of transverse strain in the jth direction to the axial strain in the ith direction, when stresses in the i-direction. The transformed stress-strain relations of an orthotropic lamina can be written as [3]:

$$\begin{Bmatrix}\sigma_{xx}\\ \sigma_{yy}\\ \sigma_{xy}\end{Bmatrix}=\begin{bmatrix}\overline{Q}_{11} & \overline{Q}_{12} & \overline{Q}_{16}\\ \overline{Q}_{12} & \overline{Q}_{22} & \overline{Q}_{26}\\ \overline{Q}_{16} & \overline{Q}_{26} & \overline{Q}_{66}\end{bmatrix}\begin{Bmatrix}\varepsilon_{xx}\\ \varepsilon_{yy}\\ \gamma_{xy}\end{Bmatrix} \qquad \textbf{2.1-7}$$

and

$$\begin{Bmatrix}\sigma_{yz}\\ \sigma_{xz}\end{Bmatrix}=\begin{bmatrix}\overline{Q}_{44} & \overline{Q}_{45}\\ \overline{Q}_{45} & \overline{Q}_{55}\end{bmatrix}\begin{Bmatrix}\gamma_{yz}\\ \gamma_{xz}\end{Bmatrix} \qquad \textbf{2.1-8}$$

where

$$\begin{aligned}
\overline{Q}_{11} &= Q_{11}\cos^4\theta+2(Q_{12}+2Q_{66})\sin^2\theta\cos^2\theta+Q_{22}\sin^4\theta\\
\overline{Q}_{12} &= (Q_{11}+Q_{22}-4Q_{66})\sin^2\theta\cos^2\theta+Q_{12}(\sin^4\theta+\cos^4\theta)\\
\overline{Q}_{22} &= Q_{11}\sin^4\theta+2(Q_{12}+2Q_{66})\sin^2\theta\cos^2\theta+Q_{22}\cos^4\theta\\
\overline{Q}_{16} &= (Q_{11}-Q_{12}-2Q_{66})\sin\theta\cos^3\theta+(Q_{12}-Q_{22}+2Q_{66})\sin^3\theta\cos\theta\\
\overline{Q}_{26} &= (Q_{11}-Q_{12}-2Q_{66})\sin^3\theta\cos\theta+(Q_{12}-Q_{22}+2Q_{66})\sin\theta\cos^3\theta\\
\overline{Q}_{66} &= (Q_{11}+Q_{22}-2Q_{12}-2Q_{66})\sin^2\theta\cos^2\theta+Q_{66}(\sin^4\theta+\cos^4\theta)\\
\overline{Q}_{44} &= Q_{44}\cos^2\theta+Q_{55}\sin^2\theta\\
\overline{Q}_{44} &= (Q_{55}-Q_{44})\cos\theta\sin\theta\\
\overline{Q}_{55} &= Q_{55}\cos^2\theta+Q_{44}\sin^2\theta
\end{aligned} \qquad \textbf{2.1-9}$$

2.1.3 One dimensional analysis of laminated plates

There are two types of laminated plates that can be treated as one-dimensional problem, laminated beam and cylindrical bending of laminated plate strips. When the width (length along y-axis) of a laminated plate is very small compared to the length along the x-axis, it is treated as a laminated beam. In cylindrical bending the laminated plate is assumed to be a plate strip that is very long along the y-axis and has a finite dimension along x-axis. Assuming the transverse load to be uniform at any section parallel to the x-axis, the deflection w_0 and displacement (u_0, v_0) of the plate are functions of only x, and all derivatives with respect to y are zero. The cylindrical bending problem is a plane strain problem, whereas the laminated beam problem is a plane stress problem.

2.2 Laminated composite beam based on the CLPT

2.2.1 Introduction

The classical lamination theory is based on the Kirchhoff hypothesis. In other words, it assumes, 1) The straight lines perpendicular to the mid-surface before deformation remain straight after deformation, 2) The transverse normals do not experience elongation and 3) The transverse normals rotate such that they remain perpendicular to the mid-surface after deformation. Assumptions one and two indicate that the transverse displacement is independent of the transverse coordinate and the transverse normal strain ε_{zz} is zero. The third assumption forces the transverse shear strains, namely ε_{xz} and ε_{yz}, to be zero. The undeformed and deformed geometries of a beam element based on the CLPT are shown in Figure 2.2-1. According to the Kirchhoff hypothesis, displacements (u,w) can be stated as [3,7]:

$$u(x,z,t) = u_0(x,t) + z\frac{\partial w_0}{\partial x} \qquad \textbf{2.2-1}$$
$$w(x,z,t) = w_0(x,t)$$

where t is the time and (u_0, w_0) are the displacements along the coordinate lines of a material point on the mid-plane (xy-plane), as shown in Figure 2.2-1.

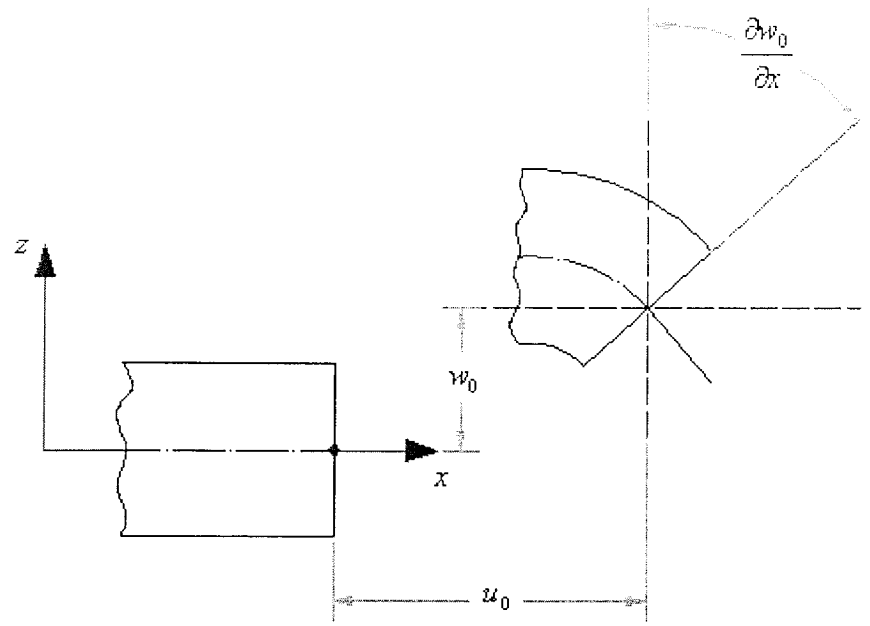

Figure 2.2-1: Undeformed and deformed geometries of a beam element based on CLPT

2.2.2 Equation of motion for Classical beam

Classical laminated beam theory states that the transverse shear stresses through the thickness of the laminate are negligible and further, the normal to the middle plane remains normal after deformation. Hence, the rotation of the mid-plane about y-axis (clockwise positive) can be written as [3]:

$$\phi_x = \frac{\partial w}{\partial x} \qquad \textbf{2.2-2}$$

where w and ϕ_x denote the deformation in the thickness direction and the rotation about y-axis respectively. The equation of motion of a beam based on classical theory is represented by:

$$\frac{\partial^2 M_x}{\partial x^2} + N_x^i \frac{\partial^2 w}{\partial x^2} + q(x) = I_0 \frac{\partial^2 w}{\partial t^2} - I_2 \frac{\partial^4 w}{\partial x^2 \partial t^2} \qquad \textbf{2.2-3}$$

where N_x^i denotes the initial axial force along x-axis, $q(x)$ denotes the distributed transverse load on the beam represented as:

$$q(x) = bq_0 \quad , \quad N_x^i(x) = bN_0 \qquad \textbf{2.2-4}$$

Here, b is the width of the beam, N_0 and q_0 are axial force and uniform transverse load (N/m^2), respectively.

M_x denotes the bending moment about the y-axis. Considering the beam element as a plate strip in cylindrical bending, M_x is given by:

$$M_x = bB_{11} \frac{\partial u_o}{\partial x} - bD_{11} \frac{\partial^2 w}{\partial x^2} \qquad \textbf{2.2-5}$$

Where u_0 is the deformation of the reference point in the mid-plane in x direction. B_{11} and D_{11} represent the coefficients of coupling stiffness and bending stiffness matrices, respectively and can be calculated as follows [3]:

$$(B_{ij}, D_{ij}) = \int_{-\frac{h}{2}}^{\frac{h}{2}} \overline{Q}_{ij}(z, z^2) dz = \sum_{k=1}^{N} \int_{z_k}^{z_{k+1}} \overline{Q}_{ij}^{(k)}(z, z^2) dz \qquad \textbf{2.2-6}$$

In the case of mid-plane symmetric laminated beams, as shown in Figure 2.2-2, $B_{11} = 0$ and Equation 2.2-5 reduces to the following equation:

$$M_x = -bD_{11} \frac{\partial^2 w}{\partial x^2} \qquad \textbf{2.2-7}$$

The terms I_0 and I_2 represents the mass and rotary inertias of the beam respectively and are defined as:

$$I_0, I_2 = \int_{-\frac{h}{2}}^{\frac{h}{2}} b\rho(1, z^2)dz \qquad \textbf{2.2-8}$$

where ρ is the density and, *-h/2* and *h/2* are the height of the upper and lower surfaces of the beam with respect to the mid-plane, respectively and z denotes the axis along the laminate thickness.

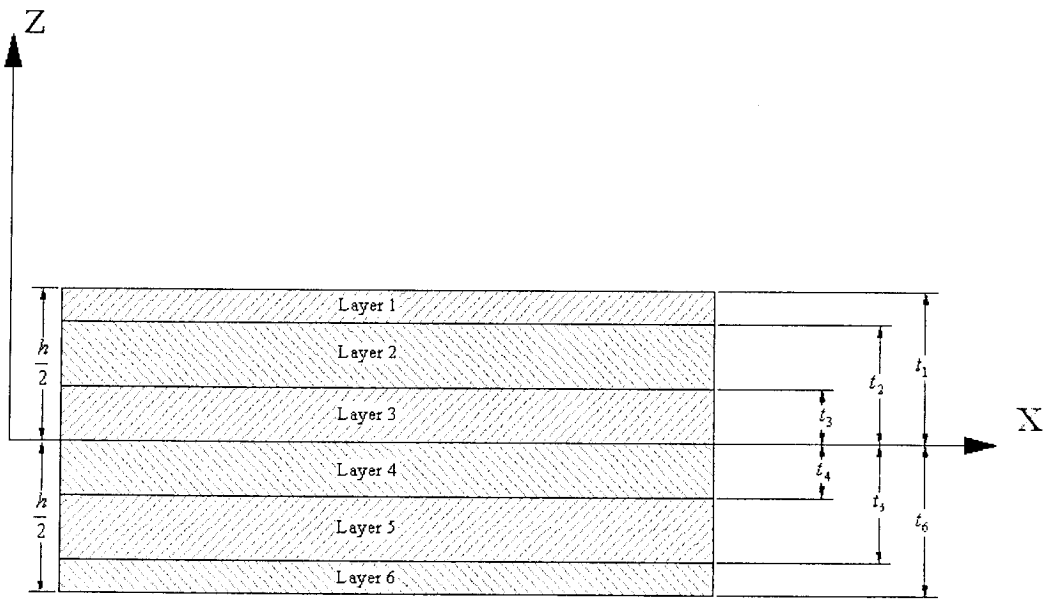

Figure 2.2-2: A symmetric laminate

Combining Equations 2.2-3 and 2.2-7, the Equation of motion for a laminated beam is obtained, in term of w, as follows:

$$\frac{\partial^2}{\partial x^2}\left(bD_{11}\frac{\partial^2 w}{\partial x^2}\right) - N_x^i\frac{\partial^2 w}{\partial x^2} - q(x) + I_0\frac{\partial^2 w}{\partial t^2} - I_2\frac{\partial^4 w}{\partial x^2 \partial t^2} = 0 \qquad \textbf{2.2-9}$$

2.2.3 Weak form of the governing equations

A typical element is isolated from the domain as shown in Figure 2.2-3 and its structural behavior is modeled. The weak form of the governing Equation 2.2-9 is used to construct the finite element model. In the weak form, w and ϕ, that are respectively the deflection and rotation as shown in Figure 2.2-3 are the primary variables. Q_i $(i = 1, 2, 3, 4)$ represent secondary variables corresponding to the primary variables. To construct the weak form of Equation 2.2-9, a function v is chosen as the weight function.

Multiplying Equation 2.2-9 by weight function v, and integrating the equation over the element, one may obtain [3]:

$$\int_0^l \left[v\frac{d^2}{dx^2}\left(bD_{11}\frac{\partial^2 w}{\partial x^2}\right) - vN_x^i\frac{\partial^2 w}{\partial x^2} - vq(x) + vI_0\frac{\partial^2 w}{\partial t^2} - vI_2\frac{\partial^4 w}{\partial x^2 \partial t^2}\right] dx = 0 \qquad \textbf{2.2-10}$$

Integrating the first term of Equation 2.2-10 by parts twice and the second term once, the weak form is obtained as follows:

$$\int_0^l \left(bD_{11}\frac{d^2 v}{dx^2}\frac{\partial^2 w}{\partial x^2} + N_x^i\frac{dv}{dx}\frac{\partial w}{\partial x} - vq(x) + vI_0\frac{\partial^2 w}{\partial t^2} + I_2\frac{\partial v}{\partial x}\frac{\partial^3 w}{\partial x \partial t^2}\right) dx$$
$$- Q_1^e v(0) - Q_3^e v(l) - Q_2^e\left(-\frac{dv}{dx}\right)_{x=0} - Q_4^e\left(-\frac{dv}{dx}\right)_{x=l} \qquad \textbf{2.2-11}$$

where

$$Q_1^e = \left[\frac{\partial}{\partial x}\left(bD_{11}\frac{\partial^2 w}{\partial x^2} - I_2\frac{\partial^2 w}{\partial t^2}\right) - N_x^i\frac{\partial w}{\partial x}\right]_{x=0} \qquad \textbf{2.2-12}$$

$$Q_3^e = -\left[\frac{\partial}{\partial x}\left(bD_{11}\frac{\partial^2 w}{\partial x^2} - I_2\frac{\partial^2 w}{\partial t^2}\right) - N_x^i\frac{\partial w}{\partial x}\right]_{x=l} \qquad \textbf{2.2-13}$$

$$Q_2^e = \left(bD_{11}\frac{\partial^2 w}{\partial x^2}\right)_{x=0} \qquad \textbf{2.2-14}$$

$$Q_4^e = -\left(bD_{11}\frac{\partial^2 w}{\partial x^2}\right)_{x=l} \qquad \textbf{2.2-15}$$

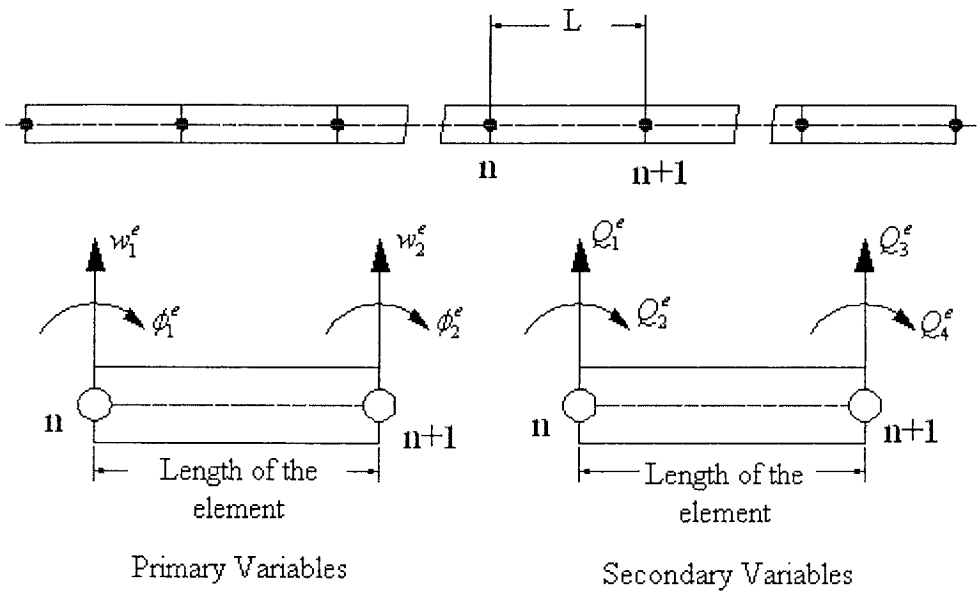

Figure 2.2-3: Domain, finite element subdivision, and typical finite element

Since, deflection, w, and slope ϕ_x, must be continuous everywhere in the domain, they should be continuous at each and every interface between two elements. The deflection w and slope, ϕ_x, at nodes 1 and 2 are given as:

$$w^e(0,t) = w_1^e$$

$$w^e(l,t) = w_3^e$$

$$\phi(0,t) = -\left.\frac{dw^e}{dx}\right|_{x=0} = w_2^e \qquad \textbf{2.2-16}$$

$$\phi(l,t) = -\left.\frac{dw^e}{dx}\right|_{x=l} = w_4^e$$

Since there are four boundary conditions per element, a fourth-order polynomial is required as:

$$w^e(x,t) = c_1^e + c_2^e x + c_3^e x^2 + c_4^e x^3 \qquad \textbf{2.2-17}$$

Using the boundary conditions stated in Equation 2.2-16:

$$w_1^e = c_1^e;\ w_2^e = -c_2^e;\ w_3^e = c_1^e + c_2^e l + c_3^e l^2 + c_4^e l^3;\ w_4^e = -c_2^e - 2c_3^e l - 3c_4^e l^2 \qquad \textbf{2.2-18}$$

Rewriting Equation 2.2-18 in matrix form, following matrix equation is obtained

$$\begin{Bmatrix} w_1^e \\ w_2^e \\ w_3^e \\ w_4^e \end{Bmatrix} = \begin{bmatrix} 1 & 0 & 0 & 0 \\ 0 & -1 & 0 & 0 \\ 1 & l & l^2 & l^3 \\ 0 & -1 & -2l & -3l^2 \end{bmatrix} \begin{Bmatrix} c_1^e \\ c_2^e \\ c_3^e \\ c_4^e \end{Bmatrix} \qquad \textbf{2.2-19}$$

Finding c_1^e to c_4^e from the Equation 2.2-19 and substituting them in Equation 2.2-17 yields:

$$w(x,t) \approx w^e(x,t) = w_1^e \varphi_1 + w_2^e \varphi_2 + w_3^e \varphi_3 + w_4^e \varphi_4 \qquad \textbf{2.2-20}$$

where $\varphi_1, \varphi_2, \varphi_3$ and φ_4 are shape functions defined as:

$$\varphi_1^e = 1 - 3\left(\frac{x}{l}\right)^2 + 2\left(\frac{x}{l}\right)^3 \quad ; \qquad \varphi_2^e = -x + 2x\left(\frac{x}{l}\right) - x\left(\frac{x}{l}\right)^2$$

$$\varphi_3^e = 3\left(\frac{x}{l}\right)^2 - 2\left(\frac{x}{l}\right)^3 \quad ; \qquad \varphi_4^e = x\left(\frac{x}{l}\right) - x\left(\frac{x}{l}\right)^2 \qquad \textbf{2.2-21}$$

Now substituting w from Equation 2.2-20 into Equation 2.2-11 and considering weight function v as φ_1, φ_2, φ_3 and φ_4, the i^{th} equation may be written as:

$$\sum_{j=1}^{4}\int_0^l \left[\left(bD_{11}\frac{d^2\varphi_i}{dx^2}\frac{d^2\varphi_j}{dx^2} + N_x^i\frac{d\varphi_i}{dx}\frac{d\varphi_j}{dx}\right)w_j^e + \left(I_0\varphi_i\varphi_j + I_2\frac{d\varphi_i}{dx}\frac{d\varphi_j}{dx}\right)\frac{d^2w_j^e}{dt^2} - \varphi_i q(x)\right]dx$$
$$- Q_1^e\varphi_i(0) - Q_3^e\varphi_i(l) - Q_2^e\left(-\frac{d\varphi_i}{dx}\right)_{x=0} - Q_4^e\left(-\frac{d\varphi_i}{dx}\right)_{x=l} = 0 \qquad \textbf{2.2-22}$$

For the sake of simplicity, the following expressions are introduced:

$$K_{ij}^e = \int_0^l bD_{11}\frac{d^2\varphi_i}{dx^2}\frac{d^2\varphi_j}{dx^2}dx \qquad \textbf{2.2-23}$$

$$G_{ij}^e = \int_0^l N_x^i\frac{d\varphi_i}{dx}\frac{d\varphi_j}{dx}dx \qquad \textbf{2.2-24}$$

$$M_{ij}^e = \int_0^l \left(I_0\varphi_i\varphi_j + I_2\frac{d\varphi_i}{dx}\frac{d\varphi_i}{dx}\right)dx \qquad \textbf{2.2-25}$$

$$q_i^e = \int_0^l \varphi_i q(x)dx \qquad \textbf{2.2-26}$$

$$F_i^e = q_i^e + Q_1^e\varphi_i(0) + Q_3^e\varphi_i(l) + Q_2^e\left(-\frac{d\varphi_i}{dx}\right)_{x=0} + Q_4^e\left(-\frac{d\varphi_i}{dx}\right)_{x=l} \qquad \textbf{2.2-27}$$

Now considering Equations 2.2-23 to 2.2-27, Equation

2.2-22 may be rewritten as:

$$\sum_{j=1}^{4}\left[\left(K_{ij}^{e}+G_{ij}^{e}\right)w_{j}^{e}+M_{ij}^{e}\frac{d^{2}w_{j}^{e}}{dt^{2}}\right]-F_{i}^{e}=0 \qquad \textbf{2.2-28}$$

Finally putting Equation 2.2-28 into matrix form will yield:

$$[M]^{e}\{\ddot{w}\}^{e}+\left([K]^{e}+[G]^{e}\right)\{w\}^{e}=\{F\}^{e} \qquad \textbf{2.2-29}$$

where $[K]^{e}$,$[G]^{e}$ and $[M]^{e}$ represent element's stiffness, geometric stiffness and mass matrices respectively, and $\{F\}^{e}$ is the external force vector.

For a uniform thickness beam, the aforementioned matrices can be derived as:

$$[K]^{e}=\frac{2bD_{11}}{l^{3}}\begin{bmatrix}6 & -3l & -6 & -3l\\ & 2l^{2} & 3l & l^{2}\\ & & 6 & 3l\\ sym & & & 2l^{2}\end{bmatrix} \qquad \textbf{2.2-30}$$

$$[M]^{e}=\frac{bl\rho h}{420}\begin{bmatrix}156 & -22l & 54 & 13l\\ & 4l^{2} & -13l & -3l^{2}\\ & & 156 & 22l\\ sym & & & 4l^{2}\end{bmatrix}+\frac{I_{2}}{30l}\begin{bmatrix}36 & -3l & -36 & -3l\\ & 4l^{2} & 3l & -l^{2}\\ & & 36 & 3l\\ sym & & & 4l^{2}\end{bmatrix} \qquad \textbf{2.2-31}$$

$$[G]^{e}=\frac{bN_{x}^{i}}{30l}\begin{bmatrix}36 & -3l & -36 & -3l\\ & 4l^{2} & 3l & -l^{2}\\ & & 36 & 3l\\ sym & & & 4l^{2}\end{bmatrix} \qquad \textbf{2.2-32}$$

where l and h are the length and height of the beam respectively

Equation 2.2-29 is the governing dynamic equation for an element. After proper assembling, the finite element formulation for the whole system can be described as:

$$[M]\{\ddot{w}\}+([K]+[G])\{w\}=\{F\} \qquad \textbf{2.2-33}$$

It should be noted that using Equation 2.2-33, one can perform static, dynamic, buckling and frequency analysis which will be elaborated later in Section 2.4.

2.3 Laminated composite beam based on the FSDT

2.3.1 Introduction

The classical laminated plate theory (CLPT), can predict, with an acceptable precision, the mechanical behavior of thin laminate. In the case of thick laminate (ratio of the length to thickness approximately less than 10), the results obtained using the CLPT shows significant difference with those in reality. In the composite materials, the effect of shear deformation is also accentuated by the relatively large ratio of Young's modulus in fiber direction to the in-plane shear modulus [3].

The first-order shear deformation theory (FSDT), improves the classical laminated plate theory (CLPT) by introducing the effects of transverse shear deformation. The basic assumptions here are similar to the CLPT except that the transverse normal does not remain perpendicular to the mid-surface after deformation. Figure 2.3-1 illustrates the rotation of the cross-section in a beam element. The displacement field of the first-order theory is as follows:

$$\begin{aligned} u(x,z,t) &= u_0(x,t) + z\phi_x(x,t) \\ w(x,z,t) &= w_0(x,t) \end{aligned} \qquad \textbf{2.3-1}$$

where (u_0, w_0) are the displacements of a point on the mid plane z = 0, ϕ_x is the rotations of transverse normal about the y axis. It must be noted that in this theory, value of ϕ_x is different from $\frac{\partial w}{\partial x}$ due to the effects of the shear deformation. Eventually the transverse shear strain will be $\gamma = \phi_x - \frac{\partial w}{\partial x}$.

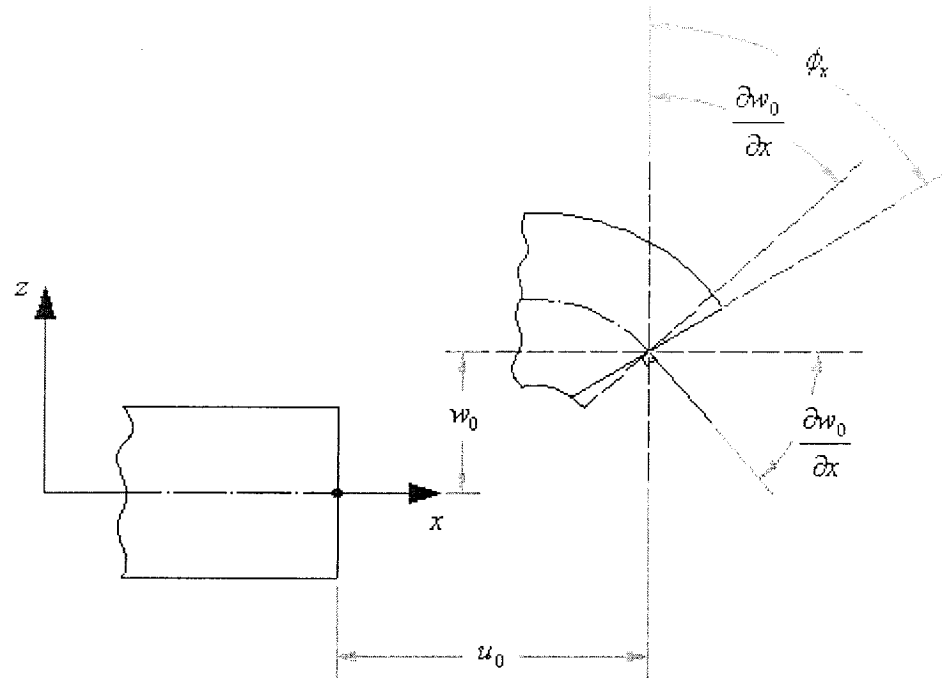

Figure 2.3-1. Undeformed and deformed geometries of a beam element based on the FSDT

2.3.2 Equation of motion for a beam based on the FSDT

The basic equations for mid-plane symmetric composite beams are given as [3]:

$$\frac{\partial Q_x}{\partial x} + N_x^i \frac{\partial^2 w}{\partial x^2} + q(x) = I_0 \frac{\partial^2 w}{\partial t^2} \qquad \textbf{2.3-2}$$

$$\frac{\partial M_x}{\partial x} - Q_x = I_2 \frac{\partial^2 \phi}{\partial t^2} \qquad \textbf{2.3-3}$$

where Q_x denotes the transverse shear force described as:

$$Q_x = b\mu F_{55}\left(\frac{\partial w}{\partial x} + \phi\right) \qquad \textbf{2.3-4}$$

and F_{55} is given by:

$$F_{55} = \sum_{k=1}^{n} (h_k - h_{k-1})(\overline{C}_{55})_k = \sum_{k=1}^{n} (t_k)(\overline{C}_{55})_k \qquad \textbf{2.3-5}$$

In Equation 2.3-5, n represents the total number of plies in the laminate, t_k the thickness of individual ply, h_k and h_{k-1} are the distances to the upper and lower surfaces of k^{th} ply from the mid-plane and b is the width of the beam and $\overline{C}_{55}$ is computed using the following relation:

$$\overline{C}_{55} = C_{44}\sin^2(\theta) + C_{55}\cos^2(\theta) \qquad \textbf{2.3-6}$$

where θ is the angle between fiber orientation and the reference axis and the values of C_{44} and C_{55} are given by:

$$C_{44} = G_{23} \quad ; \quad C_{55} = G_{13} \qquad \textbf{2.3-7}$$

in which G_{13} and G_{23} are the shear modulus in relevant planes.

The coefficient μ is the shear correction factor and it is considered in the formulations to compensate the difference between actual stress state and the constant stress state predicted by the first-order shear deformation theory. I_0 and I_2 are the mass and rotary inertias, respectively, given by Equation 2.2-8.

The bending moment is given by:

$$M_x = bD_{11}\frac{\partial \phi}{\partial x} \qquad \textbf{2.3-8}$$

Substituting Equations 2.3-4 and 2.3-8 into Equations 2.3-2 and 2.3-3 respectively, the governing differential equations for mid-plane symmetric laminated beams based on the

FSDT model are obtained as follows:

$$b\mu F_{55}\left(\frac{\partial^2 w}{\partial x^2}+\frac{\partial \phi}{\partial x}\right)+N_x^i\frac{\partial^2 w}{\partial x^2}+q(x)-I_0\frac{\partial^2 w}{\partial t^2}=0 \qquad \textbf{2.3-9}$$

$$bD_{11}\frac{\partial^2 \phi}{\partial x^2}-b\mu F_{55}\left(\frac{\partial w}{\partial x}+\phi\right)-I_2\frac{\partial^2 \phi}{\partial t^2}=0 \qquad \textbf{2.3-10}$$

2.3.3 Weak form of the governing equations

To construct the weak forms of equations, two weight functions, v_1 and v_2 are introduced. Multiplying Equation 2.3-9 and 2.3-10 by v_1 and v_2 respectively and integrating by parts of the first and second terms results in the following equations:

$$\int_0^l\left[b\mu F_{55}\frac{dv_1}{dx}\left(\frac{\partial w}{\partial x}+\phi\right)+N_x^i\frac{dv_1}{dx}\frac{\partial w}{\partial x}-v_1 q(x)+v_1 I_0\frac{\partial^2 w}{\partial t^2}\right]dx \qquad \textbf{2.3-11}$$
$$-v_1 Q_1^e(0)-v_1 Q_3^e(l)=0$$

$$\int_0^l\left[bD_{11}\frac{dv_2}{dx}\frac{\partial \phi}{\partial x}+v_2 b\mu F_{55}\left(\frac{\partial w}{\partial x}+\phi\right)+v_2 I_2\frac{\partial^2 \phi}{\partial t^2}\right]dx-v_2 Q_2^e(0)-v_2 Q_4^e(l)=0 \qquad \textbf{2.3-12}$$

where:

$$Q_1^e=-\left[b\mu F_{55}\left(\frac{\partial w}{\partial x}+\phi\right)+N_x^i\frac{\partial w}{\partial x}\right]_{x=0} \qquad \textbf{2.3-13}$$

$$Q_3^e=\left[b\mu F_{55}\left(\frac{\partial w}{\partial x}+\phi\right)+N_x^i\frac{\partial w}{\partial x}\right]_{x=l} \qquad \textbf{2.3-14}$$

$$Q_2^e=-\left[bD_{11}\frac{\partial \phi}{\partial x}\right]_{x=0} \qquad \textbf{2.3-15}$$

$$Q_4^e = \left[bD_{11} \frac{\partial \phi}{\partial x} \right]_{x=l} \qquad \textbf{2.3-16}$$

2.3.4 Generation of the finite element model

Considering primary variables at the end nodes as:

$$w(0) = w_1^e \quad w(l) = w_2^e \quad \phi(0) = \phi_1^e \qquad \phi(l) = \phi_2^e \qquad \textbf{2.3-17}$$

Assuming a linear approximation for displacement and the cross-section rotation, it can be written:

$$w = a_1 + a_2 x \quad ; \quad \phi = b_1 + b_2 x \qquad \textbf{2.3-18}$$

Applying boundary conditions in Equations 2.3-18 one can obtain:

$$w_1^e = a_1, \qquad w_2^e = a_1 + a_2 l \qquad \textbf{2.3-19}$$

$$\phi_1^e = b_1, \qquad \phi_2^e = b_1 + b_2 l \qquad \textbf{2.3-20}$$

Solving Equations 2.3-19 and 2.3-20 the variables a_1, a_2, b_1 and b_2 are determined as:

$$a_1 = w_1^e, \qquad a_2 = \frac{w_2^e - w_1^e}{l} \qquad \textbf{2.3-21}$$

$$b_1 = \phi_1^e, \qquad b_2 = \frac{\phi_2^e - \phi_1^e}{l} \qquad \textbf{2.3-22}$$

Now substituting back a_1, a_2, b_1 and b_2 into the displacement and rotation functions, Equation 2.3-18, the following shape functions can be easily identified:

$$S_1 = 1 - \frac{x}{l} \quad ; \quad S_2 = \frac{x}{l} \qquad \textbf{2.3-23}$$

$$\varphi_1 = 1 - \frac{x}{l} \quad ; \quad \varphi_2 = \frac{x}{l} \qquad \textbf{2.3-24}$$

Now, considering $v_1 = S_i$ and $v_2 = \varphi_i$ (for $i = 1,2$) in Equation 2.3-11 and 2.3-12, the following equations may be derived:

$$\int_0^l \left[b\mu F_{55} \frac{dS_i}{dx} \left(\sum_{j=1}^{2} \frac{dS_j}{dx} w_j + \varphi_j \phi_j \right) + N_x^i \frac{dS_i}{dx} \left(\sum_{j=1}^{2} \frac{dS_j}{dx} w_j \right) - S_i q(x) + S_i I_0 \left(\sum_{j=1}^{2} S_j \frac{d^2 w_j}{dt^2} \right) \right] dx$$
$$- S_i Q_1^e(0) - S_i Q_3^e(l) = 0$$

2.3-25

$$\int_0^l \left[bD_{11} \frac{d\varphi_i}{dx} \left(\sum_{j=1}^{2} \frac{d\varphi_j}{dx} \phi_j \right) + b\mu F_{55} \varphi_i \left(\sum_{j=1}^{2} \frac{dS_j}{dx} w_j + \varphi_j \phi_j \right) + \varphi_i I_2 \left(\sum_{j=1}^{2} \varphi_j \frac{d^2 \phi_j}{dt^2} \right) \right] dx$$
$$- \varphi_i Q_2^e(0) - \varphi_i Q_4^e(l) = 0$$

2.3-26

The following notations will be introduced:

$$K_{ij}^{11} = \int_0^l b\mu F_{55} \frac{dS_i}{dx} \frac{dS_j}{dx} dx$$ **2.3-27**

$$K_{ij}^{12} = \int_0^l b\mu F_{55} \frac{dS_i}{dx} \varphi_j dx$$ **2.3-28**

$$K_{ij}^{22} = \int_0^l \left[bD_{11} \frac{d\varphi_i}{dx} \frac{d\varphi_j}{dx} + b\mu F_{55} \varphi_i \varphi_j \right] dx$$ **2.3-29**

$$G_{ij} = \int_0^l bN_x^i \frac{dS_i}{dx} \frac{dS_j}{dx} dx$$ **2.3-30**

$$M_{ij}^{11} = \int_0^l I_0 S_i S_j dx$$ **2.3-31**

$$M_{ij}^{22} = \int_0^l I_2 \varphi_i \varphi_j dx$$ **2.3-32**

$$F_i^1 = \int_0^l S_i q(x)dx + S_i Q_1^e(0) + S_i Q_3^e(l) \qquad \textbf{2.3-33}$$

$$F_i^2 = \varphi_i Q_2^e(0) + \varphi_i Q_4^e(l) \qquad \textbf{2.3-34}$$

Now considering Equations 2.3-27 - 2.3-34, Equations 2.3-25 and 2.3-26, can be transformed to the following form:

$$\sum_{j=1}^{2}\left(K_{ij}^{11} + G_{ij}\right)w_j^e + \sum_{j=1}^{2} K_{ij}^{12}\phi_j^e + \sum_{j=1}^{2} M_{ij}^{11}\frac{d^2 w_j^e}{dt^2} - F_i^1 = 0 \qquad \textbf{2.3-35}$$

$$\sum_{j=1}^{2} K_{ij}^{21} w_j^e + \sum_{j=1}^{2} K_{ij}^{22}\phi_j^e + \sum_{j=1}^{2} M_{ij}^{22}\frac{d^2 \phi_j^e}{dt^2} - F_i^2 = 0 \qquad \textbf{2.3-36}$$

Writing Equations 2.3-35 and 2.3-36 in matrix form, the governing finite element model for a laminated composite beam based on the FSDT may be obtained as:

$$\begin{bmatrix}[M^{11}] & [0]\\ [0] & [M^{22}]\end{bmatrix}^e \begin{Bmatrix}\{\ddot{w}\}\\ \{\ddot{\phi}\}\end{Bmatrix}^e + \begin{bmatrix}[K^{11}] & [K^{12}]\\ [K^{12}]^T & [K^{22}]\end{bmatrix}^e \begin{Bmatrix}\{w\}\\ \{\phi\}\end{Bmatrix}^e + \begin{bmatrix}[G] & [0]\\ [0] & [0]\end{bmatrix}^e \begin{Bmatrix}\{w\}\\ \{\phi\}\end{Bmatrix}^e = \begin{Bmatrix}\{F^1\}\\ \{F^2\}\end{Bmatrix}^e \qquad \textbf{2.3-37}$$

Considering Equation 2.3-37, the element properties, namely the stiffness, mass and geometric stiffness are introduced by the following Equations:

$$[K]^e = \begin{bmatrix}[K^{11}] & [K^{12}]\\ [K^{12}]^T & [K^{22}]\end{bmatrix} \qquad \textbf{2.3-38}$$

$$[M]^e = \begin{bmatrix}[M^{11}] & [0]\\ [0] & [M^{22}]\end{bmatrix} \qquad \textbf{2.3-39}$$

$$[G]^e = \begin{bmatrix}[G] & [0]\\ [0] & [0]\end{bmatrix} \qquad \textbf{2.3-40}$$

In the case of a beam with the uniform width b, bD_{11} is constant. All coefficients of the

matrices in Equation 2.3-37 are evaluated using full integration except the coefficients associated with transverse shear strain (i.e., the second term of K^{22}), which are evaluated using reduced integration to avoid a phenomenon called *shear locking*. This phenomenon happens when both w and ϕ are approximated using linear interpolation functions. Recalling that for a thin beam, the transverse shear strain γ is neglected. Now considering that, the shear strain is determined by:

$$\gamma = \phi - \frac{\partial w}{\partial x} = b_1 + b_2 x - a_2 \qquad \textbf{2.3-41}$$

Neglecting shear strain in Equation 2.3-41 results in $b_1 - a_2 = 0$ and $b_2 = 0$, which itself results in a constant value for bending energy. Consequently, the element predicts zero solution in an attempt to satisfy the constraint, $\phi - \frac{\partial w}{\partial x} = 0$. To overcome this problem, one may use equal interpolation for both transverse deflection and rotation but use a lower-order polynomial for the shear strain. This is often realized by using reduced integration to evaluate the stiffness coefficients associated with the transverse shear strain in the element stiffness matrix. Keeping the above consideration in mind, the element stiffness matrix can be modified as:

$$[K]^e = \frac{b\mu F_{55}}{4l}\begin{bmatrix} 4 & -2l & -4 & -2l \\ & l^2+\delta & 2l & l^2-\delta \\ & & 4 & 2l \\ sym & & & l^2+\delta \end{bmatrix} \qquad \textbf{2.3-42}$$

where:

$$\delta = \frac{4D_{11}}{\mu F_{55}} \qquad \textbf{2.3-43}$$

Examination of Equation 2.3-42 reveals the following two terms corresponding to bending stiffness and shear stiffness:

$$[K_b]^e = \frac{b\mu F_{55}}{4l}\begin{bmatrix} 4 & -2l & -4 & -2l \\ & l^2 & 2l & l^2 \\ & & 4 & 2l \\ sym & & & l^2 \end{bmatrix} \qquad \textbf{2.3-44}$$

$$[K_{st}]^e = \frac{4bD_{11}}{l}\begin{bmatrix} 0 & 0 & 0 & 0 \\ & 1 & 0 & -1 \\ & & 0 & 0 \\ sym & & & 1 \end{bmatrix} \qquad \textbf{2.3-45}$$

where the subscripts b and st indicate for bending stiffness and shear stiffness, respectively. Thus, the stiffness matrix for laminated beam can be written as:

$$[K]^e = [K_b]^e + [K_{st}]^e \qquad \textbf{2.3-46}$$

The mass and geometric stiffness matrices are also obtained as:

$$[M]^e = \frac{l}{6}\begin{bmatrix} 2I_0 & 0 & I_0 & 0 \\ & 2I_2 & 0 & I_{xy} \\ & & 2I_0 & 0 \\ sym & & & 2I_2 \end{bmatrix} \qquad \textbf{2.3-47}$$

$$[G]^e = \frac{N_x^i}{l}\begin{bmatrix} 1 & 0 & -1 & 0 \\ & 0 & 0 & 0 \\ & & 1 & 0 \\ sym & & & 0 \end{bmatrix} \qquad \textbf{2.3-48}$$

Finally, after proper assembling, the finite element formulation for the whole system of a composite laminated beam is obtained as follow:

$$\begin{bmatrix} [M^{11}] & [0] \\ [0] & [M^{22}] \end{bmatrix} \begin{Bmatrix} \{\ddot{w}\} \\ \{\ddot{\phi}\} \end{Bmatrix} + \begin{bmatrix} [K^{11}] & [K^{12}] \\ [K^{12}]^T & [K^{22}] \end{bmatrix} \begin{Bmatrix} \{w\} \\ \{\phi\} \end{Bmatrix} + \begin{bmatrix} [G] & [0] \\ [0] & [0] \end{bmatrix} \begin{Bmatrix} \{w\} \\ \{\phi\} \end{Bmatrix} = \begin{Bmatrix} \{F^1\} \\ \{F^2\} \end{Bmatrix} \quad \textbf{2.3-49}$$

Equation 2.3-49 can be employed to perform static, dynamic, frequency and buckling analysis which will be discussed in the subsequent Section.

2.4 Validating the finite element models and numerical results

2.4.1 Introduction

In this Section, results obtained from the finite element models, are compared with the exact results based on the available analytical solutions. Maximum deflection of the beam, fundamental natural frequencies, maximum buckling load and transient response to impact for various boundary conditions, are among the subjects that are investigated here. Once the reliability of the models is proved, they will be served as a host for piezoelectric actuators to be bonded.

Results are obtained using the finite element code, specifically developed based on the Chapter 2.2 and 2.3 formulations and programmed in MATLAB environment.

As shown in Figure 2.4-1, the model is uniform and symmetric. The length and the width of the beam are 0.254m and 0.0254m, respectively. The beam is made of AS/3501-6 graphite/epoxy plies with the thickness of 0.00127m each. The material properties can be found in Table 2.4-1:

Table 2.4-1: Material properties for AS/3501-6 graphite/epoxy

E_1 = 144.23 Gpa	G_{12} = 4.14 Gpa
E_2 = 9.65 Gpa	G_{13} = 4.14 Gpa
ν_{12} = 0.3	G_{23} = 3.45 Gpa
ρ = 1389.23 kg m^{-3}	t = 0.000127 m

The lay-up is $[0_{10}/90_{10}]_s$ and the beam is divided into 20 elements everywhere unless it is clearly mentioned otherwise.

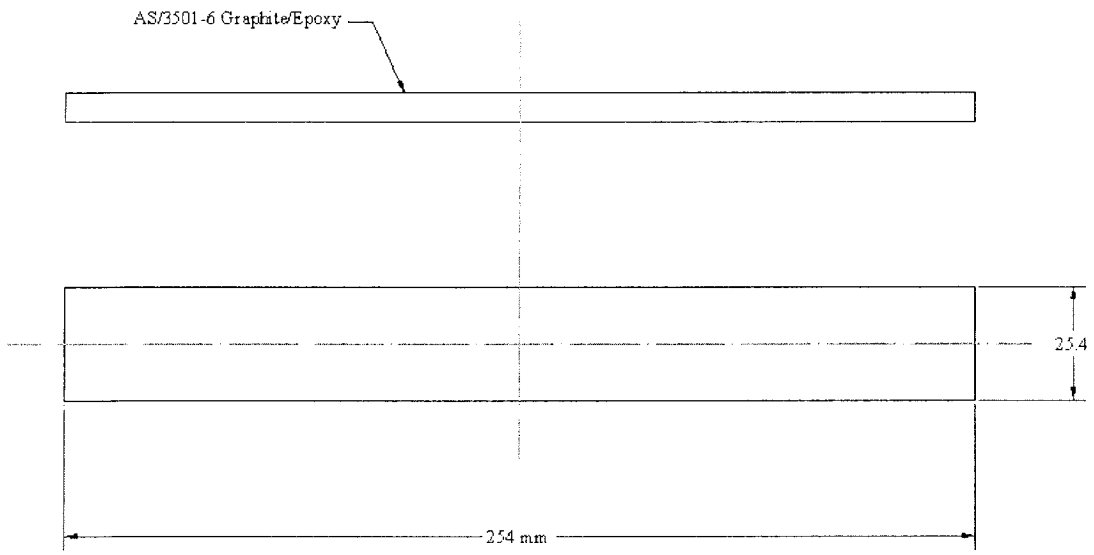

Figure 2.4-1: A uniform symmetric AS/3501-6 graphite/epoxy beam

2.4.2 Deflection of a composite beam under central and/or uniform load

To show the reliability of the model in predicting the deflections of a composite beam, some benchmark problems, having analytical solutions, have been selected. Figure 2.4-2-a,b,c show a composite beam under central point load of $F = 100N$ for various boundary conditions (Hinged-Hinged, Fixed-Fixed and Fixed-Free). Figure 2.4-2-d,e,f demonstrate the same beam under uniform load of $q_0 = 10000 N/m^2$. The exact solutions for the maximum static deflections of the beam for the aforementioned loading and boundary conditions are provided in Table 2.4-2, for both the CLPT and the FSDT. The finite element formulations for the static analysis in the absence of the axial load can be simplified as:

$$[K]\{w\}=\{F\} \qquad \textbf{2.4-1}$$

The finite element results for the problems shown in Figure 2.4-2 a-f, and the comparison to analytical solutions for both the CLPT and the FSDT are given in Table 2.4-3 and Table 2.4-4 [3], respectively.

Table 2.4-2: Exact solutions for the maximum deflections of a laminated composite beam based on the CLPT and the FSDT with various boundary conditions

Laminated beam	Maximum Deflection , w_{max}	
	CLPT	FSDT
Hinged-Hinged Central point load	$\frac{1}{48}c_1$	$\frac{1}{48}c_1+\frac{1}{4}s_1$
Uniform load	$\frac{5}{384}c_2$	$\frac{5}{384}c_2+\frac{1}{8}s_2$
Fixed-Fixed Central point load	$\frac{1}{192}c_1$	$\frac{1}{192}c_1+\frac{1}{4}s_1$
Uniform load	$\frac{1}{384}c_2$	$\frac{1}{384}c_2+\frac{1}{8}s_2$
Fixed-Free Central point load	$\frac{1}{3}c_1$	$\frac{1}{3}c_1+s_1$
Uniform load	$\frac{1}{8}c_2$	$\frac{1}{8}c_2+\frac{1}{2}s_2$

Note: $c_1=-\frac{Fl^3}{bD_{11}}$, $c_2=-\frac{ql^4}{D_{11}}$, $s_1=-\frac{Fl}{\mu F_{55}b}$, $s_2=-\frac{ql^2}{\mu F_{55}}$

Table 2.4-3: Comparison between deflections obtained from the finite element model and the exact solutions based on the classical laminate theory

Boundary conditions	w_{max} from exact solutions (mm)		w_{max} from finite element model (mm)	
	Uniform load	Central load	Uniform load	Central load
Simply-supported	-0.39	-0.96	-0.39	-0.96
Clamped	-0.08	-0.24	-0.08	-0.24
Cantilever	-3.72	-15.37	-3.72	-15.37

Table 2.4-4: Comparison between deflections obtained from the finite element model and the exact solutions based on the first-order shear deformation theory

Boundary conditions	w_{max} from exact solutions (mm)		w_{max} from finite element model (mm)	
	Uniform load	Central load	Uniform load	Central load
Simply-supported	-0.39	-0.98	-0.39	-0.98
Clamped	-0.08	-0.26	-0.08	-0.26
Cantilever	-3.74	-15.43	-3.73	-15.42

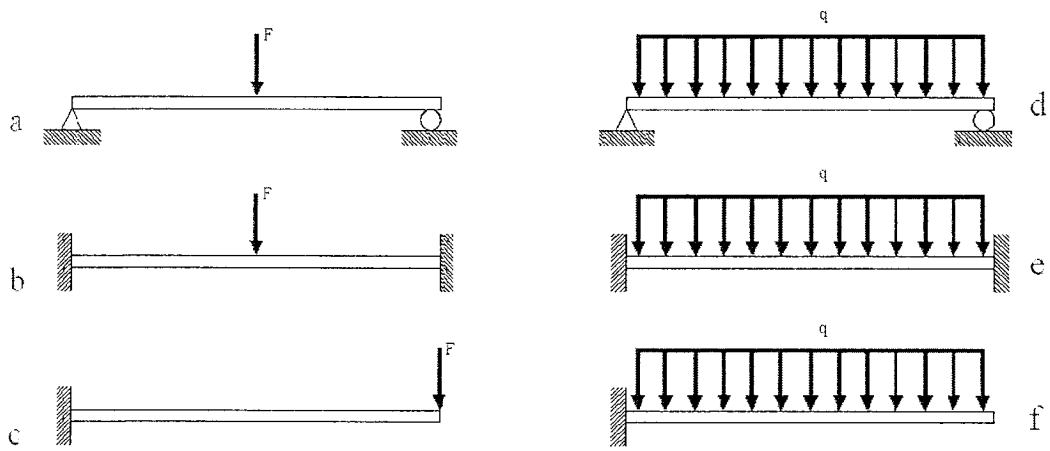

Figure 2.4-2: Laminated composite beam under different loading and various boundary conditions- a and d are simply-supported, b and e are clamped-clamped and c and f are clamped-free beams under central and uniform loading , respectively

The results show that the finite element models based on both the CLPT and the FSDT can perfectly predict deflections of the laminated composite beam under static load.

2.4.3 Free vibration analysis of laminated composite beam

To perform frequency analysis, both the initial axial force N_x^i and external applied force F are set to zero. Under these conditions, Equation 2.2-29 is simplified to:

$$[K]\{w\}+[M]\{\ddot{w}\}=\{0\} \qquad \textbf{2.4-2}$$

The nodal values are given as:

$$w_j(t)=W_j e^{i\omega t} \qquad i=\sqrt{-1} \qquad \textbf{2.4-3}$$

Substituting Equation 2.4-3 into Equation 2.4-2, one may obtain:

$$\left([K]-\omega^2[M]\right)\{W\}=\{0\} \qquad \textbf{2.4-4}$$

where ω represents natural frequency of vibration.

Considering $\lambda=\omega^2$, Equation 2.4-4 represents as eigenvalue problem and can be cast into the following form:

$$\left([K]-\lambda[M]\right)\{W\}=\{0\} \qquad \textbf{2.4-5}$$

where λ and W represent the eigenvalue and the eigenvector respectively.

Using Equation 2.4-5, first two natural frequencies of a laminated composite beam, having different boundary conditions, are calculated and compared with the frequencies obtained from the exact solutions (Table 2.4-5 and Table 2.4-6 [3]) based on both the CLPT and the FSDT. Results are presented in Table 2.4-7.

Table 2.4-5: Exact solutions for the first two natural frequencies of a laminated composite beam based on the classical lamination theory

Laminated beam	Natural frequencies	Where
Hinged-Hinged	$\omega_n = \left(\frac{n\pi}{L}\right)^2 \sqrt{\frac{D_{11}}{\rho H}}$	n=1,2,,...
Fixed-Fixed	$\omega_n = \left(\frac{\xi_n}{L}\right)^2 \sqrt{\frac{D_{11}}{\rho H}}$	$\xi_1 = 4.732$, $\xi_2 = 7.853$
Fixed-Free	$\omega_n = \frac{\xi_n}{L^2} \sqrt{\frac{D_{11}}{\rho H}}$	$\xi_1 = 3.516$, $\xi_2 = 22.034$

Table 2.4-6: Exact solutions for the first two natural frequencies of a laminated composite beam based on the first-order shear deformation theory

Laminated beam	Natural frequencies	Where
Hinged-Hinged	$\omega_n = \left(\frac{n\pi}{L}\right)^2 \sqrt{\frac{D_{11}}{\rho H}} \sqrt{\frac{\mu F_{55}}{\mu F_{55} + \left(\frac{n\pi}{L}\right)^2 D_{11}}}$	n=1,2,,...
Fixed-Fixed	$\omega_n = \left(\frac{\xi_n}{L}\right)^2 \sqrt{\frac{D_{11}}{\rho H}} \sqrt{\frac{\mu F_{55}}{\mu F_{55} + \left(\frac{\xi_n}{L}\right)^2 D_{11}}}$	$\xi_1 = 4.732$ $\xi_2 = 7.853$
Fixed-Free	$\omega_n = \frac{\xi_n}{L^2} \sqrt{\frac{D_{11}}{\rho H}} \sqrt{\frac{\mu F_{55}}{\mu F_{55} + \frac{\xi_n}{L^2} D_{11}}}$	$\xi_1 = 3.516$ $\xi_2 = 22.034$

Table 2.4-7: Comparison between the first two natural frequencies obtained from the finite element models and the exact solutions based on both the CLPT and the FSDT

Boundary conditions	Classical theory (Hz)				First-order theory (Hz)			
	1st Natural fr		2nd Natural fr		1st Natural fr		2nd Natural fr	
	Exact	FEM	Exact	FEM	Exact	FEM	Exact	FEM
S-S	343.0	343.0	1371.8	1371.9	340.3	341.2	1330.3	1345.4
C-C	778.1	777.4	2143.0	2143.1	777.8	753.5	2140.8	2012.0
C-F	122.2	122.2	765.7	765.7	122.2	121.8	765.4	750.5

As it can be seen, the error between analytical and simulation results predicted by the finite element models is less than 0.1% for the CLPT and 6% for the FSDT in its peak. However, the amount of error caused by approximation in finite element model based on the FSDT can be considerably reduced by using more elements (finer meshing) in the finite element model. Table 2.4-8 shows that by increasing the number of elements, the finite element model becomes strongly reliable in predicting the natural frequencies of a laminated beam.

Table 2.4-8: The effect of mesh refinement on the improvement of the accuracy of the results in calculating the fundamental natural frequency of a simply-supported laminated composite beam

Number of elements	Fundamental natural frequency (Hz)			
	CLPT	Error %	FSDT	Error %
4	343.0	Negligible	367.8	8.0
10	343.0	Negligible	344.4	1.2
50	343.0	Negligible	340.4	Negligible
Exact results	343.0	-	340.3	-

2.4.4 Buckling analysis of uniform-thickness composite beam

In the study of buckling problem, the axial compressive load is considered as:

$$N_x^i = -P \qquad \textbf{2.4-6}$$

As the buckling analysis is a static case with no external transverse load, Equation 2.2-29 is reduced to:

$$\left([K] - P[G^*]\right)\{W\} = \{0\} \qquad \textbf{2.4-7}$$

where matrix $[G^*]$ is defined as:

$$[G^*] = \frac{1}{N_x^i}[G] \qquad \textbf{2.4-8}$$

The matrix $[G^*]$ can be easily calculated from Equations 2.2-32 and 2.3-48 for the CLPT and the FSDT cases, respectively.

Equation 2.4-7 is an eigenvalue problem where P represents the eigenvalue. The system represented by this equation has N eigenvalues where N represents the total degrees of freedom. The smallest eigenvalue will be the critical buckling load. The exact solutions corresponding to the critical buckling loads for mid-plane symmetric composite beams, having different boundary conditions are listed in Table 2.4-9 [3]. The simulation results obtained from the finite element models are compared with the exact results in Table 2.4-10.

Table 2.4-9: Exact solutions for the critical buckling load of a laminated composite beam

Boundary conditions	CLPT	FSDT
Hinged-Hinged	$P_{cr} = \left(\frac{\pi}{L}\right)^2 D_{11}$	$P_{cr} = \left(\frac{\pi}{L}\right)^2 D_{11}\left[1 - \frac{D_{11}\left(\frac{\pi}{L}\right)^2}{D_{11}\left(\frac{\pi}{L}\right)^2 + \mu F_{55}}\right]$
Fixed-Fixed	$P_{cr} = \left(\frac{2\pi}{L}\right)^2 D_{11}$	$P_{cr} = \left(\frac{\pi}{2L}\right)^2 D_{11}\left[1 - \frac{D_{11}\left(\frac{\pi}{2L}\right)^2}{D_{11}\left(\frac{\pi}{2L}\right)^2 + \mu F_{55}}\right]$
Fixed-Free	$P_{cr} = \left(\frac{\pi}{2L}\right)^2 D_{11}$	$P_{cr} = \left(\frac{2\pi}{L}\right)^2 D_{11}\left[1 - \frac{D_{11}\left(\frac{2\pi}{L}\right)^2}{D_{11}\left(\frac{2\pi}{L}\right)^2 + \mu F_{55}}\right]$

Table 2.4-10: Comparison between the critical buckling load (N) obtained from the finite element models and exact solutions for both CLPT and FSDT

BC's	CLPT		FSDT	
	Exact	FEM	Exact	FEM
S-S	214220.1	214220.3	210872.3	211729.3
C-C	856880.5	856892.0	805720.4	818346.6
C-F	53555.0	53555.0	53343.3	53398.0

The critical buckling loads obtained from the finite element model based on the CLPT, shows almost no error compared with exact results whereas the error between the results of the FSDT model and exact solution (1.6% in its peak) can also be corrected, using finer meshes as it can be seen in Table 2.4-11.

Table 2.4-11: The effect of mesh refinement on the improvement of the accuracy of the results in calculating the critical buckling load of a simply-supported laminated composite beam

Number of elements	Critical Buckling load (N)	
	CLPT	FSDT
4	214329.8	234199.5
10	214223.0	214334.7
50	214220.1	211009.4
Exact results	214220.1	210872.3

2.4.5 Free vibration analysis of laminated beam-column

A beam under compressive axial load is well known as beam-column since it exhibits behaviors of both the beam and column. Thus for a beam-column the initial axial force $N_x^i = -P$ exists and the frequency Equation 2.4-4 changes to the following form:

$$\left([K]-P[G^*]-\lambda[M]\right)\{W\}=\{0\} \qquad \textbf{2.4-9}$$

where P is the prescribed axial load and $P < P_{cr}$. It should be noted that the compressive

axial load reduces the total stiffness of the element whereas tensional axial load increases it. This effect will be used in the following chapters to alter the natural frequencies and the critical buckling load of the beam using piezoelectric actuators (active stiffening control). Equation 2.4-9, is an eigenvalue problem where $\lambda = \omega^2$. Here ω represents the natural frequencies of the beam-column.

2.4.6 Time dependant response of the beam

In the case of time dependant response of the beam, Equations 2.2-29 and 2.3-49 are governing differential equations of motion which must be integrated using time integration techniques to obtain the nodal values at any specified time. Although in certain load cases, Equation 2.2-29 can be solved analytically, it is enormously time consuming and costly. The powerful Newmark's time-integration methods are widely-used substitutes for solving these types of time-dependant problems. In this numerical integration method, the function and its first derivative are approximated using Taylor's series and only terms up to the second derivative are included [3].

Here the Newmark's method is applied to the general form of the governing equation:

$$[M]\{\ddot{w}\}+[C]\{\dot{w}\}+([K]+[G])\{w\}=\{F\} \qquad \textbf{2.4-10}$$

where the matrix $[C]$ is the natural damping matrix of the element and $\{\dot{w}\}$ is the first derivative of the transverse deflection of the beam with respect to time.

It is assumed that the initial values of matrices $\{w\}$ and $\{\dot{w}\}$ at $t = 0$ are known. The acceleration matrix $\{\ddot{w}\}^e$ at $t = 0$ can be found from Equation 2.4-10. Considering a time

increment Δt, the predictor parameters, $\{\bar{w}\}^e_{n+1}$ and $\{\bar{\dot{w}}\}^e_{n+1}$ at the time $(n+1)\Delta t$ in terms of the known values at time $n\Delta t$ can be computed as:

$$\{\bar{w}\}_{n+1} = \{w\}_n + \Delta t\{\dot{w}\}_n + 0.5\Delta t^2(1-2\beta)\{\ddot{w}\}_n \qquad \textbf{2.4-11}$$

$$\{\bar{\dot{w}}\}_{n+1} = \{\dot{w}\}_n + \Delta t(1-\alpha)\{\ddot{w}\}_n \qquad \textbf{2.4-12}$$

Using the predictor parameters, the acceleration vector can be obtained from the following equation:

$$\left([M]+\alpha[C]+\beta\Delta t^2([K]+[G])\right)\{\ddot{w}\}_{n+1} = \left(\{F\}_{n+1} - [C]\{\bar{\dot{w}}\}_{n+1} - [K]\{\bar{w}\}_{n+1}\right) \qquad \textbf{2.4-13}$$

Knowing $\{\ddot{w}\}_{n+1}$ at time $(n+1)\Delta t$, the displacement and velocity vectors at time $(n+1)\Delta t$ are obtained from the following relations:

$$\{w\}_{n+1} = \{\bar{w}\}_{n+1} + \beta\Delta t^2\{\ddot{w}\}_{n+1} \qquad \textbf{2.4-14}$$

$$\{\dot{w}\}_{n+1} = \{\bar{\dot{w}}\}_{n+1} + \alpha\Delta t\{\ddot{w}\}_{n+1} \qquad \textbf{2.4-15}$$

Constants α and β in the above equations are the accuracy and stability parameters of the algorithm. For $\alpha = 1/2$ and $\beta = 1/4$, the Newmark method is called the average acceleration algorithm and is unconditionally stable.

In the following example, a cantilever beam with aspect ratio of L/H=10, is subjected to a dynamic step load of 1000 N for 1 millisecond, on its tip. The tip deflection of the beam versus time is plotted in Figure 2.4-3 using both the CLPT and the FSDT and are compared with static results. It should be noted that the damping ratio is considered to be 0.05 for both cases.

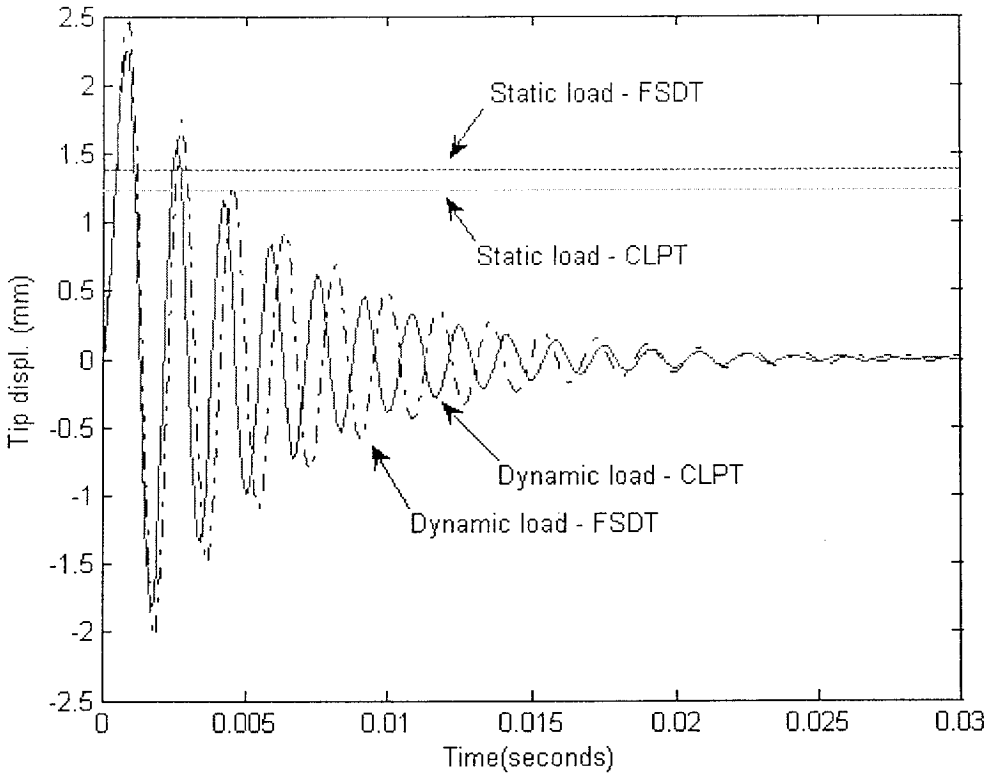

Figure 2.4-3: Response of a cantilever beam to under dynamic step load of 1 KN and duration of one millisecond using the CLPT and the FSDT

As it can be realized, the same amount of load, if applied in a short period of time (impact) can result in considerably more deflections and also, deflections obtained by the FSDT model in both static and dynamic cases are larger than those of the CLPT due to the effect of shear deformation. It is interesting to note that, the frequency predicted by the CLPT is slightly higher than that of the FSDT.

To better realize the difference in predicting the time-dependent response, the above experiment has been repeated with a considerably large load of 100000 N in a very short period of 0.01 milliseconds. Total response of the beam is plotted using both the CLPT

and the FSDT theory in Figure 2.4-4 and Figure 2.4-5.

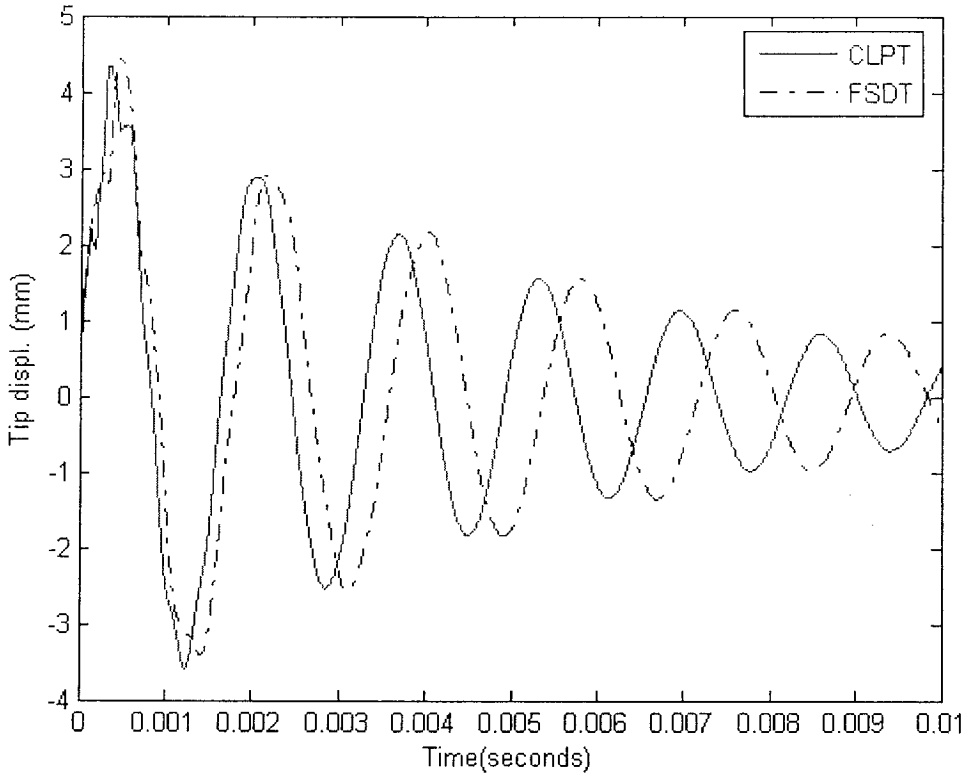

Figure 2.4-4: Response of a cantilever beam to a dynamic tip load of 100 KN applied at the period of 0.01 milliseconds predicted by both the CLPT and the FSDT

Figure 2.4-4 shows the tip displacement of the beam for the period of 0.01 second using both the CLPT and the FSDT. As it can be realized, analysis based on the CLPT produces inaccurate results and thus the theory is not suitable for predicting dynamic behavior of composite structures under impact loading.

Figure 2.4-5 shows the portion of the Figure 2.4-4 for the period of 2×10^{-3} second to better demonstrate the difference between the CLPT and the FSDT.

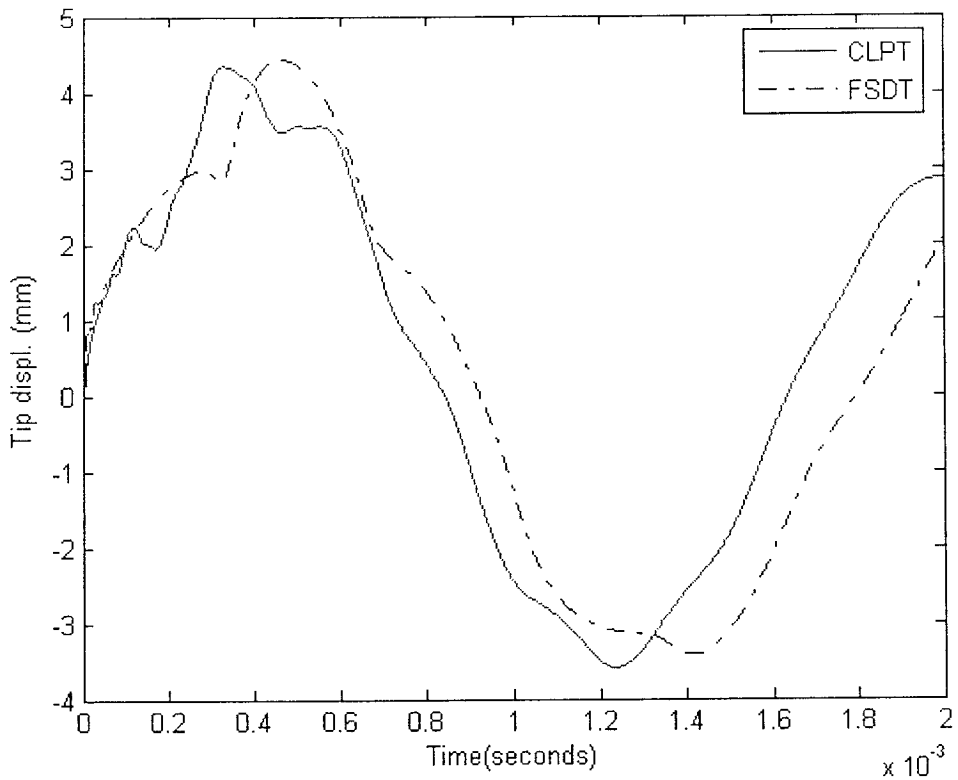

Figure 2.4-5: Response of a cantilever beam during and shortly after a dynamic tip load of 100 KN is being applied in the period of 0.01 milliseconds predicted by both the CLPT and the FSDT

Figure 2.4-6 and Figure 2.4-7 show the first three mode shapes of the beam and the total response due to these modes for both the CLPT and the FSDT, respectively:

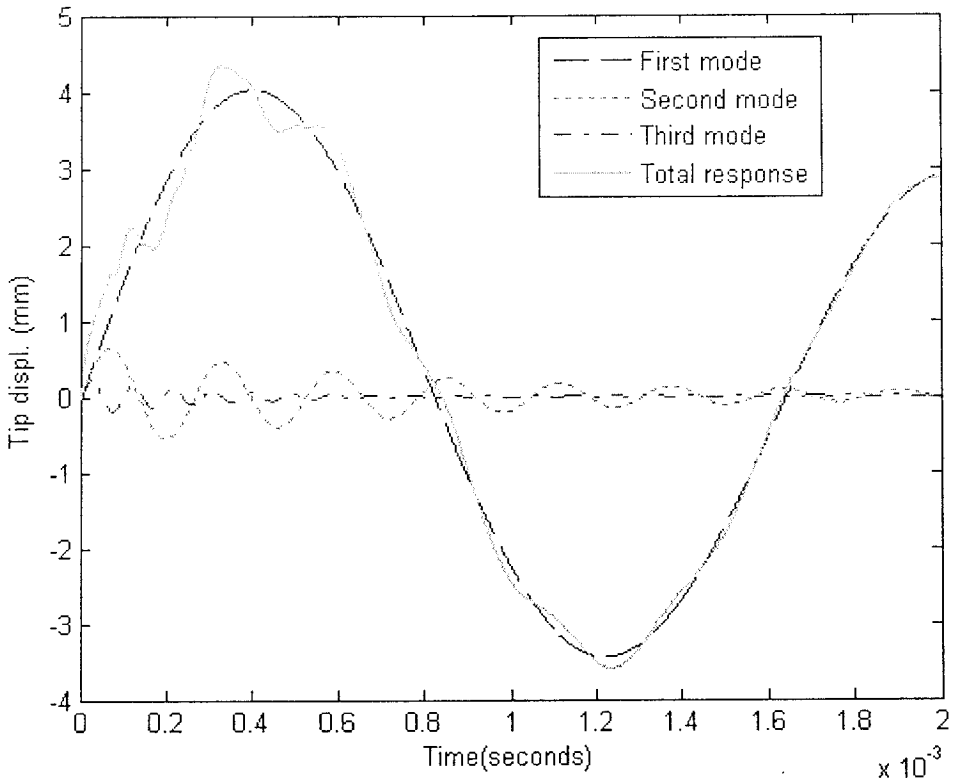

Figure 2.4-6: Total response and the first three modes of a cantilever beam during and shortly after a dynamic tip load of 100 KN is being applied in the period of 0.01 milliseconds predicted by the CLPT

By analyzing Figure 2.4-6 and Figure 2.4-7, one may see, although there is no considerable difference in the first mode of actuation predicted by the CLPT and the FSDT, the noticeable weakness of the CLPT (in comparison with the FSDT) in predicting the higher modes of actuation (here the second and the third), results in a significant difference in predicting the response of the beam under an impact loading. Increasing the impact load while decreasing the period in which the load applies (increasing the effect of impact) will result in more higher modes being activated and thus more error will be expected using the CLPT versus the FSDT.

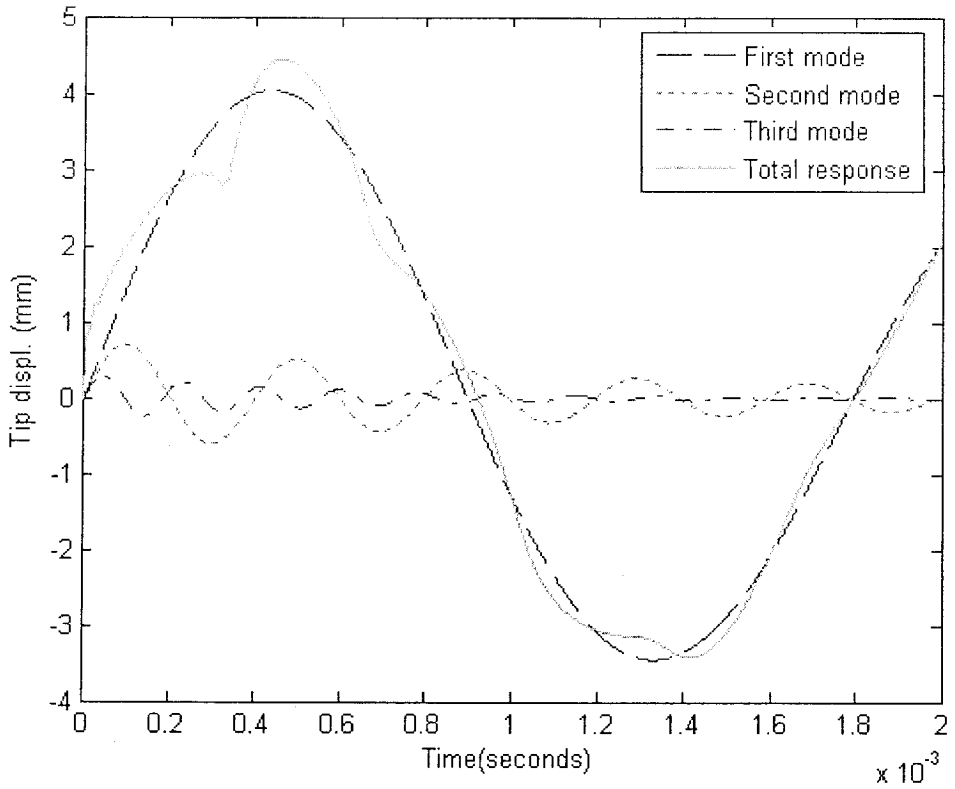

Figure 2.4-7: Total response and the first three modes of a cantilever beam during and shortly after a dynamic tip load of 100 KN is being applied in the period of 0.01 milliseconds predicted by the FSDT

It can be concluded that the effect of the shear deformation can not be ignored in analysis of laminated composite structures under impact loading as the higher modes can be better approximated using the FSDT.

2.4.7 The effect of length-to-thickness ratio (L/H) on the exactness of the theories

The CLPT can exactly predict the behavior of the laminated beam, when the thickness of the beam is relatively small compared to its length (large L/H). In this case, there is no considerable difference between the simulation results based on the CLPT and the FSDT. However for relatively thick beam (small L/H), the effect of shear deformation is noticeable hence, the CLPT is not as exact as the FSDT, even for static cases.

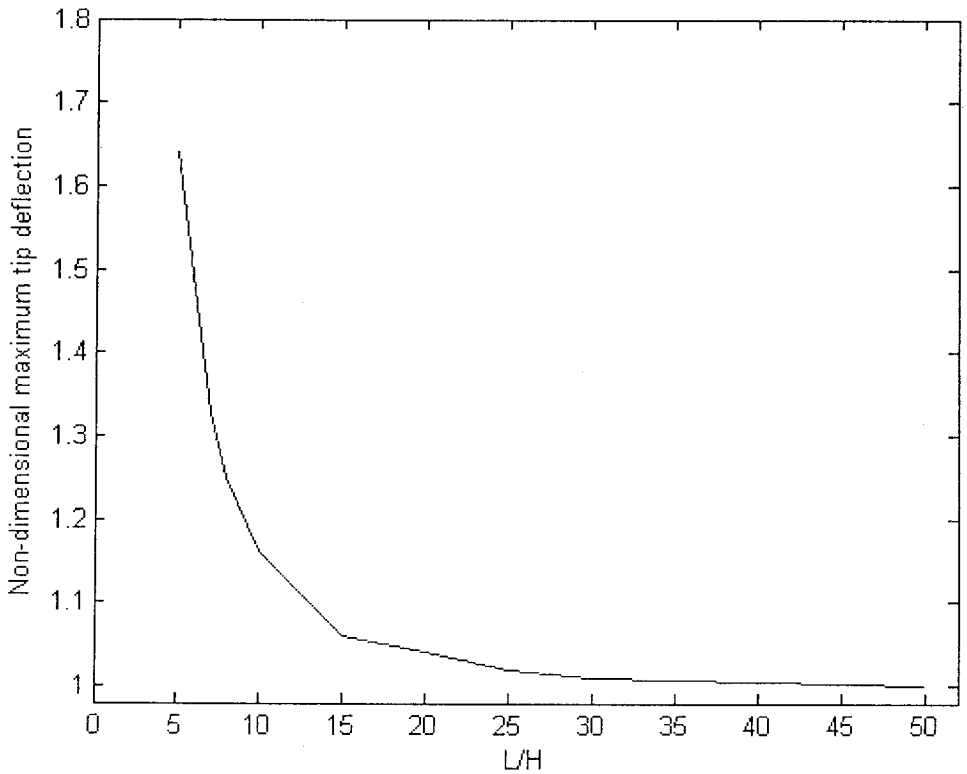

Figure 2.4-8: Non-dimensional maximum tip deflection of a cantilever beam versus length-to-thickness ratios

To find the region where the CLPT can be confidently used, non-dimensional maximum

tip deflection of the cantilever beam (ratio of maximum tip deflection based on FSDT to the maximum tip deflection based on the CLPT) is plotted versus length-to-thickness ratio for both theories in Figure 2.4-8, when a uniform loading of $100N/m^2$ is applied on the beam. The same investigation is performed on the first three natural frequencies of the cantilever beam by plotting the non-dimensional frequencies (frequencies predicted by FSDT over those predicted by the CLPT) versus length-to-thickness ratio as shown in Figure 2.4-9.

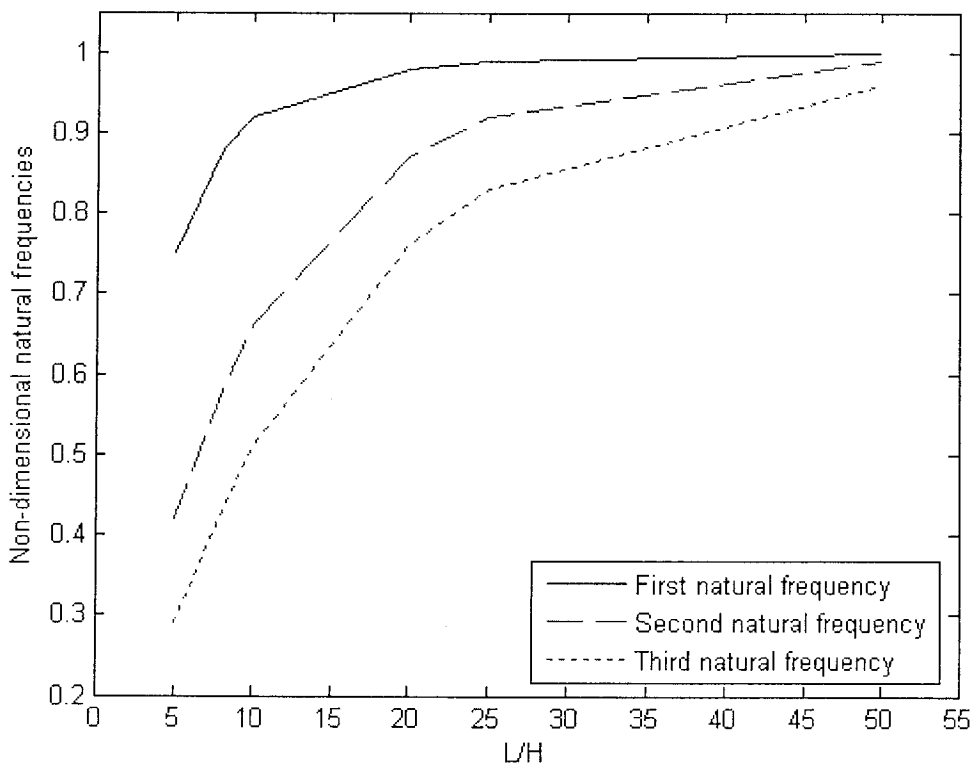

Figure 2.4-9: Non-dimensional first three natural frequencies of a cantilever beam versus length-to-thickness ratios

Figure 2.4-8 shows that there is a significant difference between predicted results for maximum deflection when L/H is relatively small (thick beam) however as L/H

increases, the difference becomes almost negligible and the CLPT is able to predict the deflections of the beam with an acceptable accuracy. It is noted that the difference in predicting the deflections is less than 1% for L/H>50. However it increases to more than 60% for L/H<5.

Figure 2.4-9 shows that the same analogy is applicable for the first natural frequency however; when it comes to predicting the higher natural frequencies, the CLPT becomes less accurate, even for relatively thin beams. This is basically confirmation of what concluded in the previous Section for response under impact loading. As L/H decreases from more than 50 to less than 5, the discrepancy in predicting the first natural frequency increases from less than 1% to more than 20%. For the second and the third natural frequencies, when L/H is smaller than 5, more than 50% and 70% of difference can be seen, between the predictions of two theories, respectively.

In general, one may conclude that using the CLPT, results in significant error when the length-to-thickness of the beam is relatively small and also when higher modes of vibration should be taken into accounts like the case of impact. However, it is still a robust theory if it is used for relatively thin beam and for the first mode of vibration. Since a finite element model using the CLPT can respond with a very good precision when extremely coarse meshes are being used (in contrary to the FSDT case in which finer meshes directly lead to more precise results), in situations rather than those explained above, it can still be a very time and cost efficient, easy to use and powerful tool in the hands of engineers and designers.

3 Piezoelectric laminate composite

3.1 Introduction

3.1.1 History

Although a peculiar property of tourmaline crystals which is attracting and then rejecting hot ashes a few moment afterwards, has been noticed centuries ago by people of Ceylan and India – the reason why it was called the Ceylan magnet when brought to Europe by Dutch tradesmen in eighteenth century- it was first scientifically analyzed in 1756 by German physicist Aepinus. The phenomenon – electrical polarization of tourmaline crystals when its temperature changes (the inverse effect is called electricaloric effect) - was named pyroelectricity by the Scottish physicist D.Brewster in 1824. However, piezoelectricity was first mentioned in 1817 by the French mineralogist Rene Just Hauy and demonstrated by Pierre and Jacques Curie in 1880. The Curies noticed that applying pressure or mechanical stress on certain nonsymmetrical crystals produces electrical charge in proportion to pressure and vice-versa. The same crystals, when subjected to an electric field, expand or contract. Although the effect was first observed in single crystals like tourmaline, quartz and Rochelle salt, it could also be induced in some polycrystalline materials, such as lead-zirconate-titanate (PZT), barium titanate and lead metaniobate [5].

3.1.2 Piezoelectricity

The Piezoelectricity is defined as transformation between the electrical and mechanical energy in certain category of materials which are composed of charged particles and can be polarized. Most of the piezoelectric materials are crystalline solids with no center of

symmetry in their crystal structures, thus exhibiting an anisotropic property such as piezoelectricity. In PZT crystals and above certain temperature called Curie temperature, the crystal structure is cubic and poses no electric dipole moment. However, below this temperature the positively charged ion shifts from its central location along one of the several allowed directions. This slightly distorts the crystal lattice into perovskite structure (a tetragonal/rhombohedral shape), and produces an electric dipole with single axis of symmetry. Immediately after sintering, groups of molecular dipoles align within small areas, or domains, to form large dipole moments. PZT is made up of many such domains; however, as they are randomly oriented, their net external electric dipole is zero.

If PZT is subjected to a large electric field at elevated temperature, as shown in Figure 3.1-1, the domain dipoles align in the allowed direction most closely in line with the field. This process is called Polarization and causes the PZT to exhibit the piezoelectric phenomenon [5].

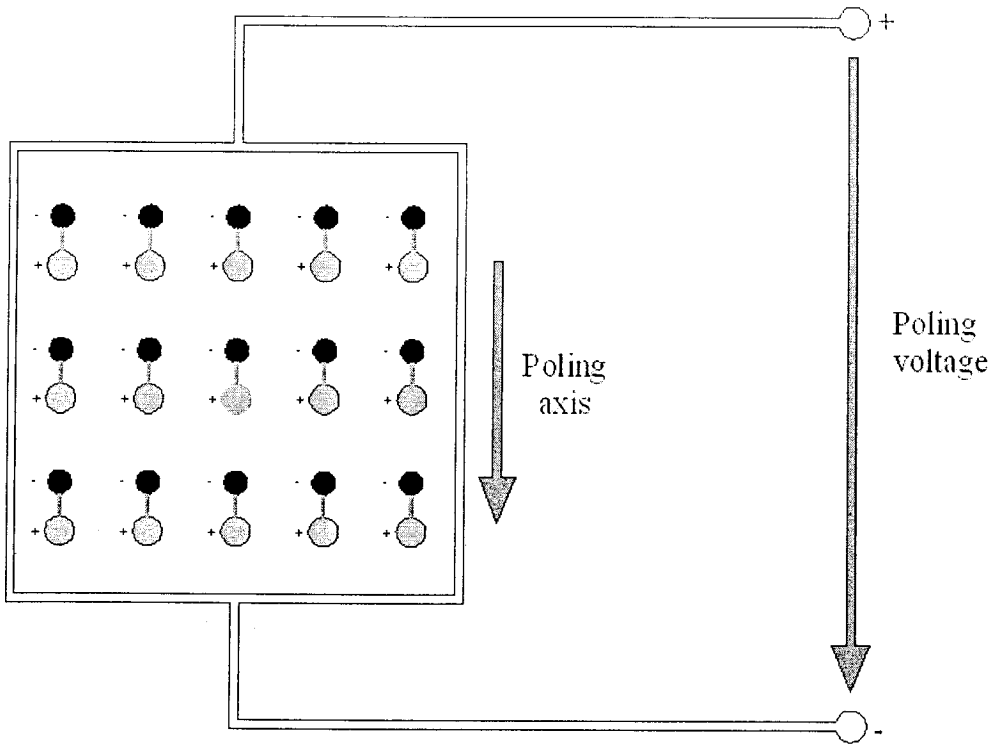

Figure 3.1-1: The phenomenon of piezoelectricity

3.1.3 Lamina Constitutive equations

The constitutive equations for a layer of piezoelectric material can be written as [7]:

$$\{\sigma\} = [C]\{\varepsilon\} - [e]\{E\} \qquad \textbf{3.1-1}$$
$$\{D\} = [e]\{\varepsilon\} - [p]\{E\}$$

where:

$\{\sigma\}$, $\{\varepsilon\}$, $\{D\}$ and $\{E\}$ are the stress, strain , electric displacement and electric field vectors, and $[C]$, $[e]$ and $[p]$ are the elasticity, piezoelectric and dielectric constant matrices, respectively. It should be noted that the first and the second equations in 3.1-1 represent the direct and reverse piezoelectric effects, respectively. The schematic representations of the direct and reverse piezoelectric effects are shown in Figure 3.1-2.

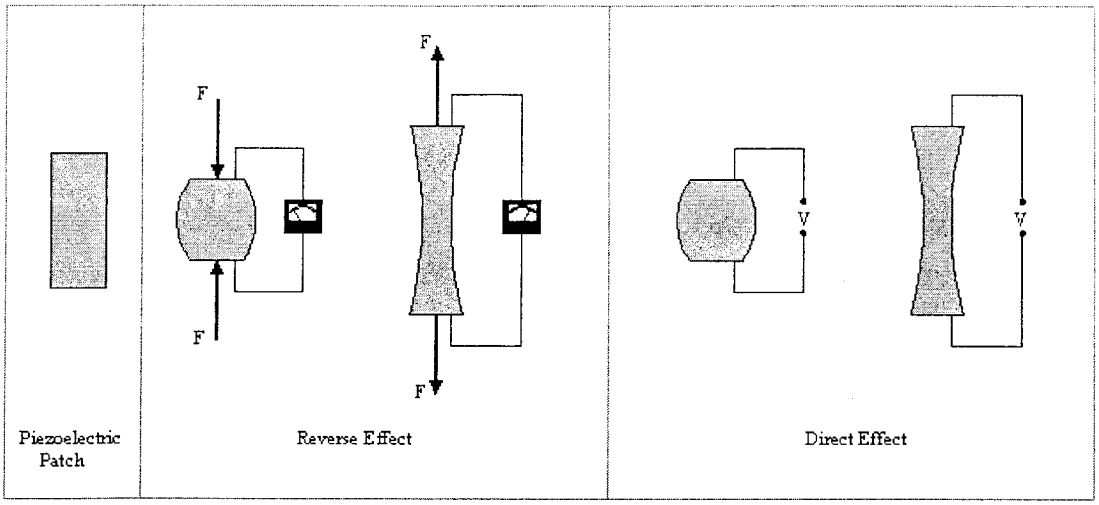

Figure 3.1-2: Schematic illustration of Direct and Reverse piezoelectric effect

In matrix form, Equation 3.1-1 can be written as:

$$\begin{Bmatrix}\sigma_1\\ \sigma_2\\ \sigma_3\\ \sigma_4\\ \sigma_5\\ \sigma_6\end{Bmatrix} = \begin{bmatrix} C_{11} & C_{12} & C_{13} & 0 & 0 & C_{16}\\ C_{12} & C_{22} & C_{23} & 0 & 0 & C_{26}\\ C_{13} & C_{23} & C_{33} & 0 & 0 & C_{36}\\ 0 & 0 & 0 & C_{44} & C_{45} & 0\\ 0 & 0 & 0 & C_{45} & C_{55} & 0\\ C_{16} & C_{26} & C_{36} & 0 & 0 & C_{66}\end{bmatrix}\begin{Bmatrix}\varepsilon_1\\ \varepsilon_2\\ \varepsilon_3\\ \varepsilon_4\\ \varepsilon_5\\ \varepsilon_6\end{Bmatrix} - \begin{bmatrix} 0 & 0 & e_{31}\\ 0 & 0 & e_{32}\\ 0 & 0 & e_{33}\\ e_{14} & e_{24} & 0\\ e_{15} & e_{25} & 0\\ 0 & 0 & e_{36}\end{bmatrix}\begin{Bmatrix}E_1\\ E_2\\ E_3\end{Bmatrix}$$

3.1-2

$$\begin{Bmatrix}D_1\\ D_2\\ D_3\end{Bmatrix} = \begin{bmatrix} 0 & 0 & 0 & e_{14} & e_{15} & 0\\ 0 & 0 & 0 & e_{24} & e_{25} & 0\\ e_{31} & e_{32} & e_{33} & 0 & 0 & e_{36}\end{bmatrix}\begin{Bmatrix}\varepsilon_1\\ \varepsilon_2\\ \varepsilon_3\\ \varepsilon_4\\ \varepsilon_5\\ \varepsilon_6\end{Bmatrix} - \begin{bmatrix} p_{11} & p_{12} & 0\\ p_{12} & p_{22} & 0\\ 0 & 0 & p_{33}\end{bmatrix}\begin{Bmatrix}E_1\\ E_2\\ E_3\end{Bmatrix}$$

For the plane-stress condition which is almost the case for piezoelectric layers, direct piezoelectric formulation becomes [7]:

$$\begin{Bmatrix}\sigma_1\\ \sigma_2\\ \sigma_6\end{Bmatrix}=\begin{bmatrix}Q_{11} & Q_{12} & 0\\ Q_{12} & Q_{22} & 0\\ 0 & 0 & Q_{66}\end{bmatrix}\begin{Bmatrix}\varepsilon_1\\ \varepsilon_2\\ \varepsilon_6\end{Bmatrix}-\begin{bmatrix}0 & 0 & e_{31}\\ 0 & 0 & e_{32}\\ 0 & 0 & 0\end{bmatrix}\begin{Bmatrix}E_1\\ E_2\\ E_3\end{Bmatrix} \qquad \textbf{3.1-3}$$

and,

$$\begin{bmatrix}0 & 0 & e_{31}\\ 0 & 0 & e_{32}\\ 0 & 0 & 0\end{bmatrix}=\begin{bmatrix}0 & 0 & d_{31}\\ 0 & 0 & d_{32}\\ 0 & 0 & 0\end{bmatrix}\begin{bmatrix}Q_{11} & Q_{12} & 0\\ Q_{12} & Q_{22} & 0\\ 0 & 0 & Q_{66}\end{bmatrix} \qquad \textbf{3.1-4}$$

where:

$$Q_{11}=\frac{E_1}{1-\nu_{12}\nu_{21}}\ ,\ Q_{12}=\frac{\nu_{12}E_2}{1-\nu_{12}\nu_{21}}=\frac{\nu_{21}E_1}{1-\nu_{12}\nu_{21}}\ ,\ Q_{22}=\frac{E_2}{1-\nu_{12}\nu_{21}}\ ,\ Q_{66}=G_{12} \qquad \textbf{3.1-5}$$

Matrix $[d]$ is the piezoelectric constant moduli matrix.

3.1.4 Applications

Here some applications of piezoelectric materials in industries are represented. Nowadays, one could hardly find any industry that still has not been touched by piezoelectric materials.

Optics and Vision: Positioning of mirrors or lenses, focusing, laser cavity tuning, alignment or deformation of fibers, scanners, choppers, interferometers, modulators and glass cutting.

Mechanics: Positioning of tools, pick and place, clamps, active wedges, damping, active control, generation of ultrasonic or sonic vibrations, health monitoring.

Fluids: Proportional valves, pumps, measuring, injections, ink jet, droplet generators and flow mass meter.

Electronics: Positioning of masks, wafers or magnetic heads, non-magnetic actuation, circuit breakers and chip testing.

Air-space: Active flaps, shape control, active wing and active helicopter blades.

Electrical energy: Piezoelectric generator, energy harvesting and electric switch.

3.2 Laminated composite beam with piezoelectric actuators (CLPT)

To obtain the finite element formulation of a laminated composite beam with piezoelectric actuators, equations of motion are presented considering the effect of piezoelectric actuators as moment and force.

From Chapter 2.2 , the equation of motion for a laminated composite beam based on the Classical beam theory was represented as:

$$\frac{\partial^2 M_x}{\partial x^2} + N_x^i \frac{\partial^2 w}{\partial x^2} + q(x) = I_0 \frac{\partial^2 w}{\partial t^2} - I_2 \frac{\partial^4 w}{\partial x^2 \partial t^2}$$

In the presence of the piezoelectric actuators, the terms M_x and N_x^i should be redefined as the combination of mechanical and piezoelectric moment/force as follows [3, 7]:

$$M_x = M_x^M + M_x^P \qquad \textbf{3.2-1}$$

The additional term M_x^P, is the piezoelectric moment and can be calculated as

$$M_x^P = \sum_{k=1}^{N_a} \int_{z_k}^{z_{k+1}} b\overline{Q}_{11}^{(k)} d_{31}^{(k)} E_z^{(k)} z dz \qquad \textbf{3.2-2}$$

Modified N_x^i in the equation of motion, also comprises both axial mechanical and piezoelectric forces. Axial piezoelectric force is represented as

$$N_x^P = \sum_{k=1}^{N_a} \int_{Z_k}^{Z_{k+1}} b\overline{Q}_{11}^{(k)} d_{31}^{(k)} E_z^{(k)} dz \qquad \textbf{3.2-3}$$

where $E_z^{(k)}$ is the electric field applied to the k^{th} layer of piezoelectric actuators in z direction, $d_{31}^{(k)}$ is the piezoelectric constant and N_a is the number of piezoelectric layers in

the laminate. It should be noted that piezoelectric actuators used in the laminates are considerably thin, thus with an acceptable accuracy one can assume that the electric field through the thickness of the laminate is constant so:

$$E_z^{(k)} = \frac{V^{(k)}}{t_k} \qquad \textbf{3.2-4}$$

where $V^{(k)}$ and t_k are the applied voltage and the thickness of the k^{th} layer of piezoelectric actuator, respectively.

Considering the effect of piezoelectric actuators and repeating the same procedure mentioned in Chapter 2.2, the effect of piezoelectric actuators is emerged in the form of actuator's moment force in Equation 2.2-29 .By performing the procedure which was explained in details in Chapter 2.2, one may obtain:

$$\left([K]^e + [G]^e\right)\{w\}^e + [M]^e\{\ddot{w}\}^e = \{F\}^e + \{F^P\}^e \qquad \textbf{3.2-5}$$

where F^P is the bending force due to the actuators and is obtained as:

$$F^P = \int_0^l M_x^P \frac{\partial^2 \varphi}{\partial x^2} dx \qquad \textbf{3.2-6}$$

Substituting shape functions φ_i^e from Equation 2.2-21 into Equation 3.2-6 yields:

$$F^P = M_x^P \begin{Bmatrix} 0 \\ 1 \\ 0 \\ -1 \end{Bmatrix} \qquad \textbf{3.2-7}$$

3.3 Laminated composite beam with piezoelectric actuators (FSDT)

Similar to the Section 3.2, the finite element model based on the FSDT must be re-derived, for the laminated beam with piezoelectric actuators. For the sake of clarity, equations of motion for a laminated composite beam based on the first-order shear deformation theory have been rewritten here:

$$\frac{\partial Q_x}{\partial x} + N_x^i \frac{\partial^2 w}{\partial x^2} + q(x) = I_0 \frac{\partial^2 w}{\partial t^2}$$

$$\frac{\partial M_x}{\partial x} - Q_x = I_2 \frac{\partial^2 \phi}{\partial t^2}$$

where transverse force, Q_x, and moment resultants, M_x, are represented as the combination of mechanical and piezoelectric forces and moments as follow [3, 7]:

$$Q_x = Q_x^M + Q_x^P \qquad \textbf{3.3-1}$$

$$M_x = M_x^M + M_x^P \qquad \textbf{3.3-2}$$

where M_x^P the moment resultant (Equation 3.2-2) and Q_x^P is the transverse shear force due to piezoelectric actuators and can be derived as:

$$Q_x^P = \sum_{k=1}^{N_a} \int_{z_k}^{z_{k+1}} b\mu F_{55}^{(k)} d_{15}^{(k)} E_x^{(k)} dz \qquad \textbf{3.3-3}$$

where $E_x^{(k)}$ is the electric field applied to the k^{th} layer of piezoelectric actuators in the x direction, $d_{15}^{(k)}$ is the piezoelectric constants and N_a is the number of piezoelectric layers in the laminate.

In presence of piezoelectric actuators, N_x^i in the equations of motions, comprise both axial mechanical and piezoelectric forces as:

$$N_x^i = N_x^M + N_x^P \tag{3.3-4}$$

where N_x^P is the axial force due to piezoelectric actuation as derived in Equation 3.2-3.

Considering the effect of piezoelectric actuators and repeating the same procedure mentioned in Section 2.3, the effect of piezoelectric actuators emerged in the form of actuator's shear and moment force in Equation 2.3-37. The final finite element formulation for the piezo-laminated composite beam can be derived as:

$$\begin{bmatrix} [K^{11}] & [K^{12}] \\ [K^{12}]^T & [K^{22}] \end{bmatrix}^e \begin{Bmatrix} \{w\} \\ \{\phi\} \end{Bmatrix}^e + \begin{bmatrix} [G] & [0] \\ [0] & [0] \end{bmatrix}^e \begin{Bmatrix} \{w\} \\ \{\phi\} \end{Bmatrix}^e + \begin{bmatrix} [M^{11}] & [0] \\ [0] & [M^{22}] \end{bmatrix}^e \begin{Bmatrix} \{\ddot{w}\} \\ \{\ddot{\phi}\} \end{Bmatrix}^e =$$
$$\begin{Bmatrix} \{F^1\} \\ \{F^2\} \end{Bmatrix}^e + \begin{Bmatrix} \{0\} \\ \{F_S^P\} \end{Bmatrix}^e - \begin{Bmatrix} \{0\} \\ \{F_B^P\} \end{Bmatrix}^e \tag{3.3-5}$$

where F_S^P and F_B^P are the shear and bending forces due to the actuators and are obtained as:

$$F_S^P = \int_{z_k}^{z_{k+1}} Q_x^P \varphi dx \tag{3.3-6}$$

$$F_B^P = \int_0^l M_{xx}^P \frac{\partial \varphi}{\partial x} dx \tag{3.3-7}$$

One should consider that due to the assumption of uniformity of the electric field in the x-direction, the term $\frac{\partial Q_{xx}^P}{\partial x}$ is neglected. Substituting shape functions φ_i^e from Equations 2.3-23 and 2.3-24 into Equations 3.3-6 and 3.3-7 yields:

$$F_S^P = \frac{Q_x^P l}{2}\begin{Bmatrix}1\\1\end{Bmatrix} \qquad \textbf{3.3-8}$$

$$F_B^P = M_{xx}^P\begin{Bmatrix}1\\-1\end{Bmatrix} \qquad \textbf{3.3-9}$$

3.4 Validating the finite element models for the piezo-laminated beam

3.4.1 Introduction

In this Section, results obtained from the finite element models with embedded and/or surface bonded piezoelectric layers/patches are compared with the results existing in the literatures. Once reliability of the models is proved, they will be used to perform sensitivity study and investigate the behavior of the piezo-laminated composite beam with variation of different parameters such as applied voltage, laminate thickness, poling directions, ply angles, distance of the embedded piezoelectric layers from mid-plane of the beam and the position of the bonded piezoelectric patches. In the next chapter, the foregoing models will be employed to perform the design optimization.

As mentioned before, results are obtained using developed finite element program in MATLAB environment based on the Sections 3.2 and 3.3 formulation.

Properties of the materials that have been used in subsequent models are presented in Table 3.4-1, so they could be addressed easier. It should be noted that since FSDT model has been proved to be more reliable, until it has been clearly mentioned otherwise, finite element model based on the FSDT has been used in the following analysis.

Table 3.4-1: Material properties

	KYNAR piezofilm	G-1195 piezoceramic	AS/3501 Graphite-epoxy
$E_1 \quad (N/m^2)$	6.85×10^9	63.0×10^9	144.8×10^9
$E_2 \quad (N/m^2)$	6.85×10^9	63.0×10^9	9.65×10^9
$G_{12} \quad (N/m^2)$	0.078×10^9	24.8×10^9	7.10×10^9
ν_{12}	0.29	0.28	0.30
$G_{13} \quad (N/m^2)$	-	-	7.10×10^9
$G_{23} \quad (N/m^2)$	-	-	5.92×10^9
$d_{31} \quad (m/V)$	22.99×10^{-12}	-166.0×10^{-12}	-
$d_{32} \quad (m/V)$	4.6×10^{-12}	-166.0×10^{-12}	-
Thickness (m)	0.00011	0.0002	0.00127

3.4.2 Bimorph beam

To validate the finite element models, first, a cantilever beam made up of two layers of KYNAR piezofilm, namely the bimorph beam as shown in Figure 3.4-1, is considered. This example is studied by Koconis et al. [33]. The data for the piezofilm are shown in Table 3.4-1. Out of phase voltage is applied to both films ($V_2 = -V_1$).

The exact tip deflection for a bimorph beam [5] can be represented as:

$$w = -\frac{3}{2}\frac{d_{31}V}{h^2}L^2 \qquad \textbf{3.4-1}$$

The tip deflections of a beam with the length of 0.08 m and the width of 0.01 m, for different applied voltages, are obtained using the finite element formulations based on both the CLPT and the FSDT and compared with exact solutions that have been

calculated using the Equation 3.4-1. The results are given in Table 3.4-2. Figure 3.4-2 also shows the variation of tip deflection versus applied voltage.

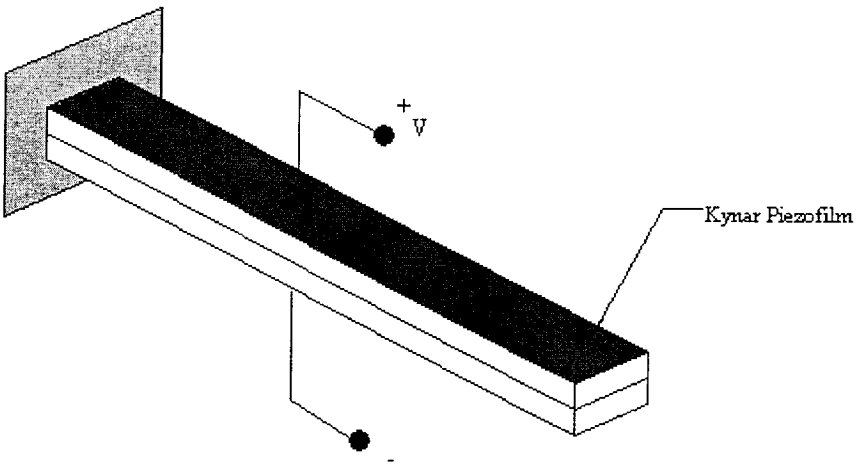

Figure 3.4-1: A Bimorph beam consist of two KYNAR piezofilm

Table 3.4-2: Tip deflection of a cantilever bimorph beam subjected to applied voltage

	Tip deflection (mm)		
Voltage (V)	Exact solution	Finite element model (CLPT)	Finite element model (FSDT)
0	0	0	0
50	0.456	0.456	0.456
100	0.912	0.912	0.912
150	1.368	1.368	1.368
200	1.824	1.824	1.824
250	2.280	2.280	2.280
300	2.736	2.736	2.736
350	3.192	3.192	3.192
400	3.648	3.648	3.648
450	4.104	4.104	4.104
500	4.560	4.560	4.560

As it can be seen, results obtained from the finite element models are in excellent agreement with those of Koconis et al. [33]. It must be noted that although the effect of shear deformation has taken into account in FSDT model, but due to considerably small thickness of the beam, the effect of shear deformation is negligible as expected.

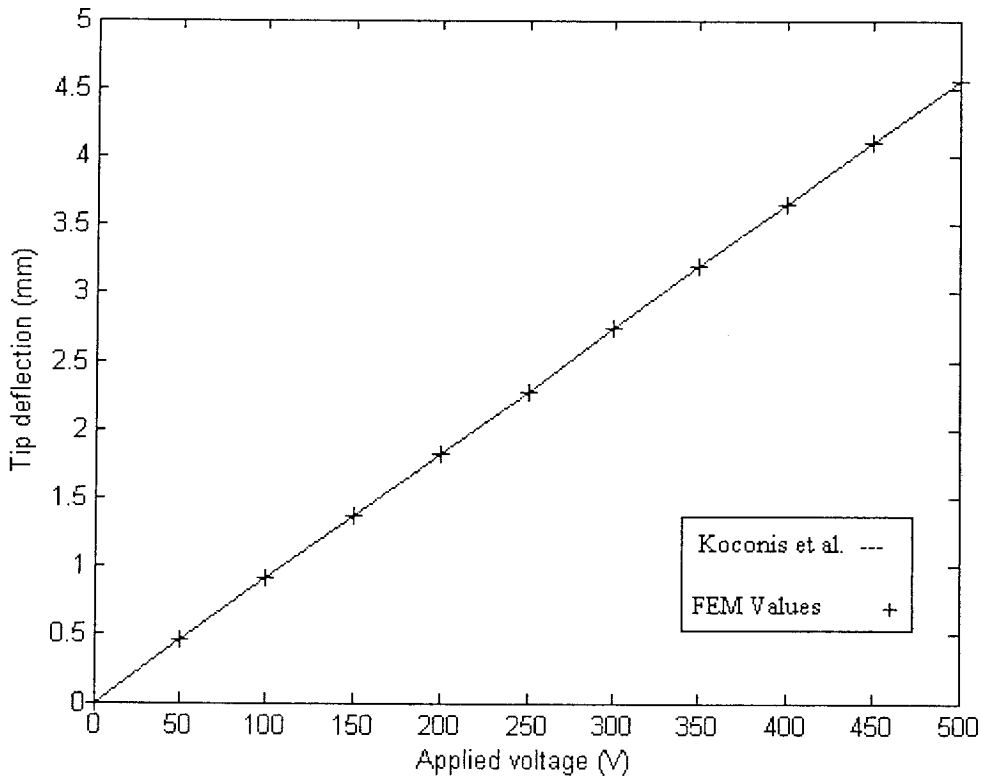

Figure 3.4-2: Comparison between the tip deflection of a bimorph beam obtained from FEM and those of Koconis et al. [33], versus applied voltage

3.4.3 Laminated composite beam with layers of piezoelectric actuator

In this example, a cross-ply symmetric laminated composite beam [0/90/90/0], made of graphite/epoxy plies (AS/3501) with two layers of piezoceramic actuators (G1195), bonded on top and bottom surfaces of the beam, is considered. The material properties can be found in Table 3.4-1. The length and width of the beam are 0.254 and 0.0254 m, respectively. Deflection of the beam with a uniformly distributed load of $q_0 = 2\times10^3 N/m^2$ and Clamped-free and simply-supported boundary conditions, for different applied voltages is plotted in Figure 3.4-3 and Figure 3.4-4 and compared with the results conducted by Donthireddy and Chnadrashekhara [27]. It must be noted that for the clamped-free beam, the top layer is polarized in the direction of the applied voltages and the bottom layer is polarized in the direction opposite to that of the applied voltage and for the simply-supported beam, the polarity is reversed.

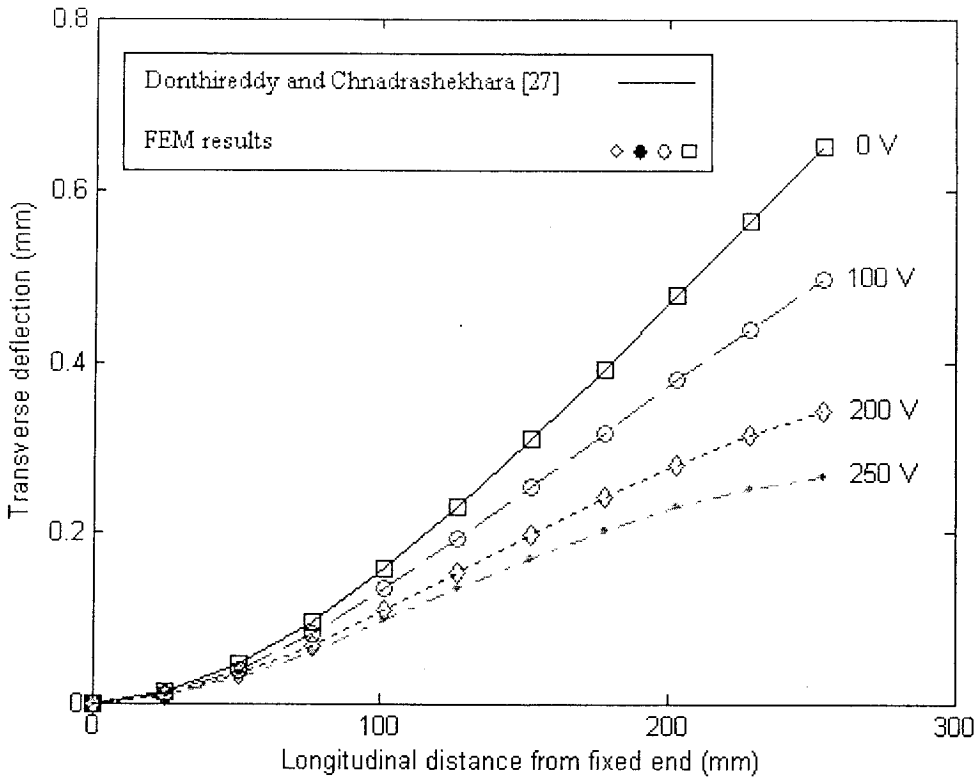

Figure 3.4-3: Effect of actuator voltage on transverse deflection of a cantilever beam subjected to uniformly distributed load – compared with the experimental results of Donthireddy and Chnadrashekhara [27]

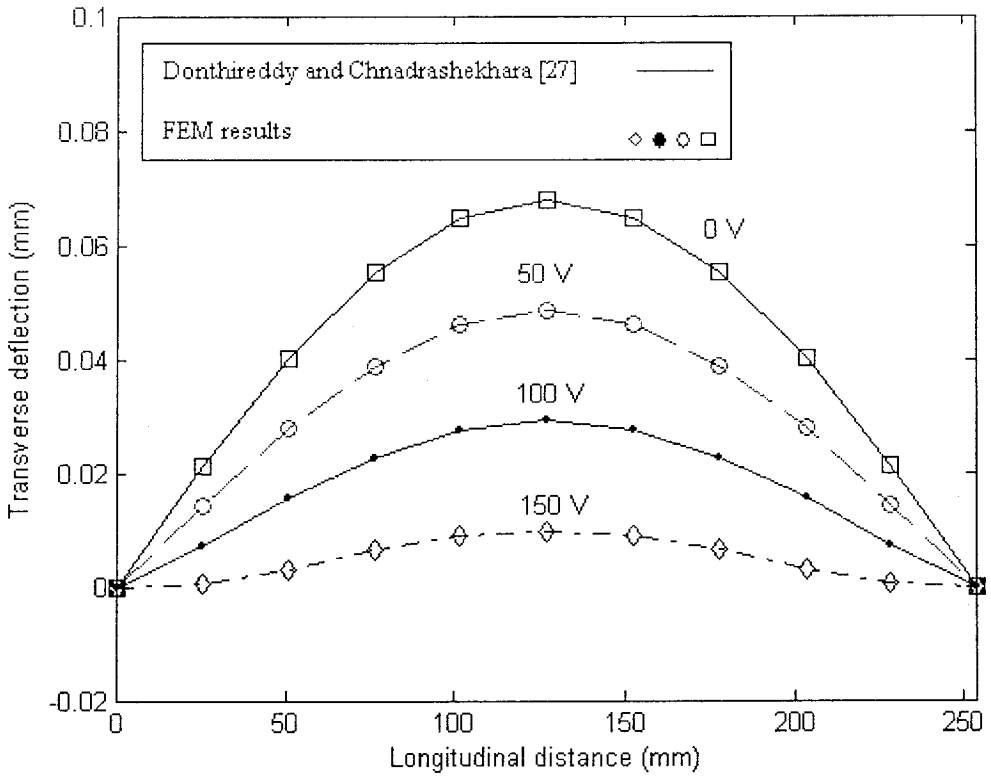

Figure 3.4-4: Effect of actuator voltage on transverse deflection of a simply supported beam subjected to uniformly distributed load- compared with the experimental results of Donthireddy and Chnadrashekhara [27]

As it can be observed, the results totally match with those in the literature [27]. Thus the finite element models are validated and the simulation results can be used with confidence in further analysis.

3.5 Parametric sensitivity study

3.5.1 Introduction

Here, the effect of various parameters such as location of piezoelectric patches, applied voltages and ply angles on the behavior of the piezo-laminated composite beam is investigated. The model used in all the following studies, is a laminated composite beam made of graphite/epoxy AS/3501-6 with two layers/patches of G-1195 piezoceramic actuators, bonded on the top and bottom surfaces of the beam. Unless it is clearly mentioned, the lay-up is $[Pz/0/90]_S$. Material properties are provided in Table 3.5-1

Table 3.5-1: Material properties

	PC5K lead zirconate titanate	G-1195 piezoceramic	AS/3501-6 Graphite-epoxy	AS4/3502 Graphite-epoxy
$E_1 \quad (N/m^2)$	60.24×10^9	63.0×10^9	144.23×10^9	131.0×10^9
$E_2 \quad (N/m^2)$	60.24×10^9	63.0×10^9	9.65×10^9	9.12×10^9
$G_{12} \quad (N/m^2)$	23×10^9	24.8×10^9	4.14×10^9	7.1×10^9
ν_{12}	0.31	0.28	0.30	0.34
$G_{13} \quad (N/m^2)$	-	-	4.14×10^9	7.1×10^9
$G_{23} \quad (N/m^2)$	-	-	3.45×10^9	5.92×10^9
$d_{31} \quad (m/V)$	-306.0×10^{-12}	-166.0×10^{-12}	-	-
$d_{32} \quad (m/V)$	-306.0×10^{-12}	-166.0×10^{-12}	-	-
$\rho \quad (Kg/m^3)$	7600	1800	1389.23	1600.23
Thickness (m)	0.0002	0.0002	0.000127	0.000127

The length and the width of the beam are assumed to be 0.254m and 0.0254m respectively, wherever it is not mentioned.

3.5.2 The effect of active stiffening on the natural frequencies of the beam

In this study, the alteration in the first three natural frequencies of the beam caused by a pair of piezoelectric layers, polarized in the same direction to stretch the beam, is investigated. The exact fundamental natural frequency of a simply-supported composite beam, stiffened by an axial tensile force N may be written as [3]:

$$\omega_n = \left(\frac{\pi}{L}\right)^2 \sqrt{\frac{D_{11}}{\rho H}} \sqrt{1 + \frac{N}{\left(\frac{\pi}{L}\right)^2 D_{11}}} \qquad \textbf{(3.5.1)}$$

To demonstrate the reliability of the finite element model, the fundamental natural frequencies are computed before and after active stiffening using the developed finite element model and are compared with the exact solution given by Equation 3.5-1. The active stiffening has been caused by applying the voltage of 200V to PZT actuators, creating an axial force of 4.54KN. The results are presented in Table 3.5-2.

Table 3.5-2:Comparison between fundamental natural frequency obtained by exact solution and finite element model for a simply supported beam, before and after stiffening

Fundamental natural frequency (Hz)				Error
Before stiffening		After stiffening		
Exact solution	FEM	Exact solution	FEM	
45.2	45.2	120	120	Negligible

Since the model proved robustly reliable, it is used to investigate the effect of applied voltage to the PZT actuators, length and position of the PZT patches on alteration in the

first three natural frequency of the beam. For this purpose, the following non-dimensional parameters are defined:

$$PL = \frac{L_P}{L} \qquad \textbf{3.5-1}$$

$$PP = \frac{L_{L2P}}{L} \qquad \textbf{3.5-2}$$

where L_P is the length of the PZT patches, L_{L2P} is the length from the support to the actuators and is the length of the beam as shown in Figure 3.5-1,

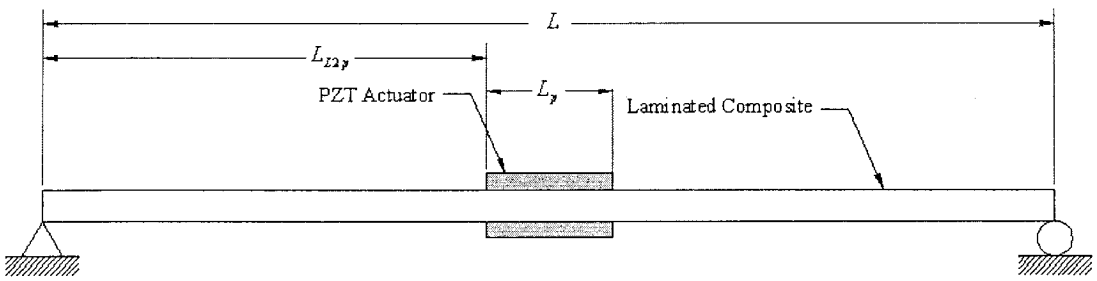

Figure 3.5-1: Two PZT actuators bonded to a piezo-laminated composite beam

To investigate the effect of the length of the actuator patches, a simply-supported beam is considered. The actuators are initially placed at the center of the beam and *PL* is increased from Zero (there are no actuators at all) to unity (the actuators cover the whole beam). Results are plotted in Figure 3.5-2 to Figure 3.5-5:

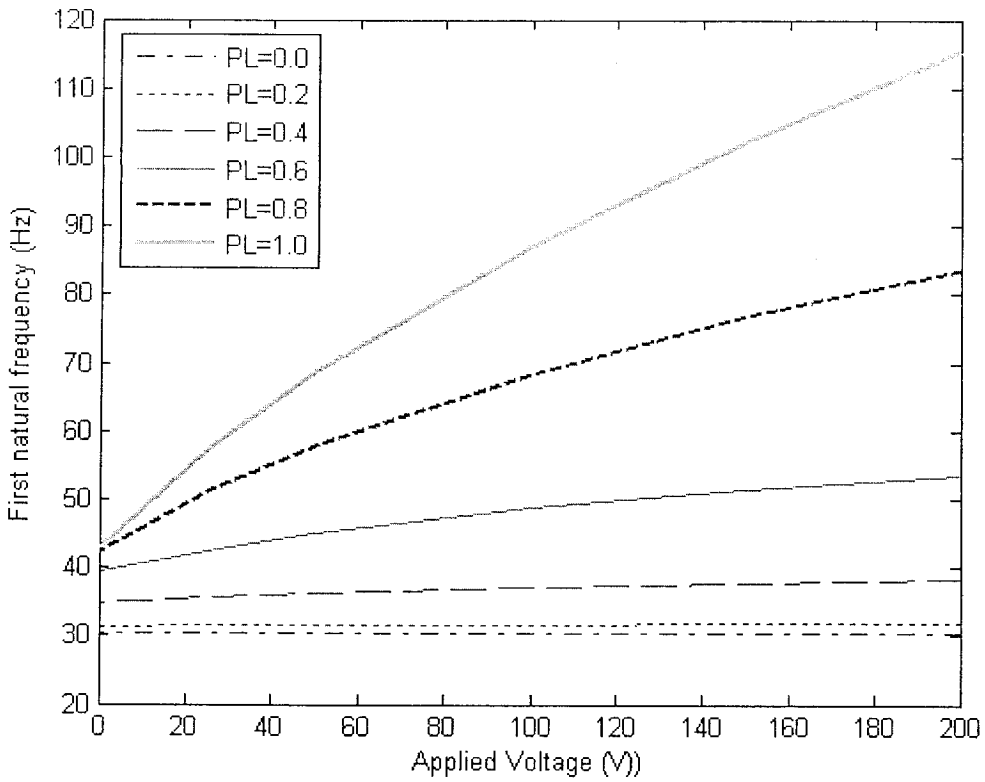

Figure 3.5-2: Variation of the fundamental natural frequency due to electrical voltage, for different PZT lengths in a simply-supported beam

Figure 3.5-2 shows that by increasing the length of piezoelectric patches, their ability to influence and therefore augment the first natural frequency of the beam increases. It is noted that with adding piezoelectric patches, with no applied voltage, can increase the first natural frequency as it will increase the stiffness of the overall system. It can also be seen that applying voltage to the patches when they are fully covered the beam can dramatically increase the first natural frequency to more than double. The result shows that for PL=0.2, the first natural frequency does not alter noticeably even for the applied voltage of 200V.

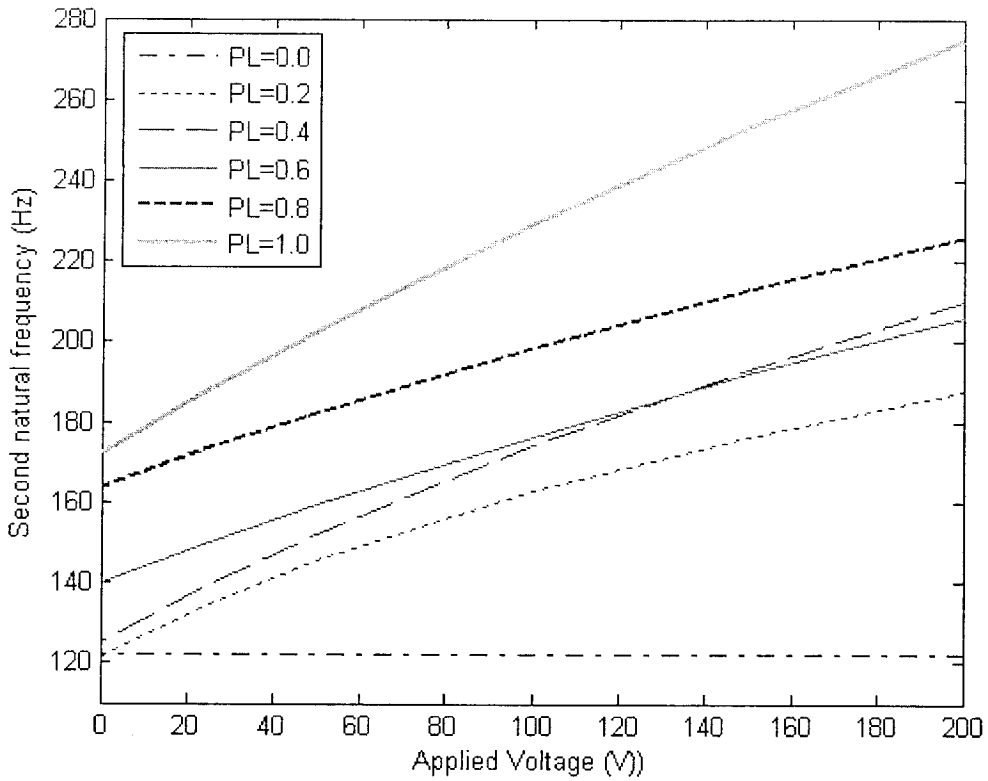

Figure 3.5-3: Variation of the second natural frequency due to electrical voltage, for different PZT lengths in a simply-supported beam.

The same analogy can be realized for the second and third natural frequencies shown in Figure 3.5-3 and Figure 3.5-4, respectively. Although the effect of active stiffening is not as drastic as it was on the first natural frequency, almost the same pattern can be found here. It must be noted that even a small patch of PL=0.2 can create a considerable effect on the second natural frequency.

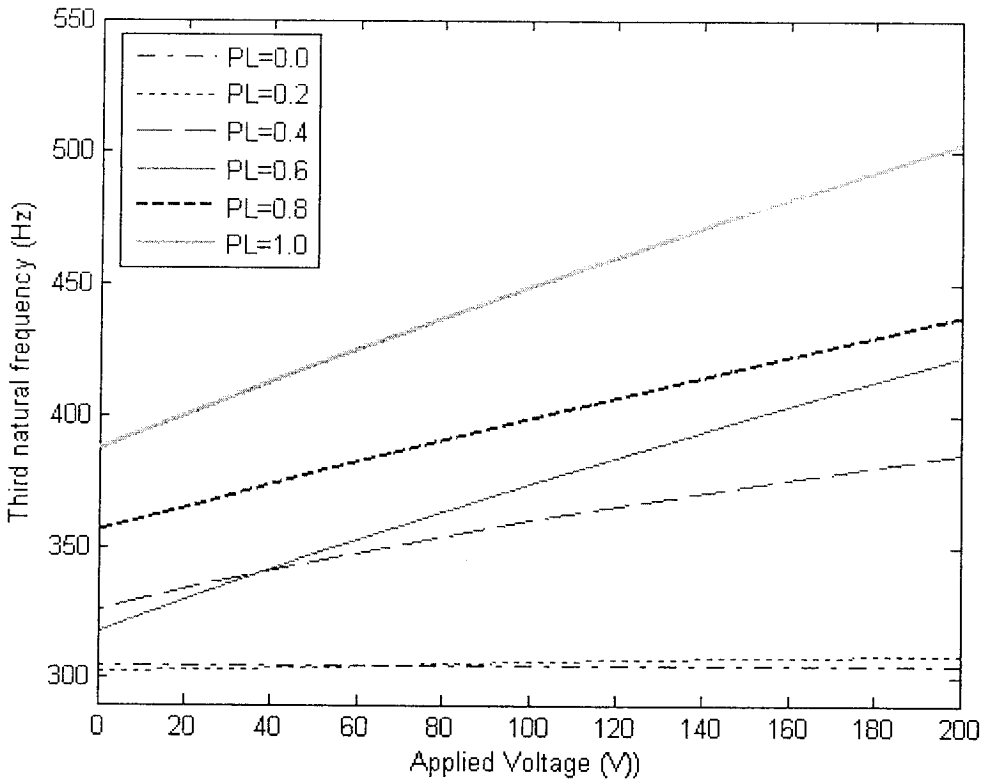

Figure 3.5-4: Variation of the third natural frequency due to electrical voltage, for different PZT lengths in a simply-supported beam.

To have an overall and conclusive idea, for the first three natural frequencies, the effect of piezoelectric patches when once there is no applied voltage (actuators acts only as a mass) and another time, when the voltage of 200V is applied on them, are plotted in Figure 3.5-5. From this Figure, the relation between the length of piezoelectric patches and their ability to alter the natural frequencies are more understandable.

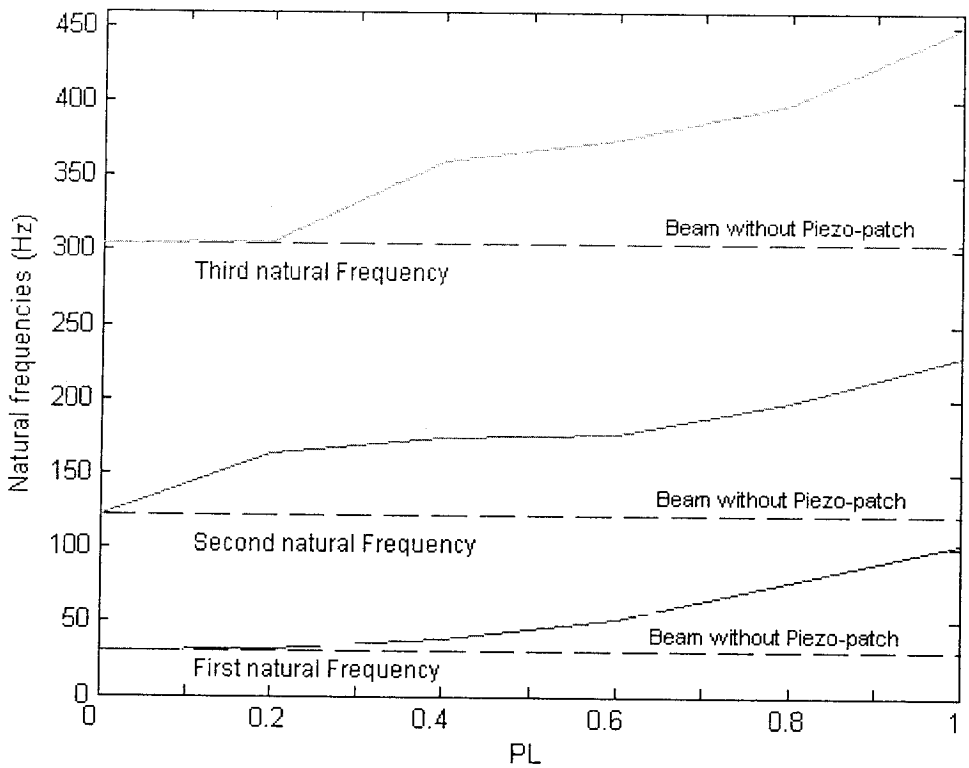

Figure 3.5-5: Effect of actuator's length on the first three natural frequencies of a simply-supported beam

Figure 3.5-5 shows that the effect of PZT patches on natural frequencies is directly related to the length of the patches. The maximum effect, in all three situations, is obtained when the actuators cover the whole beam.

In the second case, the effect of location of the piezoelectric actuators on the beam is investigated. In this case a simply-supported beam, as in Figure 3.5-6 a, is considered and the position of two pair of piezoelectric actuators (placed symmetrical with respect to middle of the beam) are subjected to change by altering the parameter *PP* from zero (where the actuators are located at the roots) to 6/7 (where the actuators are placed in the

middle of the beam), while total PL is constant and equal to 1/7. The results are shown in Figure 3.5-7 to Figure 3.5-10.

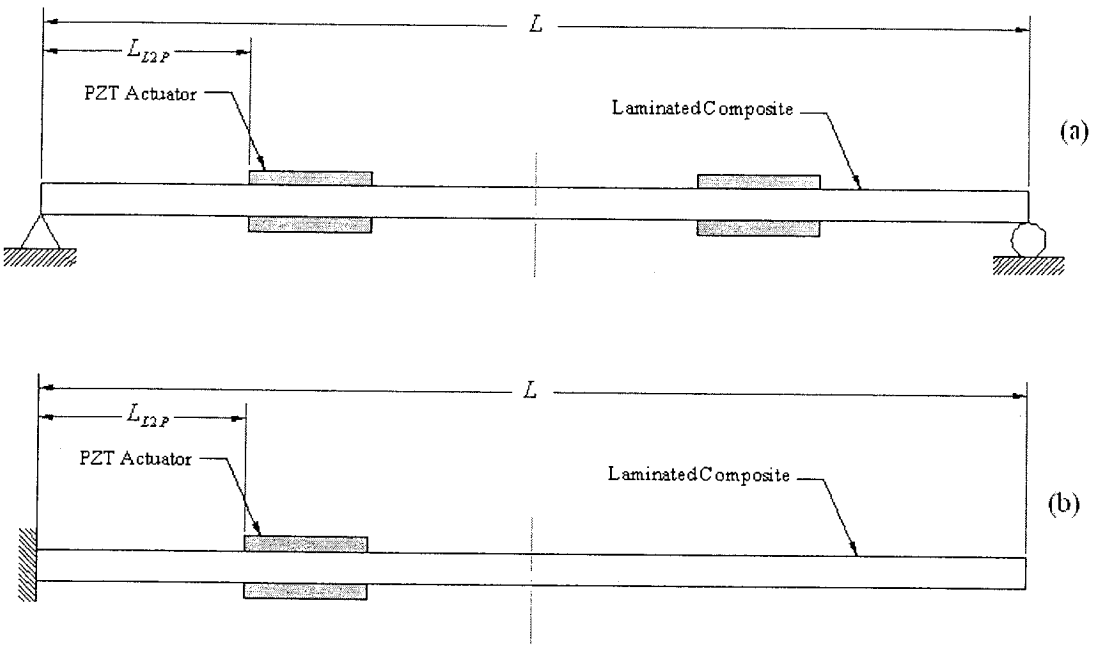

Figure 3.5-6: (a) Two sets of PZT actuators bonded to a simply-supported laminated composite beam, (b) one set of PZT actuators bonded to a cantilever laminated composite beam

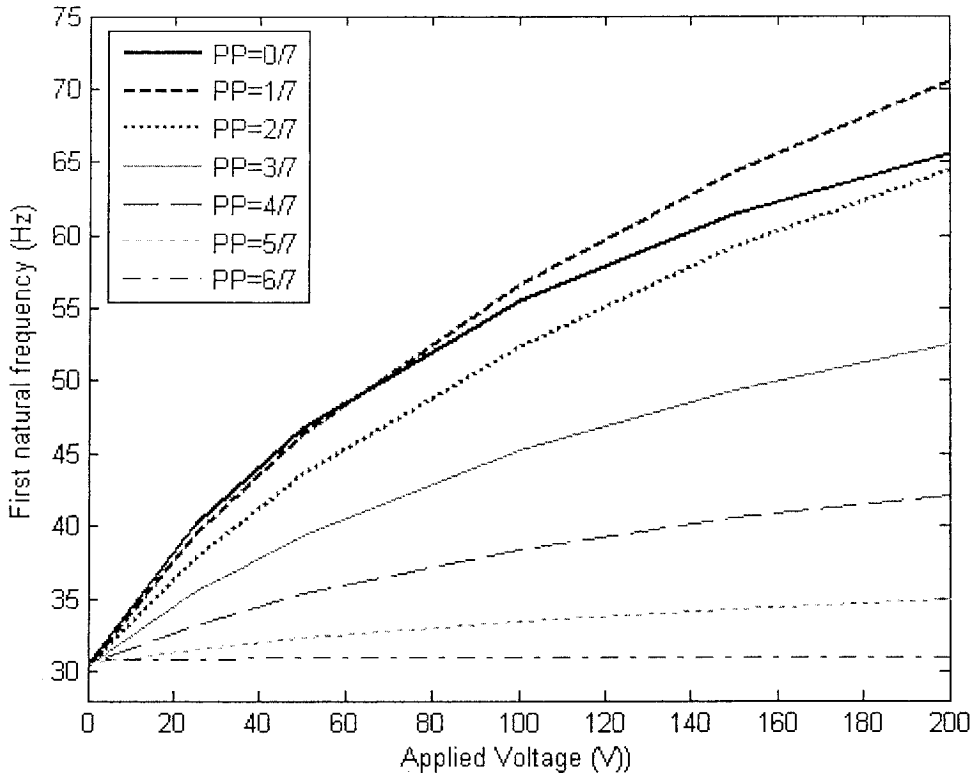

Figure 3.5-7 : The effect of actuator's position on the fundamental natural frequency of a simply-supported beam due to the applied electrical voltage to two pair of PZT with constant length of PL=1/7

Figure 3.5-7 shows that in a simply-supported beam, the actuators can have the most significant effect on the first natural frequency, when there are placed near the root. It also indicates that placing them in the middle of the beam, has little or no effect. In other words by moving actuators from roots toward the center of the beam, their effect on the fundamental natural frequency diminishes.

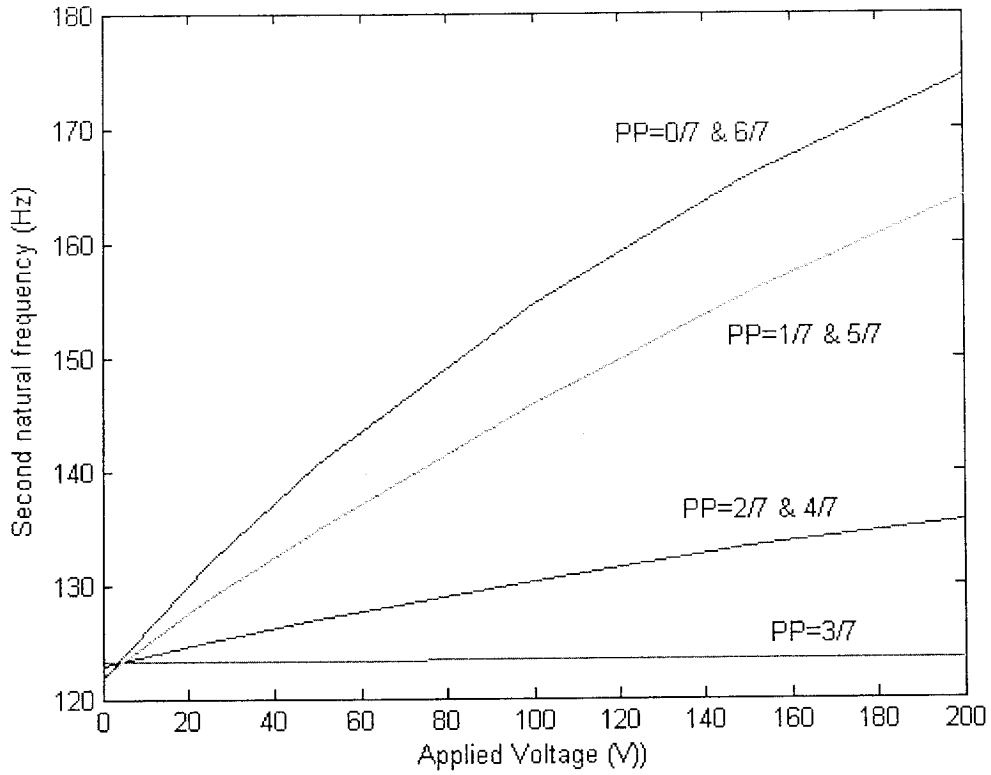

Figure 3.5-8: The effect of actuator's position on the second natural frequency of a simply-supported beam due to the applied electrical voltage to two pair of PZT with constant length of PL=1/7

Figure 3.5-8 shows that the effect of the location of piezoelectric actuators on the second natural frequency is utterly different. In this case, the roots and the middle are equally the best locations to place the actuators.

The effect of the actuator's location on the third natural frequency is shown in Figure 3.5-9. It is interesting to note that positioning the actuators in location PP=4/7 has the largest effect on the third natural frequency.

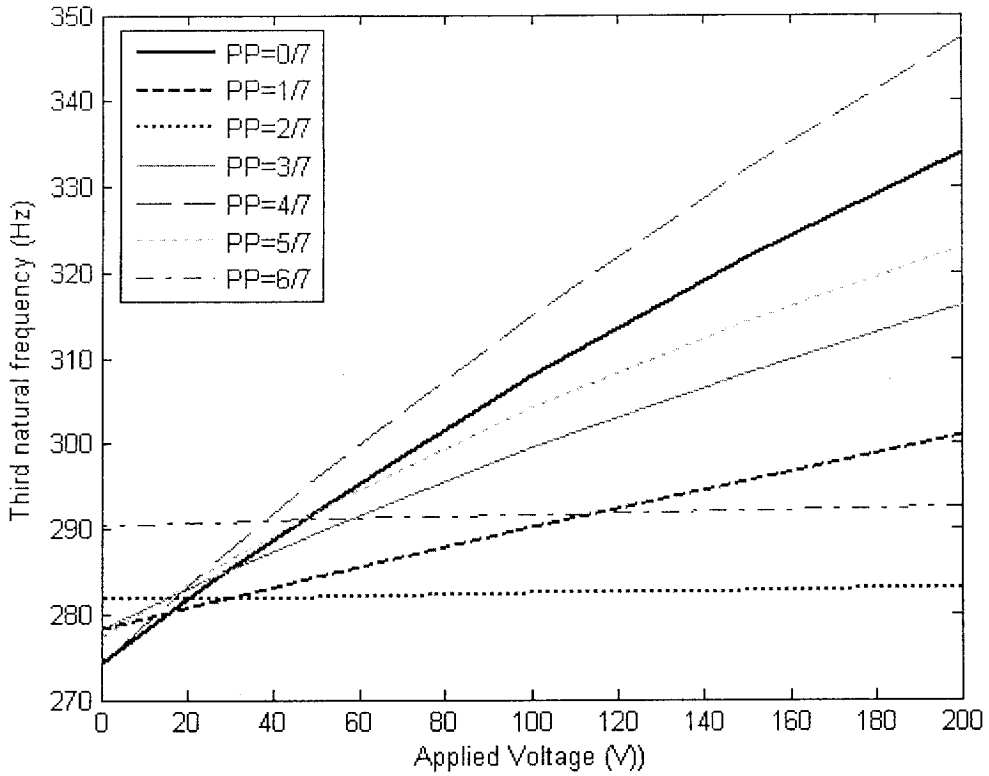

Figure 3.5-9: The effect of actuator's position on the third natural frequency of a simply-supported beam due to the applied electrical voltage to two pair of PZT with constant length of PL=1/7

To have a better overall view, the effect of location on all three natural frequencies are plotted for one applied voltage of 200V (and also when there is no voltage) in Figure 3.5-10.

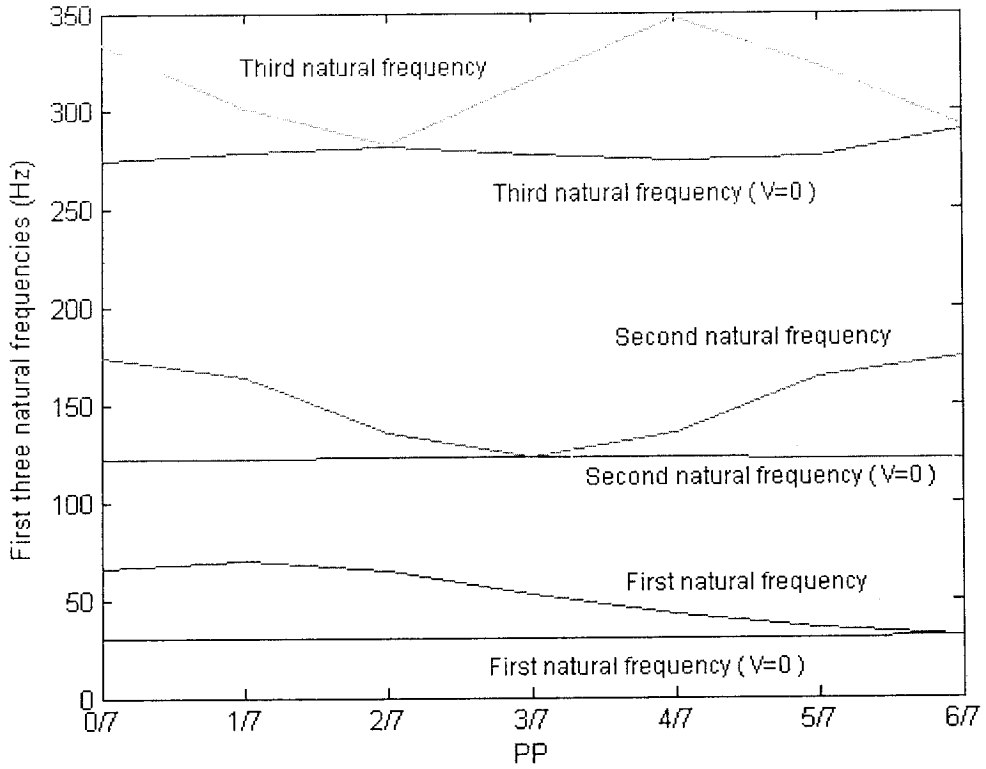

Figure 3.5-10: Effect of actuator's location on the first three natural frequencies of a simply-supported beam

As it can be realized, in general, locating the actuators close to the roots, makes them more effective on the first natural frequency than the middle of the beam. For the second natural frequency, the root and the middle are equally the most effective locations and finally, position PP=4/7 is the most effective location for the third natural frequency.

The same experiment is repeated with a cantilever beam shown in Figure 3.5-6 b, where the location of a pair of actuators are changed from zero (where the actuators are located at the roots) to 6/7 (where the actuators are placed at the tip of the beam), while the *PL* is

constant and equal to 1/7. Results are shown in Figure 3.5-11 to Figure 3.5-14.

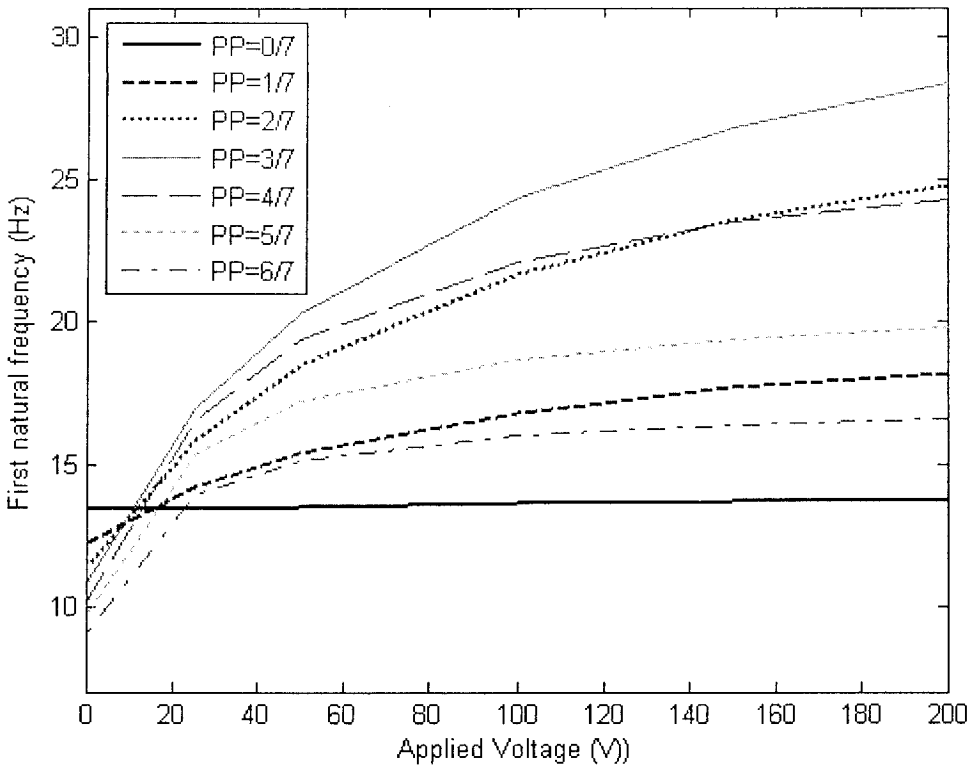

Figure 3.5-11: Variation of the fundamental natural frequency of a cantilever beam due to the applied electrical voltage to two pair of PZT with constant length of PL=1/7

By analyzing Figure 3.5-11, one may conclude that the middle of the cantilever beam is the best place for piezoelectric actuators and have the maximum effect on the first natural frequency. By approaching to the tip as well as the root of the beam, the effect of the actuators diminishes considerably.

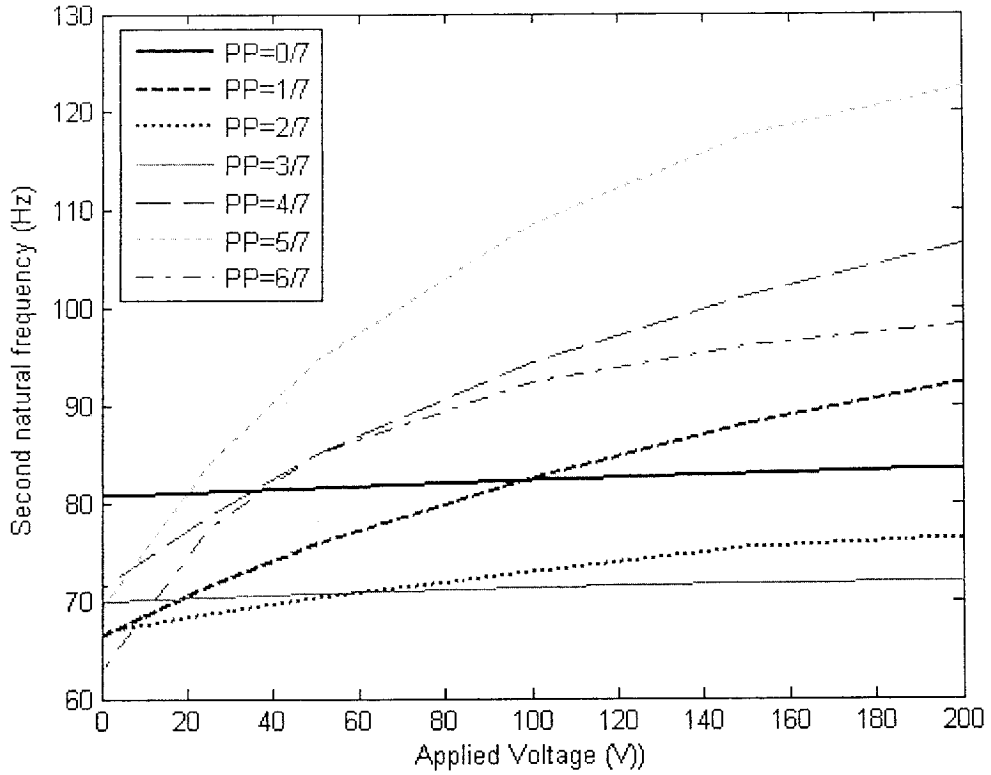

Figure 3.5-12: Variation of the second natural frequency of a cantilever beam due to the applied electrical voltage to two pair of PZT with constant length of PL=1/7

Examination of Figure 3.5-12 reveals that PP=5/7 is the location in which, Piezoelectric actuators have the most prominent effect on the second natural frequency. The locations near this optimum, which are PP=4/7 and PP=6/7, are the next suitable locations for placing the actuators to obtain a considerable effect on the second natural frequency.

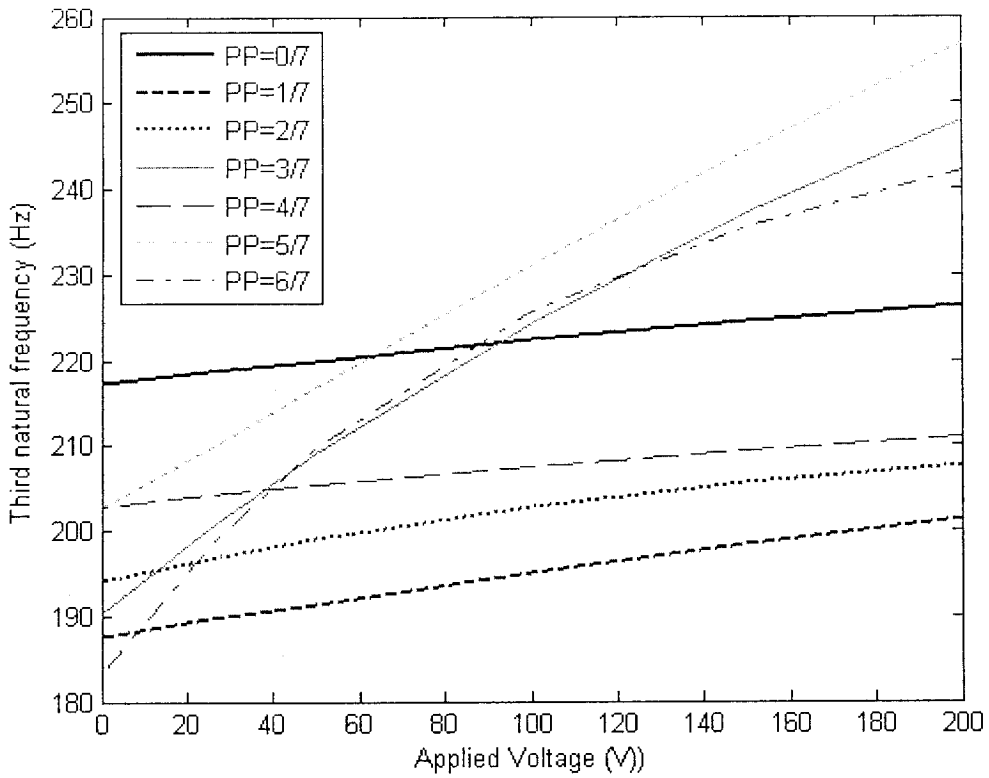

Figure 3.5-13: Variation of the third natural frequency of a cantilever beam due to the applied electrical voltage to two pair of PZT with constant length of PL=1/7

From Figure 3.5-13, it can be learn that PP=5/7 is the optimum location to place the piezoelectric actuators to alter the third natural frequency. Like the case of the second natural frequency, performing the active stiffening while the actuators have been placed near the root, has little or no effect on the third natural frequency.

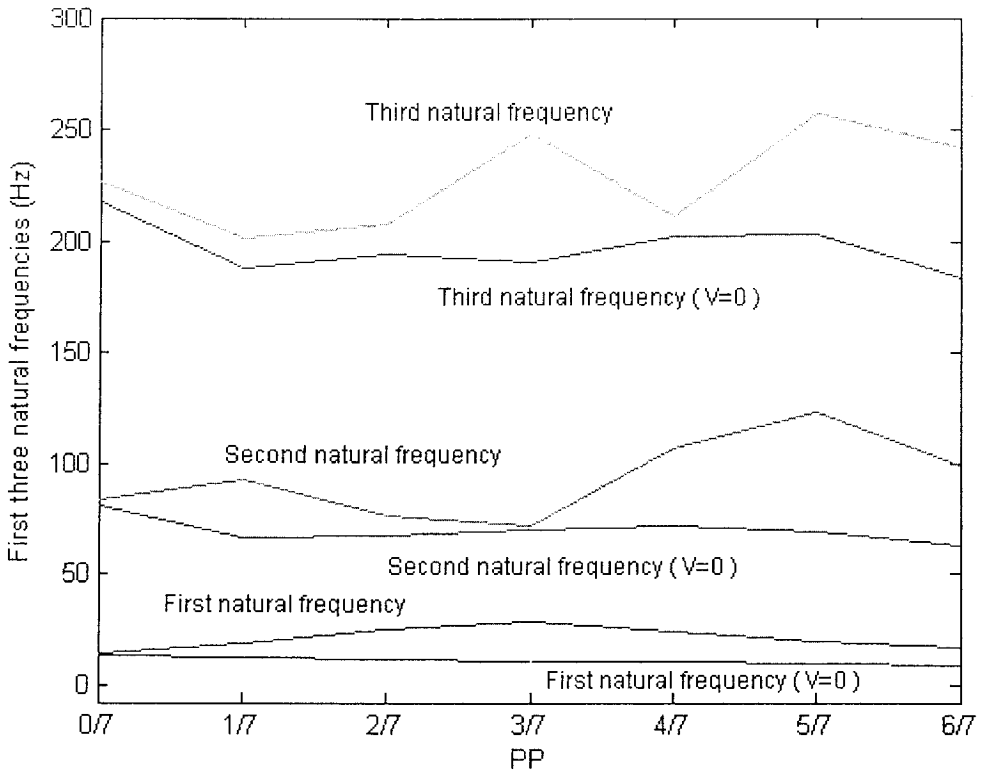

Figure 3.5-14: Effect of actuator's location on first three natural frequencies of a cantilever beam

The effect of location on all three natural frequencies may be better visualized in Figure 3.5-14, which shows the variation of the first three natural frequencies versus the location of the actuators for the given voltage of 200V. It can be seen that if the applied voltage equals zero then the actuators effect is as concentrated mass making the beam stiffer whenever placed closer to the root. When voltage is applied, placing the PZT actuators at the root has almost no considerable effect on the fundamental natural frequency whereas placing it at the tip, has even negative effect. By placing the PZT actuators, at the middle of the beam, they can considerably increase the fundamental natural frequency. Where as for second and third frequencies, PP=5/7 is the optimum location.

3.5.3 The effect of the location of the piezoelectric patches on the maximum deflection of a beam

In this study, the effect of actuator's location on the maximum deflection is investigated. Non-dimensional maximum deflection of the beam (with respect to the optimum point) when the top patch is polarized in the direction of the applied voltages of 200 V, and the bottom patch is polarized in the direction opposite to that of the applied voltage versus the location of the piezoelectric actuators with respect to the root (using the same PP notation as the previous section) is plotted in Figure 3.5-15, for both simply-supported and cantilever beam. The length of the actuators are assumed to be constant (LP=1/7).

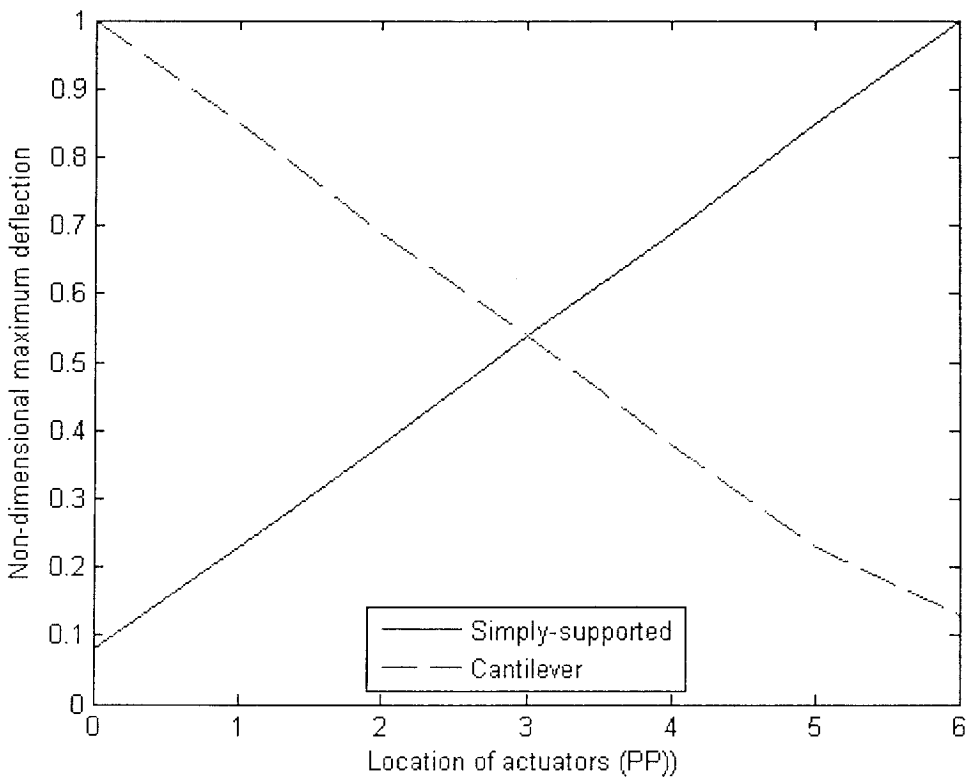

Figure 3.5-15: Non-dimensional maximum deflection of a cantilever and a simply-supported beam subjected to an applied voltage of 200 V, versus the location of piezoelectric actuators.

As Figure 3.5-15 shows for a cantilever beam, the optimum locations of actuators for maximizing deflections are close to the root and as piezoelectric actuators move to the tip of the beam, their efficiency in creating bending moment decreases drastically. For a simply-supported beam, the pattern is totally different. The actuators are the most efficient when they are placed at the middle of the beam and moving them toward the root makes the piezoelectric patches least efficient.

3.5.4 The effect of active stiffening on transient response of the beam

In this study, the effect of impact on a piezo-lamiated cantilever beam (Figure 3.5-16) is investigated by applying a step load of 1N force in the period of 1ms. The transient response of the beam a) when 0V voltage and b) when 100V voltage is applied to piezo-actuators, is presented in Figure 3.5-17.

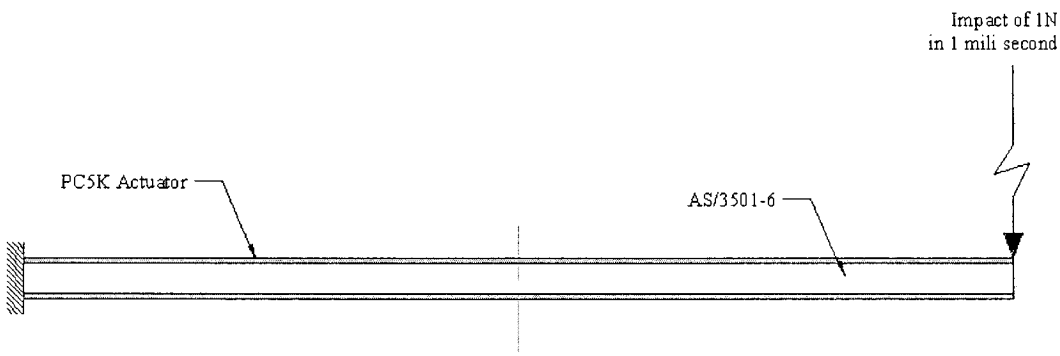

Figure 3.5-16: Cantilever piezo-laminated composite beam under impact loading at the tip.

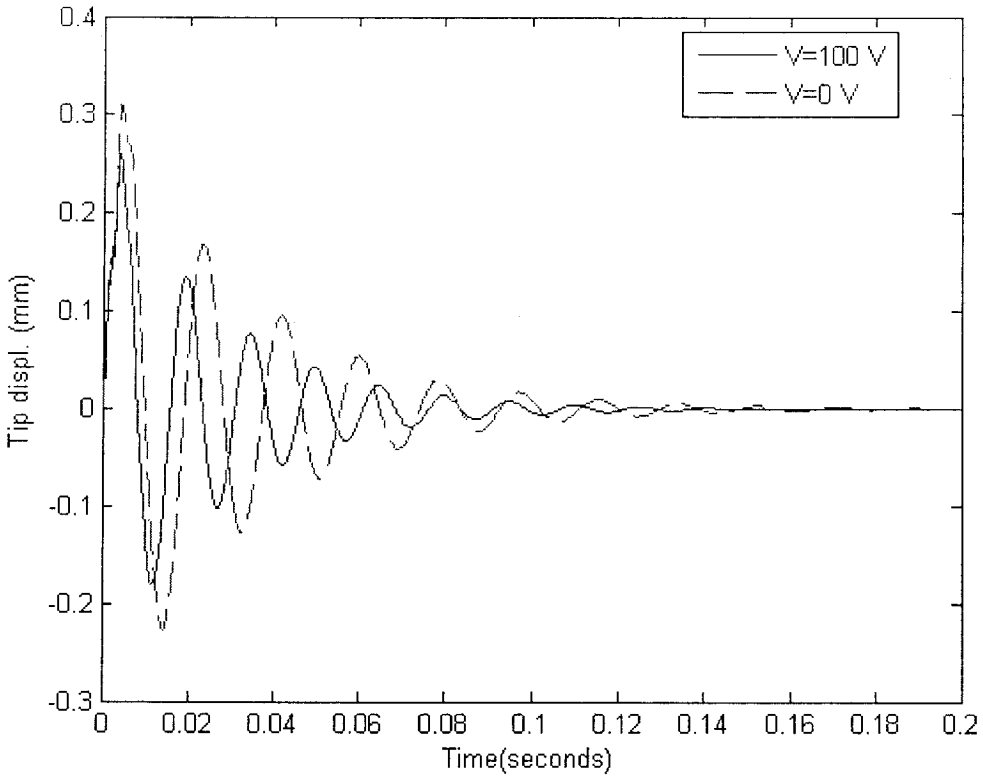

Figure 3.5-17: Transient response of a piezo-laminated cantilever beam to an step load of 1N in 1ms, with and without active stiffening

The materials are AS/3501-6 Graphite epoxy and PC5K lead zirconate titanate and the lay-up sequence is $[Pz/0_5/90_5]_S$.

It can be seen that if piezoelectric actuators are used to stiffen the piezo-laminated beam, not only the frequency increases but also the amplitude of the response to an impact can be decreased significantly. Both of these alteration can directly contribute to better damping characteristic and improved structural performance due to an impact.

4 Optimization

4.1 Introduction

One of the most important aspects of design activities in almost all disciplines is optimization. In the modern mechanical engineering, the importance of increasing the performance in every product, through design and manufacturing process, has been accentuated in today's competitive market since it can serve directly to make more efficient, accurate, environmental-friendly products with cheaper prices and less energy consumption. Aerospace industry was one of the first disciplines to intensively use optimization as a necessity in design procedure due to tremendous cost of carrying unnecessary weight in aerospace vehicles. However, the optimization is getting more popular in other industries as increasing the computational power of modern computers and introduction of more accurate and efficient optimization algorithms make the investment on the optimization more and more justifiable alongside with environmental concerns that force the designers to think about more efficient and less pollutant products, regardless of the economical aspects.

4.2 Optimization fundamentals

In the following, the most essential terminologies in optimization have been represented:

Design variables: Design variables are entities that identify a particular design. In the search for the optimal design, these entities will change over a prescribed range. In applied mathematical terminology, design variables serve as the unknown of the problem

being solved. The set of design variables is identified as the design vector.

Objective function: Design optimization problem is defined using an objective function which usually has to be minimized or maximized and must depend, explicitly or implicitly, on the design variables.

Constraint functions: As design functions, these will be influenced by the design variables. The format of these functions requires them to be compared to some numerically limiting value that is established by design requirement, or the designer. This value remains constant during the optimization of the problem. The constraint function can be classified as equality constraints or inequality constraints. Problems without constraints are called unconstrained problems. If constraints present, then meeting them is more necessary than the optimum. Constraint satisfaction is crucial before the design established by the current value of the design variables is considered valid and acceptable. If constraints are not satisfied, also called 'Violated', then there is no solution.

Side constraints: Side constraints express the range for the design variables. Each design variables must be bound by numerical values for its lower and upper limit.

The Standard format for an optimization problem can be expressed as:

Minimize $f(x_1, x_2, ..., x_n)$ (Objective function)

Subject to $h_k(x_1, x_2, ..., x_n) = 0 \quad , \quad k = 1,2,...,l$ (Equality constraints)

$g_j(x_1, x_2, ..., x_n) \leq 0 \quad , \quad j = 1,2,...,m$ (inequality constraints)

$x_i^l \leq x_i \leq x_i^u \quad , \quad i = 1,2,...,n$ (Side constraints)

Based on the above-mentioned definition, an optimal solution is one that has met the design objective while it remains in the feasible domain (is satisfying all the constraints).

4.2.1 Optimization Technique

Here the Sequential Quadratic Programming (SQP) method has been used to solve the design optimization problems. The computer implementation of the algorithm has been performed in MATLAB environment. SQP is one of the most powerful methods among the mathematical nonlinear programming techniques [48]. Using this method, Newton's method for constrained optimization can be closely mimicked just like that of unconstrained optimization. Using quasi-Newton updating method, the Hessian of the Lagrangian function has to be approximated in each iteration to create a Quadratic Programming (QP) sub-problem. The solution of the QP sub-problem is used to form a search direction for a line search procedure. One should consider that the SQP is indirectly based on the solution of the KKT conditions. An overview of the SQP is found in Arora [48] and Fletcher [49].

The main idea is to generate a QP problem based a quadratic approximation of the Lagrangian function described as:

$$L(\boldsymbol{x},\lambda) = f(\boldsymbol{x}) + \sum_{i=1}^{m} \lambda_i . g_i(\boldsymbol{x}) \qquad \textbf{4.2-1}$$

It should be noted that the bound constraints have been expressed as inequality constraints in derivation of the Lagrangian in Equation 4.2-1. The SQP implementation in MATLAB consists of three main steps: (I) a QP Sub-problem solution; (II) a line search

and objective function calculation, and (III) updating of the Hessian matrix of the Lagrangian function given by Equation 4.2-1. At each major iteration, a QP sub-problem expressed below is solved.

$$\text{Minimize } \frac{1}{2} d^T H_k d + \nabla f(x_k)^T d \qquad \textbf{4.2-2}$$

$$\nabla g_i(x_k)^T + g_i(x_k) = 0 \qquad i = 1 \ldots m_e$$
$$i = m_e + 1 \ldots m$$

where $d \in \Re$

The solution of the sub-problem (any QP algorithm can be used to solve the sub-problem), generates an estimate of the Lagrange multiplier, λ, and a search direction vector d_k in each iteration k, which is used to from a new iteration as:

$$x_{k+1} = x_k + \alpha_k d_k \qquad \textbf{4.2-3}$$

The step length parameter α_k should be determined by using an appropriate line search technique (one-dimensional minimizations) in order to produce a sufficient decrease in the merit function. At the end of the one-dimensional minimization, the Hessian of the Lagrangian, required for the solution of the next positive definitive quadratic programming problem, is updated using the Broyden-Fletcher-Goldfarb-Shanno (BFGS) updating formula as:

$$H_{k+1} = H_k + \frac{q_k q_k^T}{q_k^T s_k} - \frac{H_k^T s_k s_k^T H_k}{d_k^T H_k d_k} \qquad \textbf{4.2-4}$$

where:

$$s_k = x_{k+1} - x_k \qquad \textbf{4.2-5}$$

$$q_k = \nabla L(x_{k+1}, \lambda_k) - \nabla L(x_k, \lambda_k) \qquad \textbf{4.2-6}$$

and H_{k+1} is the approximate of the Hessian of L at x_{k+1}.

Powel [50] recommends keeping the Hessian, positive definite even though it may be positive indefinite at the solution point. If H_k is positive definite, then H_{k+1} obtained using Equation 4.2-4 is also positive definite if $q_k^T s_k$ is positive at each iteration. However, when the Lagrangian has a negative curvature at (x_{k+1}, λ_{k+1}), $q_k^T s_k$ is not positive anymore. To guarantee that the updated Hessian matrix H_{k+1} remains positive definite, Powell suggests replacing q_k by:

$$\theta q_k + (1-\theta) H_k s_k \qquad \textbf{4.2-7}$$

Where:

$$\theta = 1 \qquad \text{if } s_k^T q_k \geq 0.2 s_k^T H s_k$$

$$\theta = \frac{0.8 s_k^T H s_k}{s_k^T H s_k - s_k^T q_k} \qquad \text{if } s_k^T q_k < 0.2 s_k^T H s_k \qquad \textbf{4.2-8}$$

Additional details on the algorithm may be found in Ref. 50.

4.2.2 Local and global optimum

When non-linear programming optimization techniques such as SQP is being used, it is probable that the algorithm finds the local Minima instead of global one as Figure 4.2-1 shows.

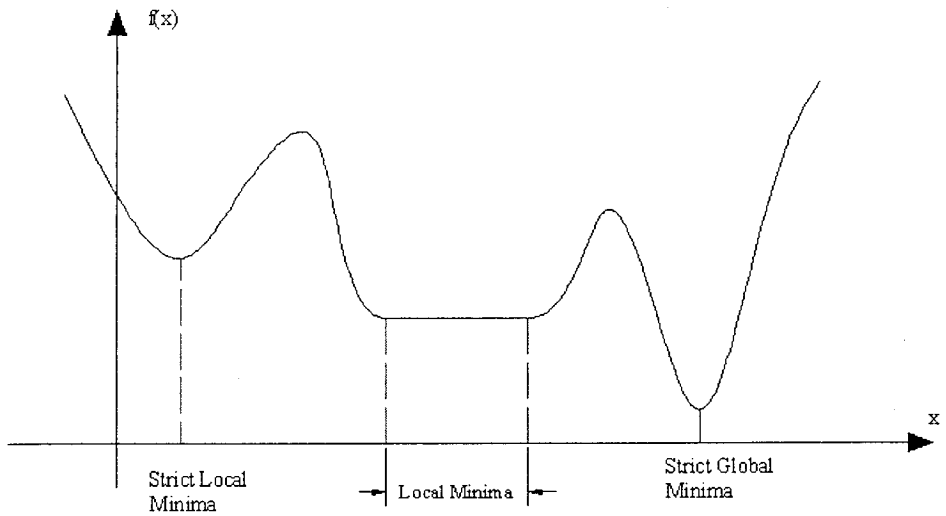

Figure 4.2-1: Local and Global minima in one dimension

In other words the mathematical programming techniques may get trapped in local optima, without having a mechanism to climb out of it. These methods may fail to discover the global optimum. In this study, to alleviate this problem, optimization algorithm has been executed for multitude of random initial points in an attempt to catch the global optimum point. This issue will be fully clarified in Example 4-3.1.

It is noted that there are non-gradient based methods such as Genetic Algorithms [51] and Simulated Annealing [52] which are able to capture the global optimum solution; however they may not be computationally efficient.

4.2.3 Objectives

In the following parts of the Chapter, two main categories of problems are investigated:

1. Shape control problems: In which, applied voltages on piezoelectric actuators are considered as variables to minimize the objective function which is the mean-square error between the actual and the desired shape of the beam. The target of this optimization is to obtain a set of appropriate voltages which can result in the closest shape possible for the beam to the desired shape.

2. Mass Minimization: In which the weight of the structure is subjected to optimization by changing the thicknesses of composite layers and/or actuators as design variables where various constrains are applied.

Some applications of piezo-laminated beams as a precise shape controller in which, optimization techniques are directly used to solve the problems are also investigated.

Table 4.2-1 demonstrates guidelines for the five different optimizations investigated in this research study. All the necessary programs in this Chapter are developed in MATLAB environment.

Table 4.2-1: General guidelines for five different optimizations

	Objective Function	Constraint(s)	Design Variable(s)	Additional information
1	Minimize the mean square error between actual and desired shape of a simply supported beam under uniform loading	Upper and lower limits on design variables	Voltages applied to each pair of piezoelectric actuators	Using 3 pairs of actuators
2	Minimize the mean square error between actual and desired shape of a cantilever beam	Upper and lower limits on design variables	Voltages applied to each pair of piezoelectric actuators	Using 5 pairs of actuators
3	Minimize the mass of a cantilever beam subjected to a uniform load	Tip deflection, Lower limit on thicknesses	Thickness of the actuators and composite layers	
4	Minimize the mass of a cantilever beam	First three natural frequencies, lower limit on thicknesses	Thickness of the actuators and composite layers	With and without active stiffening
5	Minimize the mass of a cantilever beam subjected to an impact	Maximum amplitude and fundamental natural frequency of response, lower limit on thicknesses	Thickness of the actuators and composite layers	With and without active stiffening

4.3 Static shape control of a piezo-laminated beam

This example is used to investigate the application of the static shape control optimization for beams. For this purpose, a beam, with three pairs of surface bonded piezoelectric actuators, is subjected to uniform load of 1000 N/m^2 and transverse deflections in certain control points are measured. The objective is to find the appropriate electric voltages that should be applied to the three pairs of piezoelectric actuators in order to minimize the mean-squared error between the actual shape (measured in 9 control points along the beam), and the desired shape of the beam while the upper and lower limits of ± 200 V are considered for the applied voltages. Material properties for the beam and the actuators can be found in Table 4.3-1.

Table 4.3-1: Material properties

	PC5K lead zirconate titanate	S-Glass/Epoxy
$E_1 \quad (N/m^2)$	60.24×10^9	55.0×10^9
$E_2 \quad (N/m^2)$	60.24×10^9	16×10^9
$G_{12} \quad (N/m^2)$	23.0×10^9	7.6×10^9
ν_{12}	0.31	0.28
$G_{13} \quad (N/m^2)$	-	7.6×10^9
$G_{23} \quad (N/m^2)$	-	7.6×10^9
$d_{31} \quad (m/V)$	-306.0×10^{-12}	-
$d_{32} \quad (m/V)$	-306.0×10^{-12}	-
$\rho \quad (Kg/m^3)$	7600	2000.0

Illustrative example 4.3-1: In the first attempt a simply-supported beam, as shown in Figure 4.3-1, is considered. Lamination sequence is $[0^\circ/45^\circ/-45^\circ]_S$ and beam is made of S-Glass/Epoxy layers with surface mounted PC5K (Lead Zirconate Tiatnate) actuators.

Thicknesses for both laminate and actuators are considered to be 0.5 mm.

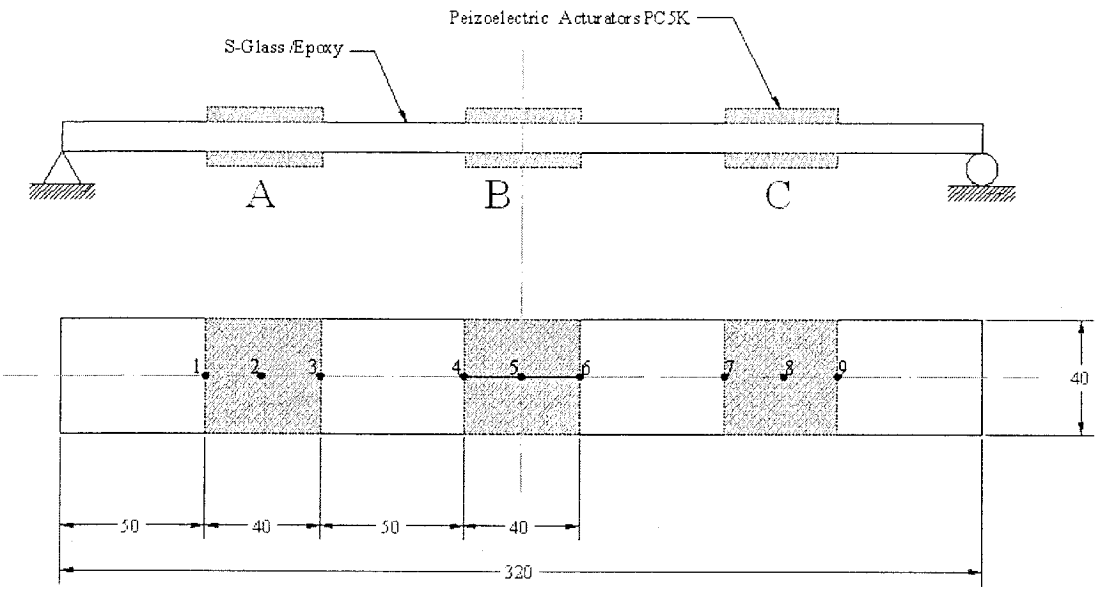

Figure 4.3-1: A simply-supported beam with three pairs of piezoelectric actuator patches

The initial, optimized and desired shapes of the beam are presented in Table 4.3-2. Table 4.3-3 provides the appropriate voltages to be applied to each pair of piezoelectric patches to obtain the minimized mean-squared error between the actual and desired shape.

Table 4.3-2: Transverse deflections of the control points of the beam

Control points	1 and 9	2 and 8	3 and 7	4 and 6	5	Mean-squared error %
Desired shape (mm)	0.400	0.580	0.730	0.900	0.920	-
Initial shape (mm) V=0	0.422	0.564	0.694	0.875	0.883	0.0813
Optimized shape (mm)	0.428	0.573	0.710	0.900	0.919	0.0504
Error (Before optimization) %	5.5	2.8	4.9	2.8	4.0	-
Error (After optimization) %	7.0	1.2	2.7	0.7	0.1	-

Table 4.3-3: Electric voltages applied to the actuator pairs (V)

Initial design			Final design		
Pair A	Pair B	Pair C	Pair A	Pair B	Pair C
0	0	0	-24.5	75.3	-24.5

As it was mentioned before, choosing the wrong initial point can easily lead the optimization algorithm to be trapped in local minima(s). One way of avoiding local minima(s), is using multitude of random initial points and choosing the best solution obtained, until all optimal solutions converge to one unique solution. Figure 4.3-2 shows the iteration history of the objective function (minimization of the mean-square error between actual and desired shape of the beam) versus number of iteration using different random initial points. In the first attempt, only one random initial point is taken, where in the other attempts, five, ten, twenty and more random initial points are taken respectively

and optimum point is chosen as the minimum of the minimums. As Figure 4.3-3 indicates, if twenty or more random initial points (for this problem) are being chosen, optimal solution can be found in every attempt. In this Chapter, above-mentioned technique has been used for all of the optimizations, to catch the global optimum.

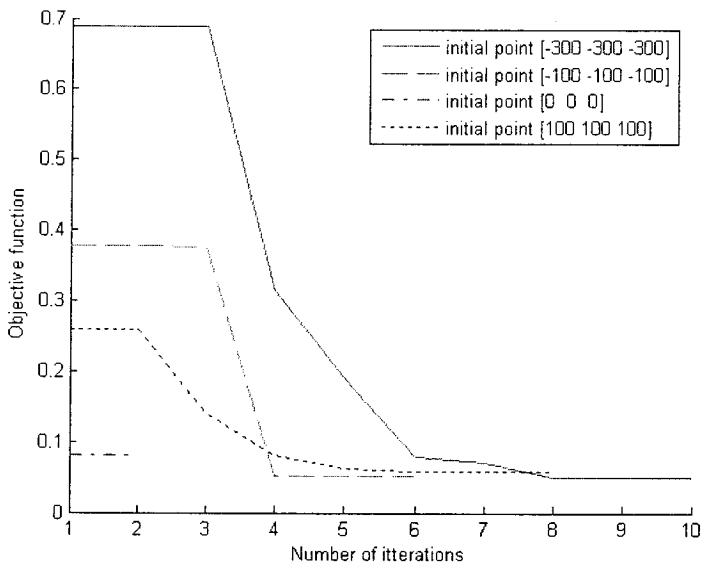

Figure 4.3-2: Finding optimal solution using various initial points

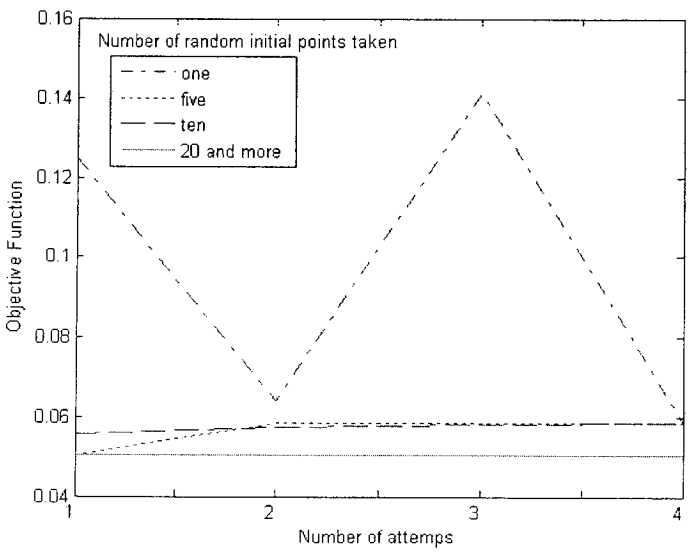

Figure 4.3-3: The effect of number of random initial points taken on the chance of finding global minimum

Illustrative example 4.3-2: This time, shape control procedure is applied on a cantilever beam with five pairs of piezoelectric actuators (as shown in Figure 4.3-4). In this example, six control points, five on mid-point of each actuator and the sixth one on the tip of the beam, are considered to monitor and control the deflections. The desired and optimized (controlled) shape of the beam are given in Table 4.3-4 and also shown in Figure 4.3-5. Appropriate set of voltages to achieve the desired shape can be found in Table 4.3-5.

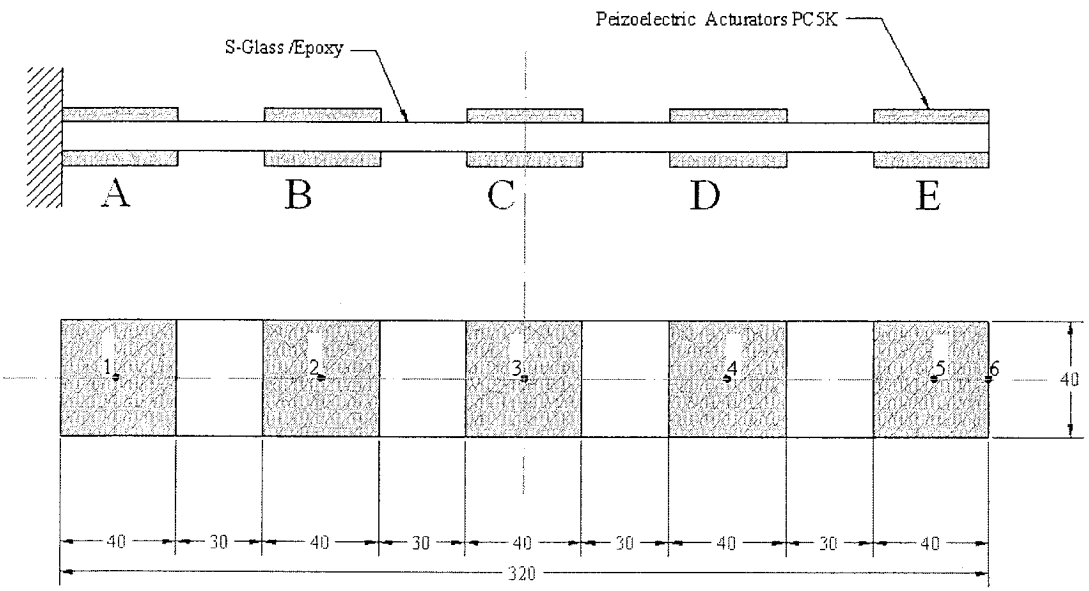

Figure 4.3-4: A cantilever beam with five pairs of piezoelectric actuator patches

Table 4.3-4:Transverse deflections of the control points of the beam (desired shape I)

Control points	1	2	3	4	5	6	Mean-squared error
Desired shape I (mm)	-0.006	-0.100	0.000	0.100	0.200	0.250	-
Initial shape (mm) V=0	0.000	0.000	0.000	0.000	0.000	0.000	0.350
Optimized shape (mm)	-0.008	0.100	0.000	0.100	0.200	0.250	0.002

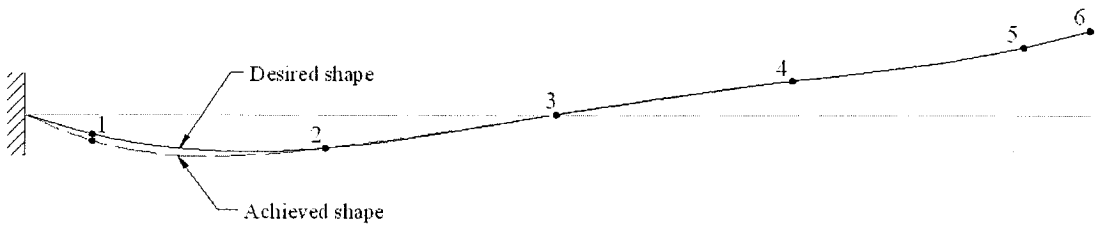

Figure 4.3-5: Desired and achieved shape of a cantilever beam

Table 4.3-5: Electric voltages applied to the actuator pairs (V)

Initial design					Final design				
Pair A	Pair B	Pair C	Pair D	Pair E	Pair A	Pair B	Pair C	Pair D	Pair E
0.0	0.0	0.0	0.0	0.0	101.4	-204.2	17.3	-0.2	-123.7

As it can be seen, the shape control is achieved within an acceptable tolerance, using the five pairs of piezoelectric actuators. Thus the mathematical model developed in chapter 3 combined with optimization technique can predict efficiently and accurately the required voltages to be applied on piezoceramic actuators (within the reach of the actuators power) in order to achieve a prescribed desired shape for adaptive laminated composite beam.

4.4 Mass Reduction of a piezo-laminated beam

In the following examples, the overall mass of a piezo-laminated beam is subjected to minimization by changing the thicknesses of both composite layers (S-Glass/Epoxy) and piezoelectric actuators (PC5K), while different constraints are applied for each optimization. It must be noted in some optimization, actuators are used to create bending moment (by polarizing the top layer in the direction of the applied voltage and the bottom layer in the direction opposite to that of the applied voltage) where as in other cases, actuators are used to stretch the beam (by polarizing both actuators in the direction of the applied voltage) and in a procedure called Active Stiffening (See 3.5.2 and 3.5.4).

Illustrative example 4.4-1: In the first optimization of this set, the mass of a cantilever adaptive composite beam subjected to a tip point load of 100 N (shown in Figure 4.4-1) is to be minimized, while the tip deflection of the beam, measured at the point 1, should remain smaller than 0.5 mm. The initial thicknesses for composite layers and actuators are 4.6 and 4.5 mm, respectively and the total mass of the structure is 0.9037 Kg and half of the beam's length is covered with actuators (PL=0.5).Table 4.4-1 shows the results of the optimization. It must be noted that the voltage of 240 V is applied to the actuators in order to help maintaining the deflection within the allowable limits. The lower limit of 0.1 mm is considered for both laminate and actuator's thicknesses. The lay-up sequence is $[45/-45]_S$.

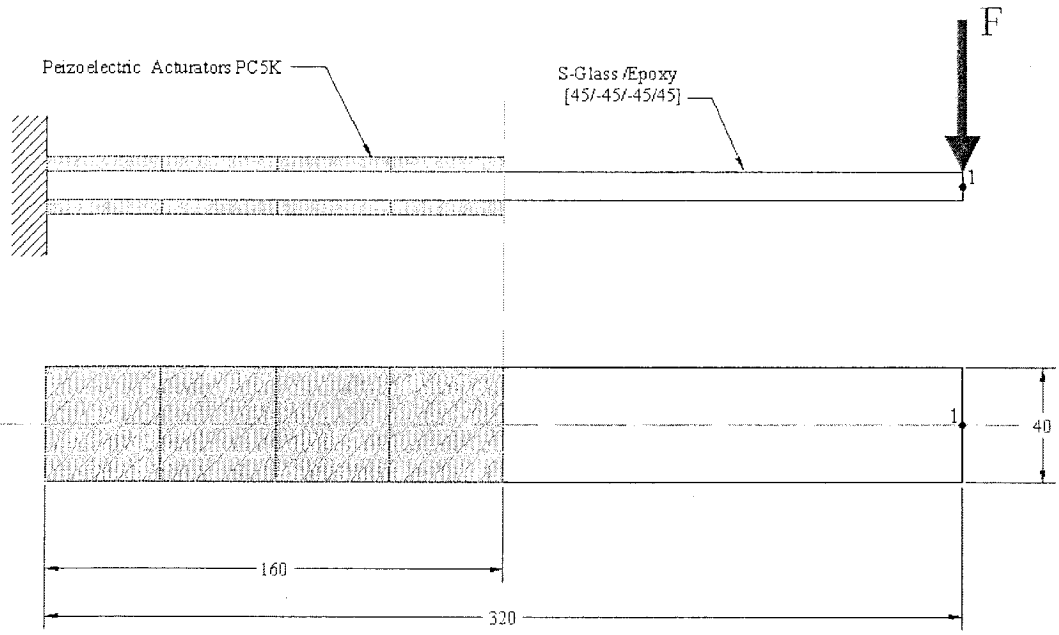

Figure 4.4-1: A piezo-laminated cantilever beam, with a tip point load of 100 N and applied voltage of 240 V, subjected to mass minimization

Table 4.4-1: Results of the overall mass minimization

Initial Values			Optimized Values		
Thicknesses		Mass (g)	Thicknesses		Mass (g)
Composite layers (mm)	Actuators (mm)		Composite layers (mm)	Actuators (mm)	
4.6	4.5	903.7	5.7	1.2	704.8

Results show the tip deflection of -0.5 mm (deflection constraint is active) and overall mass reduction of 22% in optimized structure.

Illustrative example 4.4-2: In the second optimization, a cantilever adaptive composite beam with three pairs of piezoelectric actuators as shown in Figure 4.4-2 is considered. Laminate is made of 6 layers, each with thickness of 1 mm and stacking sequence of $[45/-45/0]_S$. The thickness of each actuator is 0.1 mm. The objective function is to reduce the mass of the structure, by reducing the thicknesses of composite layers while

the first three natural frequencies are being monitored, as a constraint, not to fall below a certain boundary (First Natural Freq > 40 Hz, Second Natural frequency > 215 Hz and Third natural frequency > 580 Hz) . The optimization is being executed once where there is no voltage applied on the actuators and the second time when the voltage of 300 V is applied on each pair of actuators in a way that it polarizes both actuators in the direction of the applied voltage and therefore, increases natural frequencies of the structures by active stiffening of the structure. The results of the both optimizations can be seen in Table 4.4-2. It must be noted that the actuators placement is to make them most effective on increasing the first three natural frequencies (see section 3.5.1).

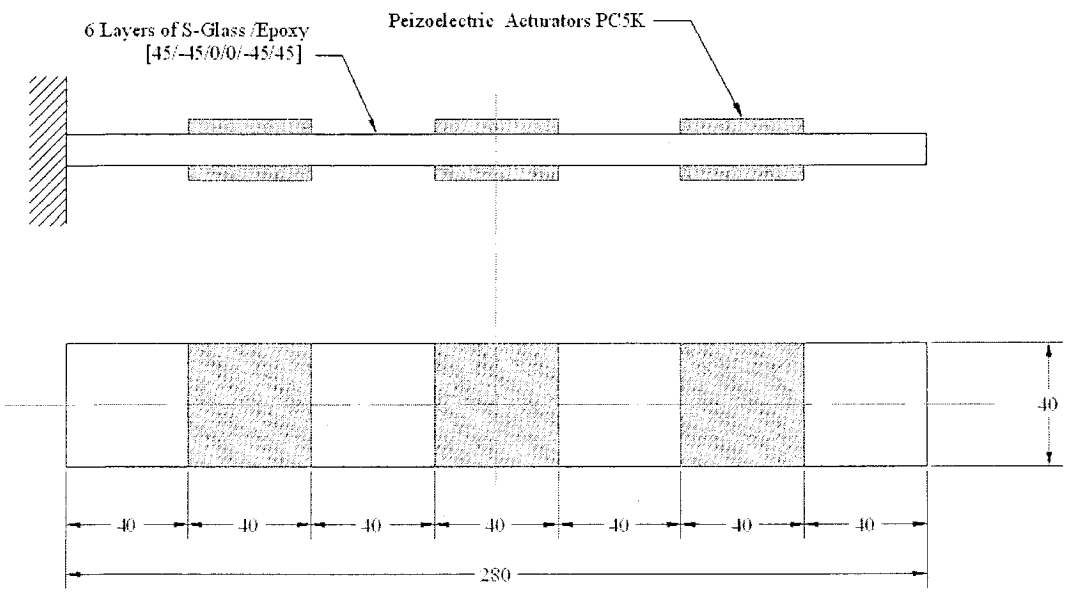

Figure 4.4-2: A piezo-laiminated cantilever beam, subjected to mass minimization with and without active stiffening

Table 4.4-2: Initial and optimized thicknesses and masses of a cantilever beam

	Thickness (mm)	Overall Mass (g)
Initial design	1.00	141.7
Optimized - without active stiffening (V=0)	0.836	119.6
Optimized -with active stiffening (V=300 V)	0.668	97.1

As Table 4.4-2 shows that the overall mass reductions of 31.5% for optimized structure with active stiffening with respect to initial designs are achieved, respectively, whereas achieved mass reductions without active stiffening with respect to initial designs is only 15.6%, respectively. The natural frequencies at the optimum point are shown in Table 4.4-3. In both cases, the optimum point is within the feasible region.

Table 4.4-3: The first three natural frequencies at the optimum point

	Without active stiffening (V=0)	With active stiffening (V=300 v)
First natural frequency (Hz)	40.0	43.8
Second natural frequency (Hz)	251.13	216.0
Third natural frequency (Hz)	705.5	580.0

Illustrative example 4.4-3 : In the third optimization of this set of optimizations, the same beam shown in Figure 4.4-2, is subjected to an impact step load of 10 N on its tip, applied during the period of 1 ms. The overall mass of the structure is minimized, while the maximum amplitude of the dynamic response is bound to be less than 2.5 mm and the fundamental natural frequency of the system is monitored not to be smaller than 40 Hz. Optimization has been accomplished, with and without active stiffening and the results are given in Table 4.4-4.

Table 4.4-4: Initial and optimized thicknesses and masses of a cantilever beam

	Thickness of each layer (mm)	Overall Mass (g)
Initial design	1.00	141.7
Optimized - without active stiffening (V=0)	0.83	119.4
Optimized -with active stiffening (V=300 V)	0.31	48.9

Table 4.4-4 shows that the overall mass reduction of 65.5% has been achieved using active stiffening (V=300 V) where as only 15.7% of this mass reduction would be

possible without it (V=0 V). The fundamental natural frequency and the maximum amplitude of the response at the optimum point can be found in Table 4.4-5. As it can be seen, in neither of cases, constraints in have not been violated.

Table 4.4-5: The fundamental natural frequency and maximum amplitude of the response at the optimum point

	Without active stiffening (V=0)	With active stiffening (V=300 v)
First natural frequency (Hz)	40	42.1
Maximum amplitude (mm)	1.2	2.5

4.5 Using Piezo-laminated beam for precise position control

Piezo-laminated beams can be used for precise control of sophisticated devices in wide range of applications. Exactness and controllability of piezoelectric actuators, compared to electro-motors and other substitutes, make them a wise choice for such applications. Although only relatively small displacements can be achieved using piezoelectric actuators, this would be sufficient in many applications. For instance, in elaborate tools for surgery or digital cameras and projectors and clearance monitoring in jet turbines and so on, relatively small amount of displacement can perform the job. Moreover, in some other applications like laser scanners used in suspension system of high-tech automobiles, in airplane's auto-pilot system or satellite's reflectors and transmitters, considerable distant between the source and the target, will result in large amount of coverage despite of very small deflections in source. Piezoelectric actuators can also be used alongside with other types of position controllers, and act as a precise controller to finish the job.

Here, two example of such exact position controlling is investigated. These examples, although schematic, can be used as a starting point to design elaborate mechanism for

real-world engineering applications.

Figure 4.5-1 shows a cantilever adaptive laminated compiste beam, designed to control the location of point P (where the laser beam, passing through a set of fiber optics, embedded at the center line of the beam, hits the target plane). The beam is covered with two sets of pizoceramic actuators which can be controlled with two separate voltages, V1 and V2. As the figure shows, the location of point P on the target plane can be calculated as follow:

$$D = w_{Tip} - d\tan(\theta_{Tip}) \qquad \textbf{4.5-1}$$

Where D is the distance of the point P from the center line (initial point), w_{Tip} and θ_{Tip} are the deflection and the angle of tip point of the beam with respect to center line and d is the distance between end point of the beam and the target plane.

Now, the appropriate set of voltages (V1 and V2), should be applied to the actuators in order to achieve the desired point P, can be obtained by solving an optimization problem in which the difference between the actual D and the desired D should be minimized as an objective function and applied voltages are the variables where transverse deflection of the middle point of the beam, should not exceed a certain limit (due to some space limits in the design of the device, in which the beam is supposed to be installed).

In this example, the thicknesses of actuators and composite laminates are 0.5 and 0.1 mm respectively, lay-up sequence is $[45/-45/0]_S$, the distance d is considered to be 100 mm

and the deflection of the middle of the beam should not exceed 1.2 mm while the laser beam should hit the target plane with distance of 6.3 mm from the base point.

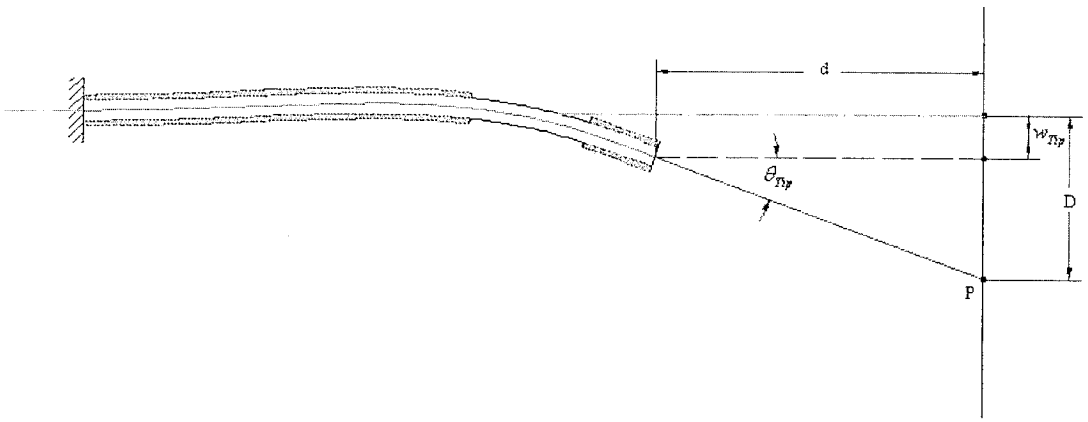

Figure 4.5-1: A piezo-laminated cantilever beam with embedded fiber optics

Results show that by applying the voltage of V1=-92.2 V to the first set of actuators and V2=-61.4 V to the second set, the desired point can be exactly achieved while the constraint is not violated.

In the second example in this category, another schematic mechanism is being analyzed.

In the second example in this category, another schematic mechanism is being analyzed.

Figure 4.5-2 shows a reflector, attached to a simply-supported piezo-laminated beam. By applying voltage to two layers of surface bonded piezoelectric actuators, the angle of the reflector can be precisely controlled. By minimizing the absolute difference between the actual and desired angle of the reflector, in an optimization problem, appropriate voltage that should be applied to the set of actuators for achieving the desired angle can be calculated. It must be noted that the voltage is considered as the design variable of the optimization problem.

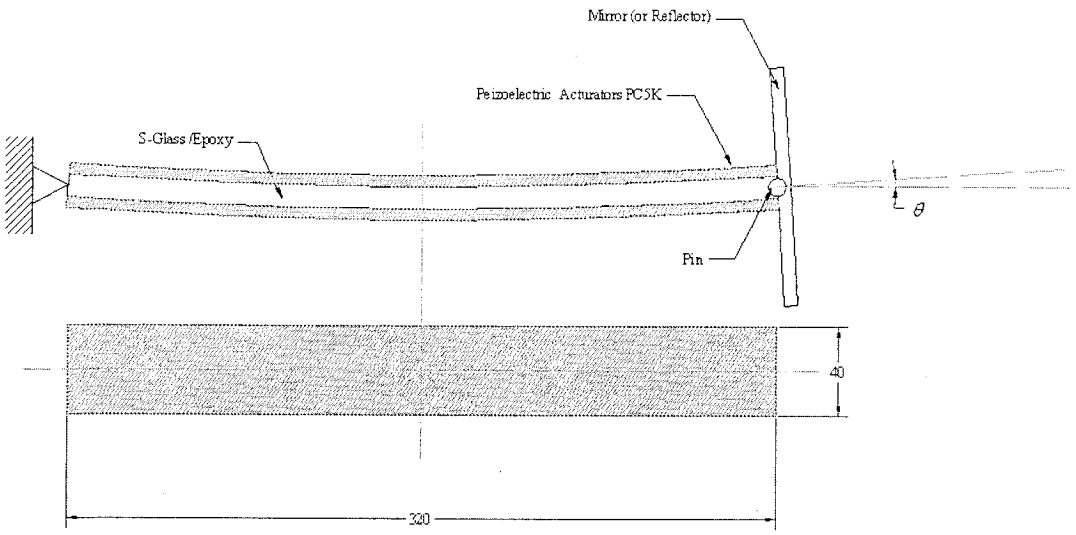

Figure 4.5-2: A piezo-laminated structure for controlling a reflector

Again for this example the thicknesses of each actuators and composite laminates are assumed to be 0.5 and 0.1 mm, respectively and the lay-up sequence is $[45/-45/0]_S$. The result shows that the voltage of 85.9 V must be applied in order to achieve the desired angle of 0.8 degree.

5 Conclusions and future works

5.1 Introduction

In this study, an efficient finite element model has been developed using classical plate lamination theory (CLPT) and first-order shear deformation theory (FSDT) to investigate the static and dynamic behavior of a laminated composite beam. The model has been validated by comparing the results with those obtained by exact solutions as well as the results available in literature. Since the model proved to be robustly reliable, it has been used to investigate overall dynamic response of a laminated composite beam.

Later, using the above mentioned theories, the finite element model has been modified to investigate the static and dynamic interaction between piezoelectric actuators and host laminated composite structure. Piezoelectric actuators have been used to create bending moment for shape control purposes as well as active stiffening to change the natural frequencies and amplitude of the dynamic response.

Finally, the developed analysis tools have been used to conduct the design optimization procedure using Sequential Quadratic Programming (SQP) technique. Two sets of constrained optimizations have been performed: 1-Shape control problems in which the mean-square error between the actual and desired shape has been minimized while the applied voltages to actuators have been set as the design variables and 2- Mass reduction problems in which the mass of the structure has been subjected to minimization by changing the thickness of composite layers and/or piezoelectric actuators. In both cases,

different constraints have been introduced to the optimization problems. The optimization techniques have also been used to find the appropriate voltages to control the shape of a piezo-laminated beam and to control a laser beam or a reflection mirror with precision.

5.2 Conclusions

The most important conclusions and contributions of the current work are as follows:

1. Although CLPT is robust and reliable theory while the structure is subjected to static load and the length-to-thickness ratio of the beam is relatively large (in fact in this situations, the difference between the results obtained by both theories are almost negligible), the theory encounters significant errors for the relatively thick beam and for the dynamic loading where higher modes of actuations (and natural frequencies) should be taken into accounts. Failure to predict the higher modes of actuation with precision also makes CLPT unable to predict the overall response of the beam to an impact.
2. By using piezo-electric patches as active stiffener, it is possible to change the stiffness of a piezo-laminated beam and therefore, later the natural frequencies and buckling load. The results show that the length and position of piezoelectric patches has a direct effect on active stiffening and subsequently on natural frequencies, buckling load and dynamic response of the structure.
3. The response of the beam to an impact can be also improved using active stiffening technique. By making the beam stiffer, not only the frequency increases but also the maximum amplitude of the response can be decreased and faster

damping is achievable.

4. The optimum locations for piezoelectric actuators to create the maximum bending effect are close to the root for cantilever and in the middle for simply-supported beam.
5. By minimizing the mean-square error between the actual and the desired shape of a beam, elaborate shape controls are achievable for piezo-laminated beam
6. Overall mass of the structure can also be reduced dramatically while piezoelectric actuators (by creating bending moment or active stiffening where it is needed) help the structure to maintain its characteristics within certain limits to meet the design conditions
7. A cantilever beam is used to control the point, created by a laser beam on the target wall. This is achieved by applying the appropriate voltages to a set of piezoelectric actuators, bonded on top and bottom of the laminated beam. The voltages are obtained by optimizing the distance between the actual and the desired point through an optimization process. Also a simply supported adaptive composite beam designed to control a reflection mirror precisely by applying appropriate voltages to the piezo actuators.
8. Sequential Quadratic Programming (SQP) does not guaranty the global optimum point (in fact for non-convex set, it is almost impossible to distinguish the local optimum from the global one). To alleviate this problem, initial points have been generated randomly. By randomly introducing multitude of starting point, in a loop, it has been found that the global optimum, if exits, can be achieved by monitoring the convergence of the results to a single point, after a certain number

of iterations. By using this methodology, non-linear programming and classical optimization techniques may be used to find the global optimum.

5.3 Future works

Although important steps towards the understanding of the analysis and design optimization of the adaptive laminated composite beam have been accomplished in this thesis, other important and intersecting subjects for the future work are identified as follows:

1. The piezoceramic actuators are mounted on the surface of the adaptive campsite beam in this study, it would be interesting to formulate the problem to show their effects when they are embedded in the structure.
2. Using piezoceramics as both sensors and actuators for vibration suppression applications through appropriate control strategy.
3. Using more refined finite element models such as layerwise theory to predict accurately transverse shear and normal stresses through the thickness. This is specifically important to study delamination between host structure and piezoceramic actuators.
4. Using global non-gradient optimization techniques such as Genetic Algorithm and Simulated Annealing to find the global optimum point in the studied design optimization problems and comparing the results with the gradient based mathematical programming technique.
5. Extending the formulation and application to plate and shell types of structure.

References

[1] Hyer, M. W., "Stress analysis of fiber-reinforced composite materials", WCB ,Mcgraw-Hill

[2] Jones R. M., "Mechanics of composite materials", 1999, Taylor & Francis

[3] Reddy J. N., "Mechanics of laminated composite plates", 1997, CRC press

[4] S. Abrate, S., "Impact on composite structures",1998, Cambridge university press

[5] Pieftort V., "Finite element modeling of piezoelectric active structure"

[6] Lee S. J., Reddy J. N., Rostam-Abadi F., "Transient analysis of laminated composite plates with embedded smart-material layers", Finite elements in analysis and design, in press.

[7] Reddy J.N., "On laminated composite plates with integrated sensors and actuators", Engineering structures, 21, 1999, 568-593

[8] Ghosh K. and Batra R. C., "Shape control of plates using piezoelectric elements", AIAA, 33, 1995, 1354-1357

[9] Eisenberger M. and Abramovich H., "Shape control of non-symmetric piezolaminted composite beam", Composite structure, Vol. 38, No. 1-4, 565-571,1997

[10] Abramovic H., "Deflection control of laminated composite beams with piezocermaic layers-closed form solution", Composite structures, 43, 1998, 217-231

[11] Ray M. C., Bhattacharya R. and Samanta B., "Exact solutions for static analysis of intelligent structures", AIAA, 31, No. 9, 1993, 1684-1691

[12] Aldraihem O., Khedir A., "Precise deflection analysis of beams with piezoelectric patches", Composite structures, 60, 2003, 135-143

[13] Wang Z., Chen S.,Han W., "The static shape control for intelligent structures", Finite element in analysis and design, 26, 1997, 303-314

[14] Varadarajan S., Chandrashekhara K. and Agarwal S, "Adaptive shape control of laminated composite plates using piezoelectric materials", AIAA journal, Vol. 36, No. 9, September, 1998

[15] Chattopadhyay A. and Seeley E., "A higher order theory fro modeling composite laminates with induced strain actuators", Composite part B, 28B, 1997, 243-252

[16] Ha, Kyu S., Keilers Ch. and Chang F., "Finite element analysis of composite structures containing distributed piezoelectric sensors and actuators", AIAA, 30, 1992, 772-776

[17] Hwang W. and Park H. C., "Finite element modeling of piezoelectric sensors and actuators", AIAA, 31, No. 5 1993, 930-937

[18] Detwiler D.T., Shen M.H.H., Venkayya V.B., "Finite element analysis of laminated composite structures containing distributed piezoelectric actuators and sensors", Finite elements in analysis and design, 20, 1995, 87-100

[19] Lin C. C., Hsu C. Y. and Huang H. N., "Finite element analysis on deflection control of plates with piezoelectric actuators", composite structures, 35, 1996, 423-433

[20] Goswami S., Kant T., "Shape control of intelligent composite stiffened structures using piezoelectric materials- A finite element approach", Journal of reinforced plastic and composite, Vol. 17, No. 5/1998

[21] Zu-Qing Q., "An efficient modeling method for laminated composite plates with piezoelectric sensors and actuators", Smart materials and structures, 10, 2001, 807-818

[22] Zhang N. and Kirpitchenko I., "Modelling dynamic of continous structure with

piezoelectric sensor/actuator for passive structural control

[23] Benjeddou A., "Advances in piezoelectric finite element modeling of adaptive structural elements: a survey, Coputers and structures, 76, 2000, 347-363

[24] Edery-Azulay L. and Abromovich H., "Piezoelectric actuation and sensing mechanism-closed form solutions", composite structures, 64, 2004, 443-453

[25] Suleman A. and Venkayya V. B., "A simple finite element formulation for a laminated composite plate with piezoelectric layers", Journal of intelligent material systems and structures, 6, 1995

[26] Ray M.C., Battacharyya R. and Samanta B., "Static analysis of an intelligent structure by the finite element method", Computers and structures, 52, No. 4, 1994, 617-631

[27] Donthireddyand P. and Chandrashekhara K., "Modeling and shape control of composite beams with embedded piezoelectric actuators", Composite Structures, 35, 1996, 237-244

[28] Benjeddou A., Deu J. F. and Letombe S., "Free vibrations of simply-supported piezoelectric adaptive plate: an exact sandwich formulation", Thin-walled structures, 40, 2002, 573-593

[29] Thirupathi S. R., Seshu P. and Naganathan N. G., "A finite element static analysis of smart turbine blades", Smart Materials and structures, 6, 1997, 607-615

[30] Waisman H., Abramovich H., "Active stiffening of laminated composite beam using piezoelectric actuators", Composite structures, 58, 2002, 109-120

[31] Waisman H., Abramovich H., "Variation of natural frequencies of beams using the active stiffening effect, Compoiste part B 33, 2002, 415-424

[32] Clinton, Y.K. Chee, Liyong Tong and G. P. Steven, "A mixed model for composite beams with piezoelectric actuators and sensors",

[33] Koconis D. B., Kollar L. P., and Springer G. S., "Shape control of composite plates and shells with embedded actuators", Journal of composite materials, 28, 1994, 415-458

[34] Soares C.M.M., Soares C.A.M., Correia, V.M.F., "Optimal design of piezolaminated structures", Composite Structures 1999, 47, (1–4), 625– 34.

[35] Correia VMF, Gomes MAA, Suleman A, Soares CMM, Soares CAM. "Modeling and design of adaptive composite structures", Computer Methods in Applied Mechanics and engineering 2000, 185(2–4), 325–46.

[36] Birman V, Simonyan A. "Optimum distribution of smart stiffeners in sandwich plates subjected to bending or forced vibrations", Composite Part B—Eng 1996, 27, (6),657–65.

[37] Bruant, G. Coffignal and F. Lene, "A methodology for determination of piezoelectric actuator and sensor location on beam structures, Journal of sound and vibration, 2001, 243(5), 861-882

[38] Carlos A. Mota Soares, Cristóvão M. Mota Soares and Victor M. Franco Correia, "Modeling and Design of Laminated Composite Structures with Integrated Sensors and Actuators", Computational Mechanics for the Twenty-First Century, Edinburg, U.K., 2000, 165-185

[39] Yan Y. J., Yam L. H., "Mechanical interaction issues in piezoelectric composite structures", Composite Structures, 59, (2003), 61–65

[40] Barboni R., Mannini A., Fantini E. and Gaudenzi P., "Optimal placement of PZT actuators for the control of beam dynamics", Smart material structure, 9, 2000, 110-120,

U.K

[41] Batra RC, Geng TS, "Enhancment of the dynamic buckling load for a plate by using piezoceramic actuators" Smart material structures, 2001, 10:925-33

[42] Victor M., Correia F., Cristovao M. Mota Soares, Carlos A. Mota Soares, "Buckling optimization of composite laminated adaptive structures" Composite structures, 62, 2003, 315-321

[43] Baz, A., and Poh, S., "Performance of an active control system with piezoelectric actuators", Journal of sound and vibration,, Vol.126, No.2, 1988, 327-343

[44] Aldraihem J. O., "Optimal Size and location of piezoelectric actuators/sensors: practical considerations", Journal of guidance, control, and dynamics, Vol.23, No.3, May-June 2000, 509-515

[45] Suleman A., Goncalves M. A., "Multi-objective optimization of an adaptive composite beam using the physical programming approach", Journal of intelligent material system and structures, V.10, 1999, 56-70

[46] Venkataraman P., "Applied Optimization with MATLAB Programming", 2002, John Wiley & Sons Inc

[47] Frecker, Mary, I., "Recent advances in optimization of smart structures and actuators", Journal of intelligent materials systems and structures, 14, 2003, 207-216.

[48] Arora, J., S., "Introduction to optimum design", 2004, Elsevier academic press.

[49] Fletcher, R., "Practical methods of optimization", 2nd edition, 1987, John Wiley.

[50] Powel, M., J., "Algorithms for nonlinear constraints that use Lagrangian functions", Mathematical programming, Vol. 14, 1978, 224-248.

[51]. Goldberg, D. E., "Genetic Algorithms in search, Optimization, and Machine Learning," 1989, Addison-Wesley Publishing Co. Inc., Reading, Massachusetts.

[52]. Aarts, E., and Korast, J., "Simulated Annealing and Boltzman Machines, A Stochastic Approach to Combinational Optimization and Neural Computing," ,1989, John Wiley & Sons.